AD-A195 335 ROLE OF ORDINARY TO EXTRAORDINARY MODE WAVE COUPLING IN 1/2
IONOSPHERIC HEATI..(U) OHIO STATE UNIV RESEARCH
FOUNDATION COLUMBUS B ABALI ET AL. MAR 88 RS-S-121
UNCLASSIFIED RADC-TR-88-22 F19628-83-K-0005 F/G 12/3 NL

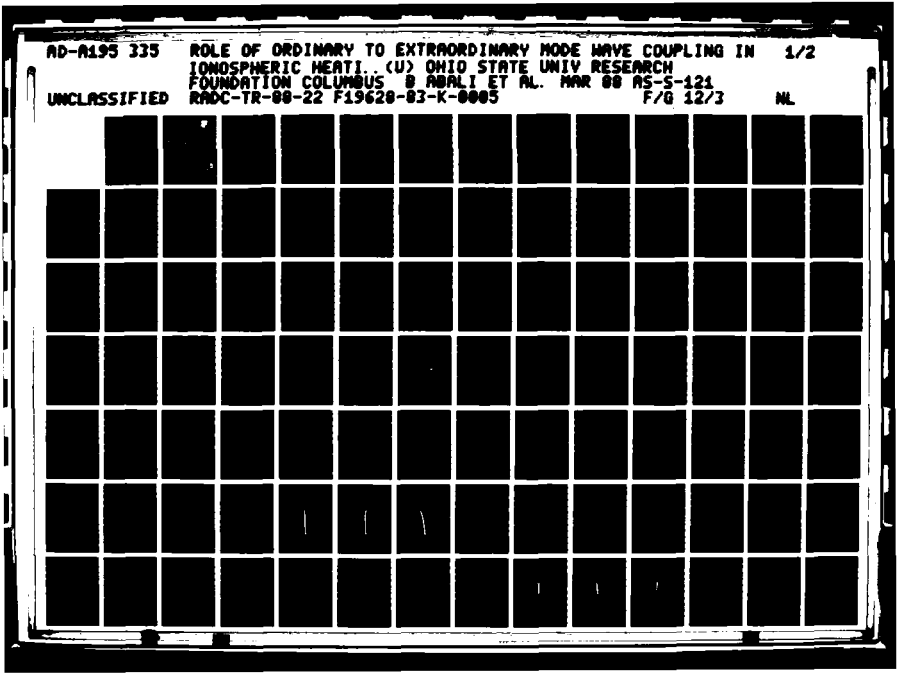

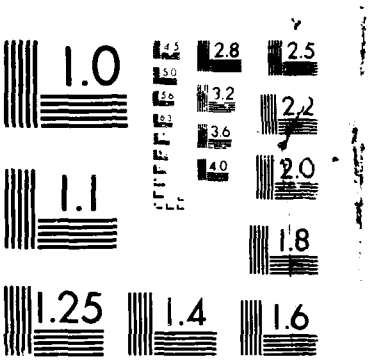

MICROCOPY RESOLUTION TEST CHA
NATIONAL BUREAU OF STANDARDS 1963

DTIC FILE COPY

AD-A195 335

RADC-TR-88-22
Final Technical Report
March 1988

ROLE OF ORDINARY TO EXTRAORDINARY MODE WAVE COUPLING IN IONOSPHERIC HEATING EXPERIMENTS

The Ohio State University

B. Abali, T. A. Seliga and K. Aydin

APPROVED FOR PUBLIC RELEASE; DISTRIBUTION UNLIMITED.

DTIC ELECTE MAY 13 1988 S D

ROME AIR DEVELOPMENT CENTER
Air Force Systems Command
Griffiss Air Force Base, NY 13441-5700

088 12 031

UNCLASSIFIED

SECURITY CLASSIFICATION OF THIS PAGE

REPORT DOCUMENTATION PAGE

Form Approved OMB No. 0704-0188

1a. REPORT SECURITY CLASSIFICATION UNCLASSIFIED	1b. RESTRICTIVE MARKINGS N/A
2a. SECURITY CLASSIFICATION AUTHORITY N/A	3. DISTRIBUTION/AVAILABILITY OF REPORT Approved for public release; distribution unlimited.
2b. DECLASSIFICATION/DOWNGRADING SCHEDULE N/A	
4. PERFORMING ORGANIZATION REPORT NUMBER(S) AS-S-121	5. MONITORING ORGANIZATION REPORT NUMBER(S) RADC-TR-88-22
6a. NAME OF PERFORMING ORGANIZATION The Ohio State University 6b. OFFICE SYMBOL (If applicable)	7a. NAME OF MONITORING ORGANIZATION Rome Air Development Center (EECP)
6c. ADDRESS (City, State, and ZIP Code) Research Foundation 1314 Kinnear Road Columbus OH 43212	7b. ADDRESS (City, State, and ZIP Code) Hanscom AFB MA 01731-5000
8a. NAME OF FUNDING/SPONSORING ORGANIZATION Rome Air Development Center 8b. OFFICE SYMBOL (If applicable) EECP	9. PROCUREMENT INSTRUMENT IDENTIFICATION NUMBER F19628-83-K-0005
8c. ADDRESS (City, State, and ZIP Code) Hanscom AFB MA 01731-5000	10. SOURCE OF FUNDING NUMBERS PROGRAM ELEMENT NO. 61102F; PROJECT NO. 2305; TASK NO J2; WORK UNIT ACCESSION NO 39

11. TITLE (Include Security Classification)
ROLE OF ORDINARY TO EXTRAORDINARY MODE WAVE COUPLING IN IONOSPHERIC HEATING EXPERIMENTS

12. PERSONAL AUTHOR(S)
B. Abali, T.A. Seliga, K. Aydin

13a. TYPE OF REPORT	13b. TIME COVERED	14. DATE OF REPORT (Year, Month, Day)	15. PAGE COUNT
Final	FROM Jul 83 TO Aug 85	March 1988	150

16. SUPPLEMENTARY NOTATION
N/A

17. COSATI CODES			18. SUBJECT TERMS (Continue on reverse if necessary and identify by block number)
FIELD	GROUP	SUB-GROUP	Ionospheric heating; Full wave solution; Ordinary mode waves; Mode coupling; Extraordinary mode waves; Plasma resonance level
20	14		

19. ABSTRACT (Continue on reverse if necessary and identify by block number)

Electromagnetic wave propagation in a plane stratified ionospheric plasma and its possible applications to high power, high frequency (HF) experiments are investigated. A theoretical and computational examination of ordinary to extraordinary mode wave coupling is made. This coupling occurs when the propagation is in the magnetic meridian, near the critical angle of incidence. The importance of the mode coupling phenomenon in ionospheric heating experiments is discussed and demonstrated with numerical full wave solutions of the generalized differential equations governing radiowave propagation in a stratified ionosphere. Computational results indicate that mode coupling leads to intense absorption of radiowave energy near the plasma resonance level. The angular shape of the coupling window, in which the coupling is most effective, is found to be approximately circular with its width being a function of the gradient of the electron density.

20 DISTRIBUTION/AVAILABILITY OF ABSTRACT ☐ UNCLASSIFIED/UNLIMITED ☒ SAME AS RPT ☐ DTIC USERS	21 ABSTRACT SECURITY CLASSIFICATION UNCLASSIFIED
22a NAME OF RESPONSIBLE INDIVIDUAL Elihu J. Tichovolsky	22b TELEPHONE (Include Area Code) (617) 377-2897 22c OFFICE SYMBOL RADC (EECP)

DD Form 1473, JUN 86 *Previous editions are obsolete*

SECURITY CLASSIFICATION OF THIS PAGE

UNCLASSIFIED

CONTENTS

		Page
LIST OF TABLES		v
LIST OF FIGURES		vi
1. INTRODUCTION		1
1.1	Introduction	1
1.2	Ionospheric Heating Experiments	3
1.3	Research Approach	5
2. REVIEW OF RELATED THEORY		7
2.1	Assumptions	7
2.2	Basic Equations	8
2.3	Wave Polarization in the Magneto-ionic Medium	16
2.4	The Appleton-Hartree Equation	17
2.5	The Z-Echo	22
2.6	The Booker Quartic	26
2.7	Radio Windows and Mode Coupling in the Ionosphere	30
2.8	Differential Equations Governing Radiowave Propagation in the Ionosphere	36
2.9	Full Wave Solution Technique	42
2.10	Deriving the Boundary Conditions	44
2.11	Integration	45
2.12	Numerical Swamping	47
2.13	Matching Solutions to the Incident Wave	50
2.14	Decomposing Total Field Components in the Lower Boundary	52

3. MODEL COMPUTATIONS 55

3.1 Parameters of the Ionospheric Model . . 55
3.2 Parameters of the Full Wave Solution Program 59
3.3 Interpretation of the Results 61
3.4 Width of the Coupling Window 90

4. CONCLUSIONS AND RECOMMENDATIONS 105

REFERENCES 111

APPENDICES 116

A. Cartesian Components of Electric and Magnetic Fields for the Ionospheric Models 1 and 2 116

B. Reflection Coefficients for the Ionospheric Models 1, 2 and 3 129

Accession For
NTIS GRA&I
DTIC TAB
Unannounced
Justification
By
Distribution/
Availability Codes
Dist | Avail and/or Special
A-1

LIST OF TABLES

Table		Page
2.1	Symbols and Notation	9
3.1	Parameters of the Selected Ionospheric Models	56
3.2	Collision Frequencies for the Ionospheric Models	57
3.3	Critical Level Heights for the Ionospheric Models.	59
3.4	Integration Increments Used for Each Ionospheric Model	60
3.5	Average Execution Times for the Ionospheric Models	61
3.6	Angular Widths of the Coupling Windows	91
B.1	Reflection Coefficients - Model 1, in the Magnetic Meridian	130
B.2	Reflection Coefficients- Model 1, off the Magnetic Meridian	131
B.3	Reflection Coefficients - Model 2 - in the Magnetic Meridian	132
B.4	Reflection Coefficients - Model 2, off the Magnetic Meridian	133
B.5	Reflection Coefficients - Model 3, in the Magnetic Meridian	134
B.6	Reflection Coefficients - Model 3, off the Magnetic Meridian	135

LIST OF FIGURES

Figure		Page
2.1	Square of refractive index vs. magnetoionic parameter X for intermediate inclination of the magnetic field	20
2.2	Demonstration of mode-propagation regions as a function of the plasma frequency parameter X	21
2.3	Square of refractive index versus plasma frequency parameter X when Earth's magnetic field is nearly vertical	23
2.4	n^2 versus X when the wave normal is nearly parallel to the Earth's magnetic field at the X-1 level	25
2.5	Relationships between the propagation parameters (n, q, θ_i, θ)	28
2.6	Roots of the Booker quartic for the vertical incidence case	31
2.7	Roots of the Booker quartic for the critical angle of incidence (propagation towards magnetic south)	33
2.8	Roots of the Booker quartic for the critical angle of incidence (propagation towards magnetic north)	34
2.9	Ray paths in the magnetic meridian; critical coupling rays are indicated by dashed lines \42, 43}.	37
3.1	Geomagnetic field conditions at Platteville, Colorado	58
3.2	x-component of electric field intensity; vertical incidence case	63

3.3 y-component of electric field intensity; vertical incidence case 64

3.4 z-component of electric field intensity; vertical incidence case 65

3.5 Real part of q; vertical incidence case 66

3.6 Imaginary part of q; vertical incidence case 67

3.7 Ray path for the vertical incidence case 69

3.8 x-component of electric field intensity; critical angle of incidence case (towards magnetic north) 71

3.9 y-component of electric field intensity; critical angle of incidence case (towards magnetic north) 72

3.10 z-component of electric field intensity; critical angle of incidence case (towards magnetic north) 73

3.11 Real part of q; critical angle of incidence case (towards magnetic north) 75

3.12 Imaginary part of q; critical angle of incidence case (towards magnetic north) 76

3.13 Real part of q near the x=1 level; critical angle of incidence case (towards magnetic north) 77

3.14 Imaginary part of q near the x=1 level; critical angle of incidence case (towards magnetic north) 78

3.15 Ray path in the magnetic meridian; critical angle of incidence case (towards magnetic north) 79

3.16 x-component of electric field; critical angle of incidence case (towards magnetic south) 81

3.17 y-component of electric field; critical angle of incidence case (towards magnetic south) 82

3.18 z-component of electric field; critical angle of incidence case (towards magnetic south) 83

3.19 Real part of q; critical angle of incidence case (towards magnetic south) 85

3.20 Imaginary part of q; critical angle of incidence case (towards magnetic south) 86

3.21 Real part of q near the X=1 level; critical angle of incidence case (towards magnetic south) 87

3.22 Imaginary part of q near the X=1 level; critical angle of incidence case (towards magnetic south) 88

3.23 Ray path in the magnetic meridian; critical angle of incidence case (towards magnetic south) 89

3.24 Reflection coefficient vs. angle of incidence: Model 1, in the magnetic meridian, towards magnetic north 92

3.25 Reflection coefficient vs. angle of incidence: Model 1, in the magnetic meridian, towards magnetic south 93

3.26 Reflection coefficient vs. angle of incidence: Model 2, in the magnetic meridian, towards magnetic north 94

3.27 Reflection coefficient vs. angle of incidence: Model 2, in the magnetic meridian, towards magnetic south 95

3.28 Reflection coefficient vs. angle of incidence: Model 3, in the magnetic meridian, towards magnetic north 96

3.29 Reflection coefficient vs. angle of incidence: Model 3, in the magnetic meridian, towards magnetic south 97

3.30 Reflection coefficient vs. angle of incidence: Model 1, off the magnetic meridian, towards magnetic north 98

3.31 Reflection coefficient vs. angle of incidence: Model 1, off the magnetic meridian, towards magnetic south 99

3.32 Reflection coefficient vs. angle of incidence: Model 2, off the magnetic meridian, towards magnetic north 100

3.33 Reflection coefficient vs. angle of incidence: Model 2, off the magnetic meridian, towards magnetic south 101

3.34 Reflection coefficient vs. angle of incidence: Model 3, off the magnetic meridian, towards magnetic north 102

3.35 Reflection coefficient vs. angle of incidence: Model 3, off the magnetic meridian, towards magnetic south 103

A.1 Model 1, x, y, z components of electric field for the vertical incidence case. . 117

A.2 Model 1, x, y, z components of magnetic field for the vertical incidence case. . 118

A.3 Model 1, x, y, z components of electric field for the critical angle case. . . . 119

A.4 Model 1, x, y, z components of magnetic field for the critical angle case . . . 120

A.5 Model 1, x, y, z components of electric field for the critical incidence case. . 121

A.6 Model 1, x, y, z components of magnetic field for the critical incidence case. . 122

A.7 Model 2, x, y, z components of electric field for the vertical incidence case. . 123

A.8 Model 2, x, y, z components of magnetic field for the vertical incidence case. . 124

A.9 Model 2, x, y, z components of electric field for the critical incidence case. . 125

A.10 Model 2, x, y, z components of magnetic field for the critical incidence case. . 126

A.11 Model 2, x, y, z components of electric field for the critical incidence case. . 127

A.12 Model 2, x, y, z components of magnetic field for the critical incidence case. . 128

CHAPTER 1

INTRODUCTION

1.1 - INTRODUCTION

The ionosphere is the region of the atmosphere in which sufficient numbers of free electrons and ions exist to affect radio wave propagation. This ionization is mostly caused by solar radiation interacting with the Earth's atmosphere. The electron density distribution of the local ionosphere changes with solar variability, such as day and nighttime difference, seasonal variations, sunspot number, etc.

Although free electrons and ions are distributed randomly on small spatial scales, they often act upon electromagnetic waves as a continuous refracting medium because of their statistical uniformity. In the high frequency (HF) range the ionosphere may be considered as composed of only free electrons, since the ions have heavy mass and are relatively immobile.

The collisions free electrons make with other particles such as ions, molecules and atoms have a viscous damping effect on radio waves which is equivalent to ohmic heating in a conductive medium. This is the major reason for radio wave absorption in the ionosphere.

The Earth's magnetic field complicates the refracting properties of the ionosphere. The presence of a constant magnetic field makes the medium anisotropic and complicates the relationship between the electric polarization $\vec{P}$ and electric field intensity $\vec{E}$,

$$\vec{P} = \varepsilon_0 M \vec{E} \qquad (1.1)$$

where M is the 3 x 3 susceptibility tensor of the ionized medium and ε_0 is the free space permittivity.

As an anisotropic medium, the ionosphere exhibits many interesting properties. For special cases, complete penetration of the layers which would generally be reflecting is possible through ordinary to extraordinary mode wave coupling. This occurs when propagation is near the critical angle of incidence which lies in the magnetic meridian. Total energy deposition of the coupled wave may occur near the resonance region using this mechanism. In the future this may prove to be an efficient heating mechanism for ionospheric modification experiments as well as a viable explanation for many experimental observations.

A theoretical and computational examination of this phenomenon is made in this study.

1.2 - IONOSPHERIC HEATING EXPERIMENTS

High power HF heating experiments began in the 1970s and produced many interesting and often unexpected results [1,2]. The motivation of the early experiments was to understand the nature of the ionospheric plasma. Experimental observations have been summarized in numerous references [3,5,5,6,7,8,9, 10,11,12,13]. Among the most interesting observations derived from these experiments are:

- Plasma instabilities associated with the non-linearity behavior of the medium.
- Generation of short scale irregularities.
- Generation of large scale irregularities.
- Airglow excitation.
- Nonlinear demodulation (ELF, VLF generation).
- Production of extrathermal electrons.

These experimental findings may have their greatest impact on long-range communications systems. For example, scattering from small-scale irregularities

(0.5 - 5m size) have been observed which may be useful for establishing long range VHF and UHF communication links [33,34]. Large scale irregularities were found to scatter HF signals [14,15,16,17] which might be useful for injecting HF waves into ionospheric waveguides for so-called duct mode propagation [18,19, 20,21,22]. Nonlinear demodulation capability of the ionosphere has also been reported [23,24]. When the heater wave is amplitude modulated with a frequency between 0.5-10KHz, the heated volume irradiates waves at the modulating frequency which may be received at far distances. This is believed to occur because of the modulation of the natural ionospheric currents (dynamo, polar electrojet, equatorial electrojet, etc.) passing through the periodically varying heated region.

The potential of HF ionospheric heating/ modification has been well recognized. However, to date, most of the experiments have been performed with vertically directed antennas. Both theoretically and experimentally, very little attention has been paid to oblique propagation. This work shows that, for certain angles of incidence, oblique propagation should provide an efficient way of depositing energy into the ionospheric plasma. This, then, should enhance the

utility of HF radiowave heating for communications and basic plasma research purposes.

1.3 - RESEARCH APPROACH

Electromagnetic wave propagation in a plane stratified ionospheric plasma and its possible application to high power, high frequency (HF) heating experiments are investigated. Theory shows that mode coupling from ordinary (o-) to extraordinary (x-) waves in the vicinity of the plasma resonance level is possible if certain conditions are met. This may result in deposition of radiowave energy into the ionospheric plasma. The conditions under which coupling is most effective, and the amount of coupling, are investigated for several ionospheric models using the numerical full wave solution technique and the roots of the Booker quartic.

The theory of wave propagation in the ionospheric plasma, the Booker quartic and the full wave solution technique are presented in Chapter 2. Computational results which demonstrate the theory and coupling efficiencies for several directions of propagation are presented in Chapter 3. Summary of results, conclusions and recommendations are presented in

Chapter 4. This study clearly shows that coupling from o- to x-waves may result in significant absorption of radiowave energy in a very narrow region just below the level at which the wave frequency equals the plasma frequency. This heating mechanism should have important implications for using ionospheric high-power radiowaves to produce irregularities from which scattering of other radiowaves for communications purposes may be possible.

CHAPTER 2

REVIEW OF RELATED THEORY

In this chapter the theory of HF electromagnetic plane wave propagation in a plane stratified ionospheric plasma is reviewed [25,26,27,28,29,30]. The theory provides the basis for understanding HF wave propagation phenomena through related numerical full wave solutions.

2.1 - ASSUMPTIONS

- The electromagnetic fields are assumed to arise from harmonic plane waves. The time dependence $\exp(i\omega t)$ is suppressed for all field variables.
- The rationalized M.K.S. units are used.
- The ionosphere is assumed to be horizontally stratified.
- As a magnetoionic medium, the ionosphere is assumed to consist of free electrons which are distributed locally with statistical uniformity. The effects of heavy ions are neglected.
- Cold plasma conditions are assumed to exist, and the possibility of energy loss caused by generation of other types of waves such as plasma waves and acoustic waves is ignored.

- Definition of the symbols and basic quantities are listed in Table 2.1.

2.2 - BASIC EQUATIONS

The electromagnetic fields in the ionosphere are governed by the Maxwell's equations:

$$\nabla \cdot \vec{D} = 0 \qquad (2.1) \qquad \nabla \times \vec{E} = 1i\omega \mu_0 \vec{H} \qquad (2.3)$$

$$\nabla \cdot \vec{B} = 0 \qquad (2.2) \qquad \nabla \times \vec{H} = i \omega \vec{D} \qquad (2.4)$$

If the z-axis is taken to be the wave normal, Eqs. 2.3, 2.4 become

$$\frac{\partial}{\partial z} E_y = i \omega \mu_0 H_x \qquad \frac{\partial}{\partial z} H_x = i \omega D_y$$

$$\frac{\partial}{\partial z} E_x = -i \omega \mu_0 H_y \qquad \frac{\partial}{\partial z} H_y = -i \omega D_x \qquad (2.5)$$

$$D_z = 0 \qquad H_z = 0$$

$D_z = 0$ leads to $E_z = 0$ in an isotropic medium. However, in an anisotropic medium such as the ionosphere this is not true, and in general the longitudinal component E_z is non-zero.

Table 2.1 - Symbols and Notation

c	velocity of light in free space
ε_0	free space permittivity
μ_0	free space permeability
i	$\sqrt{-1}$
e	electron charge
m	electron mass
k	wave number
K	Boltzmann constant
T	electron temperature
n	refractive index
N	electron density
E	electric field
P	electric polarization
D	electric displacement
H	magnetic field
B	magnetic induction
$\vec{H}$	$n_o \vec{H}$
ω	wave frequency
ω_N	plasma frequency
ω_H	gyro frequency

$\vec{B}_0$	Earth's magnetic induction
X	plasma frequency parameter
Y	normalized gyro frequency parameter
Z	normalized collision frequency
M	3 x 3 susceptibility tensor
ℓ,m,n	x,y,z direction cosines of $\vec{Y}$
U	$1 - iZ$
ν	collision frequency
ν_m	collision frequency of monoenergetic electrons
ν_e	effective collision frequency
g_n	complex collision frequency
$C_n(y)$	Dingle integral of order n
ρ	wave polarization
Y_T	transverse component of Y
Y_L	longitudinal component of Y
X_R	$= \frac{1-Y^2}{1-Y^2_Z}$ resonance condition
θ	angle of incidence
θ_I	angle of incidence in free space
θ_B	magnetic dip
n_o	intrinsic impedance of free space

$\vec{H}$ is often used as a measure of magnetic field intensity and is defined as:

$$\vec{H} = \eta_0 \vec{H} \tag{2.6}$$

where η_0 is the intrinsic impedance of free space. H has the units of electric field intensity which makes it more convenient for this application. Using this definition Eqs. 2.3, 2.4 become

$$\nabla \times \vec{E} = -ik \vec{H} \tag{2.7}$$

$$\nabla \times \vec{H} = \frac{ik}{\varepsilon_0} \vec{D} \tag{2.8}$$

In the ionospheric plasma the equation of electron motion, arising from excitation of an HF electromagnetic wave, defines the polarisation state of the plasma according to Eq. 2.9 [26]

$$-\varepsilon_0 X \vec{E} = \vec{P} (1 - i Z) + i \vec{P} \times \vec{Y} \tag{2.9}$$

where X, $\vec{Y}$, Z are defined in terms of basic quantities as

$$X = \frac{N e^2}{\varepsilon_0 m \omega^2} = \frac{\omega_N^2}{\omega^2} \tag{2.10}$$

$$\vec{Y} = \frac{e B_0}{m \omega} = \frac{\omega_H}{\omega} \tag{2.11}$$

$$Z = \frac{\nu}{\omega} \tag{2.12}$$

The variable X is proportional to the electron density. Plasma frequency ω_N is a characteristic frequency of the plasma at which electrons tend to oscillate. The variable $\vec{Y}$ is the normalized gyrofrequency, and its direction is anti-parallel to the superimposed magnetic field $\vec{B}_0$. The gyrofrequency ω_H is another characteristic frequency of the magnetoionic plasma and is the frequency at which free electrons oscillate in a circular motion about the magnetic field $\vec{B}_0$. The variable Z is the normalized collision frequency.

If (ℓ, m, n) are the direction cosines of $\vec{Y}$, Eq. 2.9 becomes

$$-\varepsilon_0 X \begin{bmatrix} E_x \\ E_y \\ E_z \end{bmatrix} = \begin{bmatrix} U & i\,n\,Y & -i\,m\,Y \\ -i\,n\,Y & U & i\,\ell\,Y \\ i\,m\,Y & -i\,\ell\,Y & U \end{bmatrix} \begin{bmatrix} P_x \\ P_y \\ P_z \end{bmatrix} \tag{2.13}$$

Inverting this 3 x 3 matrix gives the classical form of the constitutive relations [25]

$$\begin{bmatrix} P_x \\ P_y \\ P_z \end{bmatrix} = \frac{-\varepsilon_0 X}{U(U^2-Y^2)} \begin{bmatrix} U^2-\ell^2Y^2 & -in\,Y\,U - l\,m\,Y^2 & i\,m\,Y\,U - \ell\,n\,Y^2 \\ i\,n - \ell\,m\,Y^2 & U^2 - m^2Y^2 & -i\,\ell\,Y\,U - m\,n\,Y^2 \\ -i\,m\,Y\,U - \ell n\,Y^2 & i\ell\,Y\,U - m\,n\,Y^2 & U^2 - n^2Y^2 \end{bmatrix} \begin{bmatrix} E_x \\ E_y \\ E_z \end{bmatrix} \tag{2.14}$$

Uses of the parameter Z suggests that there is a single effective collision frequency which can be substituted in the constitutive relations. Actually, because of the dependence of the collision frequency on thermal energy of the electrons there is no single collision frequency applicable, except under certain conditions. Sen and Wyller (1960) [31] developed a modified form of the constitutive relations for weakly ionized gases which accounts for the thermal energies of electrons using Boltzmann's transport equation. As a result one obtains three different collision frequencies g_n (n=1,2,3) [32].

$$g_n = \omega_n \left\{ \frac{5}{2} \left(\frac{\omega_n}{\nu_m}\right) C_{\frac{5}{2}} \left(\frac{\omega_n}{\nu_m}\right)^2 C_{\frac{3}{2}} \left(\frac{\omega_n}{\nu_m}\right) \right\} - i\,\omega_n \tag{2.15}$$

where

$$\omega_1 = \omega \qquad \omega_2 = \omega - \omega_H \qquad \omega_3 = \omega + \omega_H \tag{2.16}$$

and

$$\nu_m = a\ K\ T \tag{2.17}$$

where a is a proportionality constant, K is the Boltzmann constant and T is the electron temperature. The $C_{\frac{5}{2}}(y)$ and $C_{\frac{3}{2}}(y)$ are the Dingle integrals which are defined as

$$C_n(y) = \frac{1}{n!} \int_0^\infty \frac{x^n e^{-x}}{x^2 + y^2}\, dx \tag{2.18}$$

Using these new collision frequency terms, the susceptibility tensor M takes the form given by Eq. 2.21, which is equivalent to the classical form of the constitutive relations 2.14 at the asymptotical limits $\nu_m << |\omega - \omega_H|$ and $\nu_m >> |\omega + \omega_H|$ with ν_e defined as the effective collision frequency [32].

$$\nu_m << \left|\omega - \omega_H\right| \qquad \nu_e = \frac{5}{2}\nu_m \tag{2.19}$$

$$\nu_m \gtrsim \left|\omega + \omega_H\right| \qquad \nu_e = \frac{3}{2}\nu_m \tag{2.20}$$

$$\cdot \chi \left[\begin{array}{ccc} \frac{\ell^2}{U_1} + \frac{1/2(1-\ell^2)}{U_2 - Y} + \frac{1/2(1-\ell^2)}{U_3 + Y} & \frac{\ell m}{U_1} + \frac{1/2(-in-\ell m)}{U_2 + Y} + \frac{1/2(in-\ell m)}{U_3 + Y} & \frac{\ell n}{U_1} \quad \frac{1/2(im-\ell n)}{U_2 - Y} + \frac{1/2(-im-\ell n)}{U_3 + Y} \\ \frac{m\ell}{U_1} + \frac{1/2(in-m\ell)}{U_2 - Y} + \frac{1/2(-in-m\ell)}{U_3 + Y} & \frac{m_2}{U_1} + \frac{1/2(1-m^2)}{U_2 - Y} + \frac{1/2(1-m^2)}{U_3 + Y} & \frac{mn}{U_1} \quad \frac{1/2(-i\ell-mn)}{U_2 - Y} \quad \frac{1/2(i\ell-mn)}{U_3 + Y} \\ \frac{n\ell}{U_1} \quad \frac{1/2(-im-n\ell}{U_2 - Y} \quad \frac{1/2(im-n\ell}{U_3 + Y} & \frac{nm}{U_1} \quad \frac{1/2(i\ell-nm)}{U_2 - Y} \quad \frac{1/2(-i\ell-nm)}{U_3 + Y} & \frac{n^2}{U_1} \quad \frac{1/2(1-n^2)}{U_2 - Y} \quad \frac{1/2(1-n^2)}{U_3 + Y} \end{array} \right] \quad (2.21)$$

The susceptibility tensor M which accounts for the thermal energies of electrons

2.3 - WAVE POLARIZATION IN THE MAGNETOIONIC MEDIUM

The polarization of a plane wave propagating in the z-direction is defined as

$$\rho = \frac{E_y}{E_x} \tag{2.22}$$

In a magnetoionic medium the following relationships also hold:

$$\rho = \frac{D_y}{D_x} = \frac{P_y}{P_x} = \frac{-H_x}{H_y} \tag{2.23}$$

If $\vec{B}_o$ is chosen to lie in the x-z plane, then the constitutive relations 2.13 become

$$\begin{aligned} -\varepsilon_o X E_x &= U P_x + i n Y P_y \\ -\varepsilon_o X E_y &= U P_y - i n Y P_x + i \ell Y P_z \\ -\varepsilon_o X E_z &= U P_z - i \ell Y P_y \end{aligned} \tag{2.24}$$

Combining Eqs. 2.22-2.24,2.25 leads to a solution of the polarization equation

$$\rho = \frac{i Y^2 T_\bullet}{2 Y_L (U-X)} \pm i \left\{ \frac{Y^4 T}{4 Y^2_L (U-X)^2} + 1 \right\}^{1/2} \tag{2.25}$$

where $Y_T = \ell Y$ and $Y_L = nY$. This equation shows that there exists two possible polarizations for an electromagnetic wave propagating in a given direction in a magnetoionic medium [26].

2.4 - THE APPLETON-HARTREE EQUATION

Appleton (1932) and Hartree (1931) developed the theory and derived the refractive index for vertically propagating radiowaves in a magnetoionic medium such as the ionosphere [26,29,30]. Their derivation of the refractive index is often referred to as the Appleton-Hartree equation which is given by

$$n^2 = 1 - \frac{X}{U - \frac{Y^2_T}{2(U-X)} \pm \left\{\frac{Y^4_T}{4(U-X)^2} + Y^2_L\right\}^{1/2}} \qquad (2.26)$$

Eq. 2.26 demonstrates the complexity of radiowave propagation in the presence of a superimposed magnetic field. Notice that in general there are two possible refractive indices for any X, due to the ± sign in the denominator. This shows that the ionosphere is a doubly refracting medium. Thus, for any given direction of propagation two characteristic waves are possible, each having different polarisations and different refractive indices. These two characteristic

waves propagate independently and have different reflection levels. It is customary to call these two waves "ordinary" and "extraordinary." The ordinary (o-) wave is the wave component whose propagation characteristics are influenced minimally by the superimposed magnetic field. On the other hand, the extraordinary (x-) wave's propagation is influenced maximally by the superimposed magnetic field.

If the superimposed magnetic field is removed ($Y_L = Y_T = 0$), the refractive index reduces to that for an isotropic plasma.

$$n^2 = 1 - \frac{X}{U} \qquad (2.27)$$

If collisions are neglected and the wave frequency equals the plasma frequency ($X = 1$), $n^2 = 0$. This is the level of reflection. Beyond this level ($X > 1$) the wave becomes evanescent and does not propagate.

The Appleton-Hartree equation exhibits a zero refractive index at three levels:

$$X = 1, \quad X = 1 - Y, \quad X = 1 + Y \quad (U = 1) \qquad (2.28)$$

The X = 1 reflection level for the o-wave is also the reflection level in an isotropic plasma. X = 1 - Y and X = 1 + Y are the reflection levels for x-waves. There is another level X = X_R where η^2 becomes infinity for a collisionless plasma, or very large when the collision frequency is small. The x-wave may be significantly absorbed at this level, given by

$$X_R = \frac{1 - Y^2}{1 - Y^2_Z} \qquad (2.29)$$

For an intermediate inclination of the magnetic field and Y < 1, the variation of η^2 with X is as shown in Fig 2.1. Figure 2.2 demonstrates the relative levels of reflection and absorption in terms of X as well as the regions in which the o- and x-waves can propagate. If a wave is incident from below the ionosphere with a monotonically increasing electron density, the x-mode will reflect at the X = 1 - Y level. The o-mode, being unaffected at this level, will propagate up to X = 1 and reflect there. The arrival times of these two reflected components will be different due to the height difference between these two levels. This double reflection phenomenon is called "magneto-ionic splitting" and its cause is the

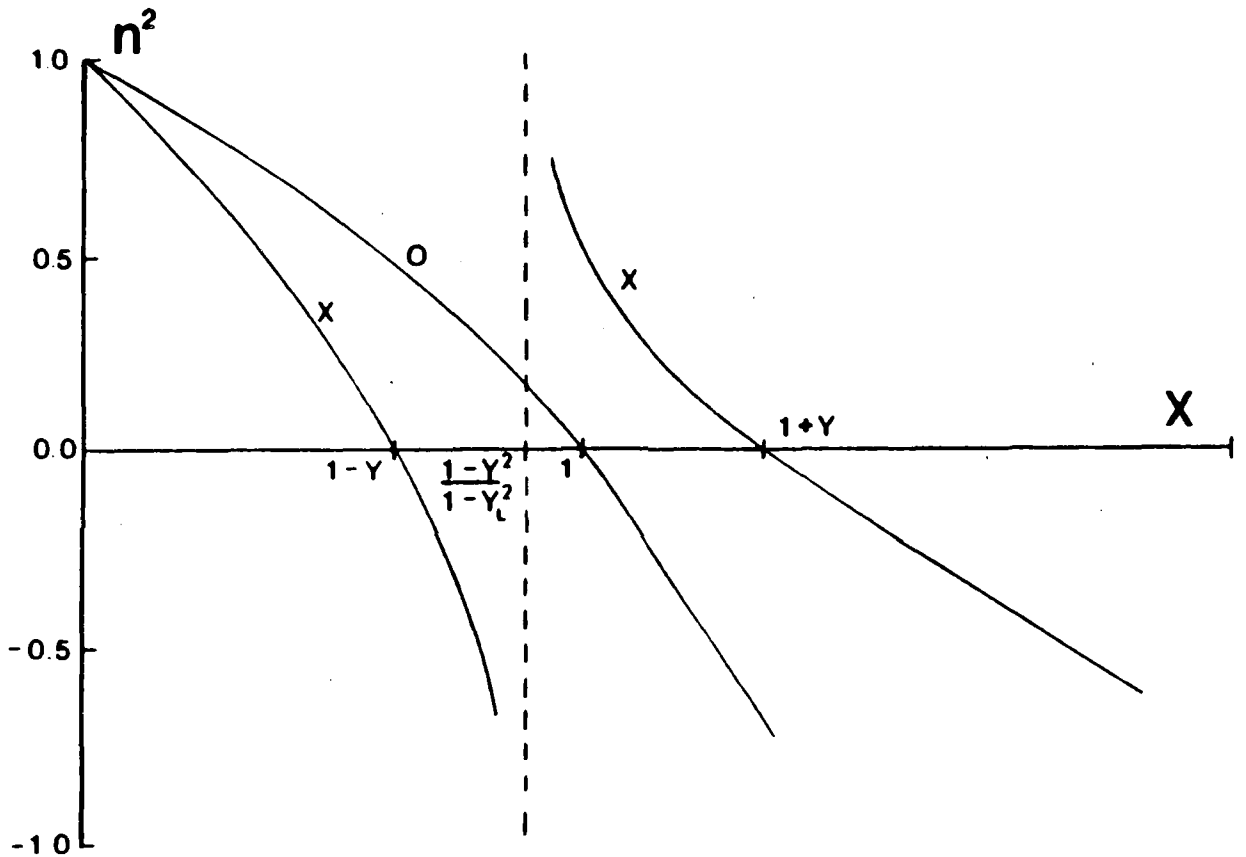

Fig. 2.1 Square of refractive index vs. magnetoionic parameter X for intermediate inclination of the magnetic field

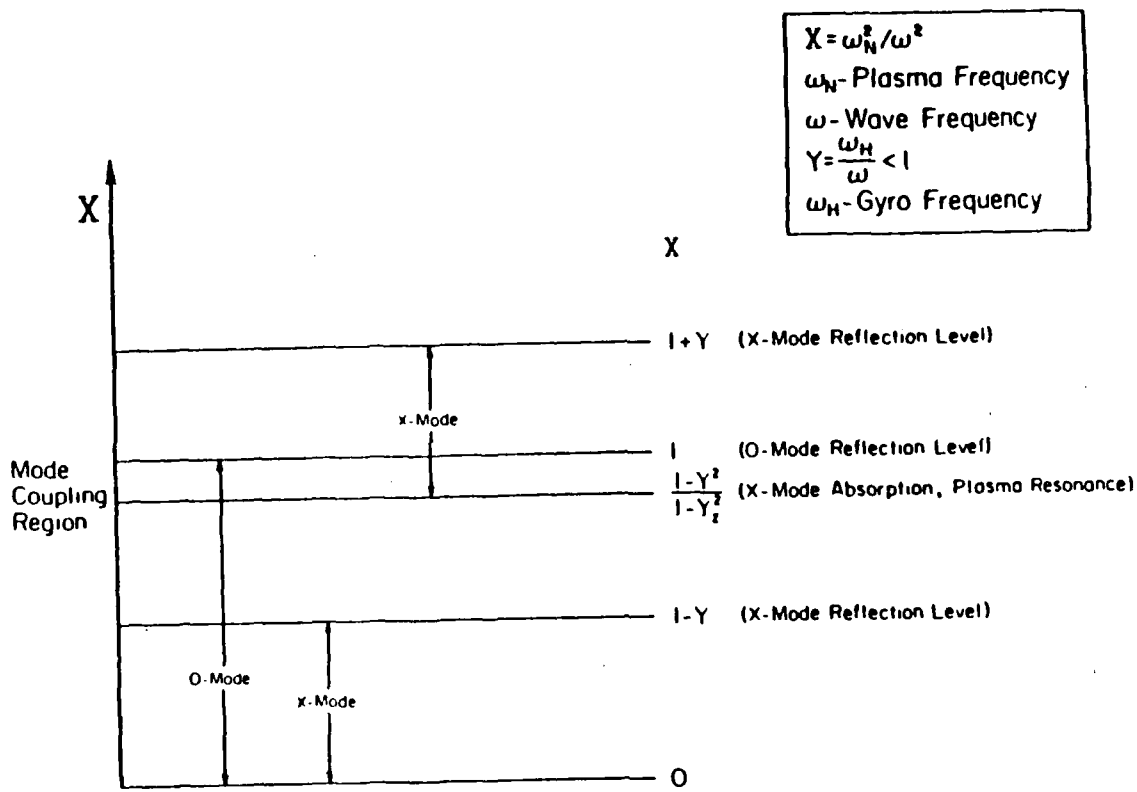

Figure 2.2 Demonstration of mode-propagation regions as a function of the plasma frequency parameter X

doubly refracting properties of the plasma containing the Earth's magnetic field [25, 26, 27].

2.5 - THE Z-ECHO

At locations where the Earth's magnetic field is nearly vertical, experimenters have occasionally observed a third echo (named z-echo) during ionosonde soundings. Eckersley (1950) and Rydbeck (1950,1951) explained this observation by reflection from the X=1+Y level through the mechanism of mode coupling from o- to x-waves at the X = 1 level [27]. If the angle between the wave normal and the Earth's magnetic field is small, η^2 versus X behaves as shown in Fig. 2.3. This figure shows that around X = 1 the curves for the o-mode and x-mode refractive indices are nearly equal. There is also a rapid change of the o-mode polarization at this level. This rapid change of polarization may lead to a coupling between the o- and x-modes and cause the transfer of energy into the region between X = 1 and X = 1 + Y as an x-wave. This wave would then travel up to the level X = 1 + Y where it would be reflected, and, after coupling back to o-mode polarisation, it would appear as a z-echo on an ionogram.

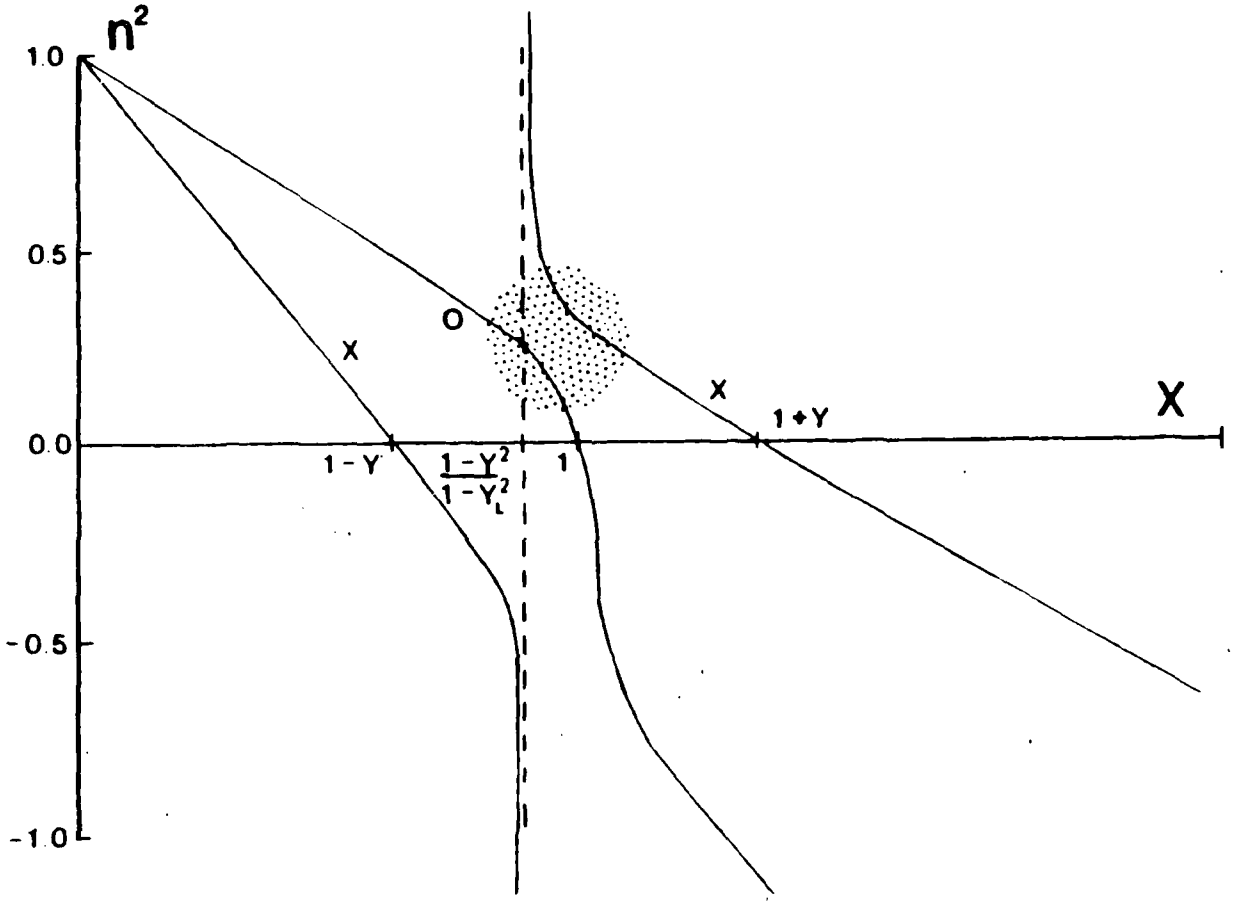

Fig. 2.3 Square of refractive index versus plasma frequency parameter X when Earth's magnetic field is nearly vertical

Ellis pointed out that for vertical incidence the collision frequency in the F-region of the ionosphere is not great enough for coupling energy effectively above the X = 1 level [35,36,37,38]. He suggested an alternative explanation. At X = 1, if the wave normal is parallel to the Earth's magnetic field ($Y_T = 0$), even with a small number of collisions η would be non-zero, which may cause the o-wave to penetrate into that region through mode coupling.

Fig. 2.4 shows η^2 versus X for this case. It is seen that the refractive indices of o- and x-modes are almost equal at X = 1. This condition may always be met provided the o-wave direction of propagation is near a critical angle of incidence θ_c below the ionosphere, given by

$$\sin \theta_c = \pm \sqrt{\frac{Y}{1 + Y}} \sin \theta_B \qquad (2.30)$$

Having penetrated the X = 1 layer, the x-wave then would propagate up to the X = 1 + Y level and would reflect in a direction which would not be observable from the ground. However, Ellis surmised that irregularities at the X = 1 + Y level might cause backscattering which would then be observed at the

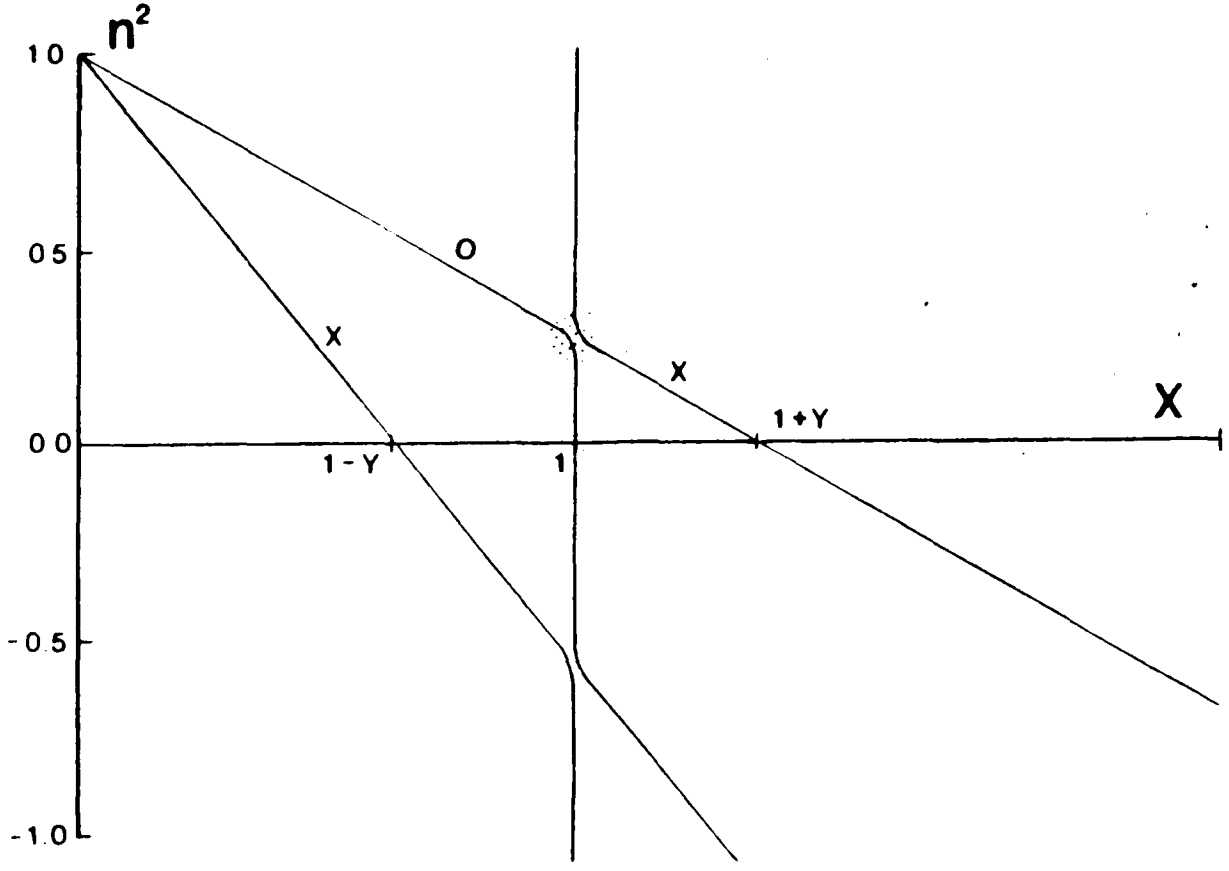

Fig. 2.4 n^2 versus X when the wave normal is nearly parallel to the Earth's magnetic field at the X=1 level

transmitter location as a z-echo [35]. It should be noted that the term z-echo or z-mode wave is used for historical reasons. Theory shows that it is actually a downgoing o-wave which underwent successive transformation from o- to x- to o- polarizations near the X = 1 level.

2.6 - THE BOOKER QUARTIC

The Appleton-Hartree formulation introduced in the previous section is most useful for vertically incident waves. For oblique incidence a more general formulation is desirable for investigating radio wave propagation in a magnetoionic medium.

Assume a wave is represented by the following wave function in which the y dependence is not included for ease of discussion.

$$\exp\{ik(ct - n(x \sin\theta + z \cos\theta))\} \qquad (2.31)$$

For an isotropic medium the refractive index n is independent of the direction of the wave normal. Therefore, to determine the propagation angle θ of the wave for a particular n, Snell's law applies

$$\sin \theta_I = n \sin \theta \qquad (2.32)$$

where θ_I is the angle of incidence in free space (n=1) below the ionosphere.

For anisotropic media the small wave function can be used to represent either o- or x-waves. Snell's law still applies, giving

$$\sin \theta_I = n_X \sin \theta_X = n_O \sin \theta_O \qquad (2.33)$$

where (n_X, θ_X) and (n_O, θ_O) are the refractive indices and propagation angles of the x-and o-waves, respectively. However, in this case, because of the anisotropy both n_X and n_O depend on the direction of the wave normal. That is, n_X and n_O are functions of θ_X and θ_O. Since θ's and n's are both unknown, one cannot simply use Snell's law to determine the parameters of Eq. 2.31.

A more general method for investigating oblique propagation was developed by Booker [38,39,26]. Booker introduced the variable q, which is more meaningful than n for oblique propagation in the ionosphere. Consider n as a vector in the direction of the wave normal inclined at an angle θ from the vertical, as

shown in Fig. 2.5. Then q is defined as the vertical component of n

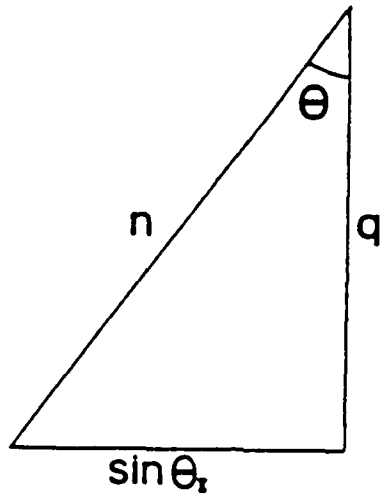

Fig. 2.5 Relationships between the propagation parameters (n, q, θ_I, θ)

and satisfies the following relationships:

$$\sin \theta_I = n \sin \theta \qquad (2.34)$$

$$q = n \cos \theta \qquad (2.35)$$

Substitution of these variables into the wave function Eq. 2.31 gives

$$\exp\{ik(ct - x \sin \theta_I - qz)\} \qquad (2.36)$$

Booker has shown that q is a root of a fourth-order polynomial which is known as the Booker quartic:

$$F(q) = \alpha q^4 + \beta q^3 + \gamma q^2 + \delta q + \epsilon = 0 \qquad (2.37)$$

where

$$\begin{aligned}
\alpha &= U^2(U-X) - UY^2 + n^2Y^2X \\
\beta &= 2nXY \ (S_1\ell = S_2m) \\
\gamma &= -2U(U-X)\ (C^2U - X) + 2Y^2(C^2U - X) \\
&\quad + XY^2\left\{1-C^2n^2+ (S_1\ell + S_2m)^2\right\} \\
\delta &= 2C^2n^2XY^2(S_1\ell + S_2m) \\
\epsilon &= (U-X)\ (C^2U - X)^2 - C^2Y^2(C^2U - X) - C^2XY^2(S_1\ell+S_2m)^2
\end{aligned} \qquad (2.38)$$

The four roots of the Booker quartic correspond to the upgoing ordinary, downgoing ordinary, upgoing extraordinary and downgoing extraordinary waves. The roots are in general complex because of the damping effect of collisions. The real part of q governs the phase change of the wave, and the imaginary part governs the attenuation of the wave as it progresses in the medium. Upgoing and downgoing waves can be identified from the imaginary part of the root. The conservation of energy principle requires that the

waves attenuate in the direction of energy flow, so for a wave propagating in the positive z-direction (upgoing), the imaginary part of q must be negative. Conversely, for waves travelling in the negative z-direction (downgoing), it must be positive.

In certain regions of the ionosphere it is possible that the roots of the Booker quartic may have real and imaginary parts with different signs. This means that the direction of energy flow and phase propagation are different [39,25]. This is explained by the fact that for anisotropic media the wave normal and ray directions are, in general, different. For the same reason the reflection level for anisotropic media is the level where two roots become equal, not where q=0.

Fig. 2.6 shows the real part of q for the vertical incidence case when there are no collisions. It is seen that the reflection levels for the o- and x-waves are at $X = 1$ and $X = 1 \pm Y$, respectively. Also note that at the $X = X_R$ level the x-wave roots approach infinity.

2.7 - RADIO WINDOWS AND MODE COUPLING IN THE IONOSPHERE

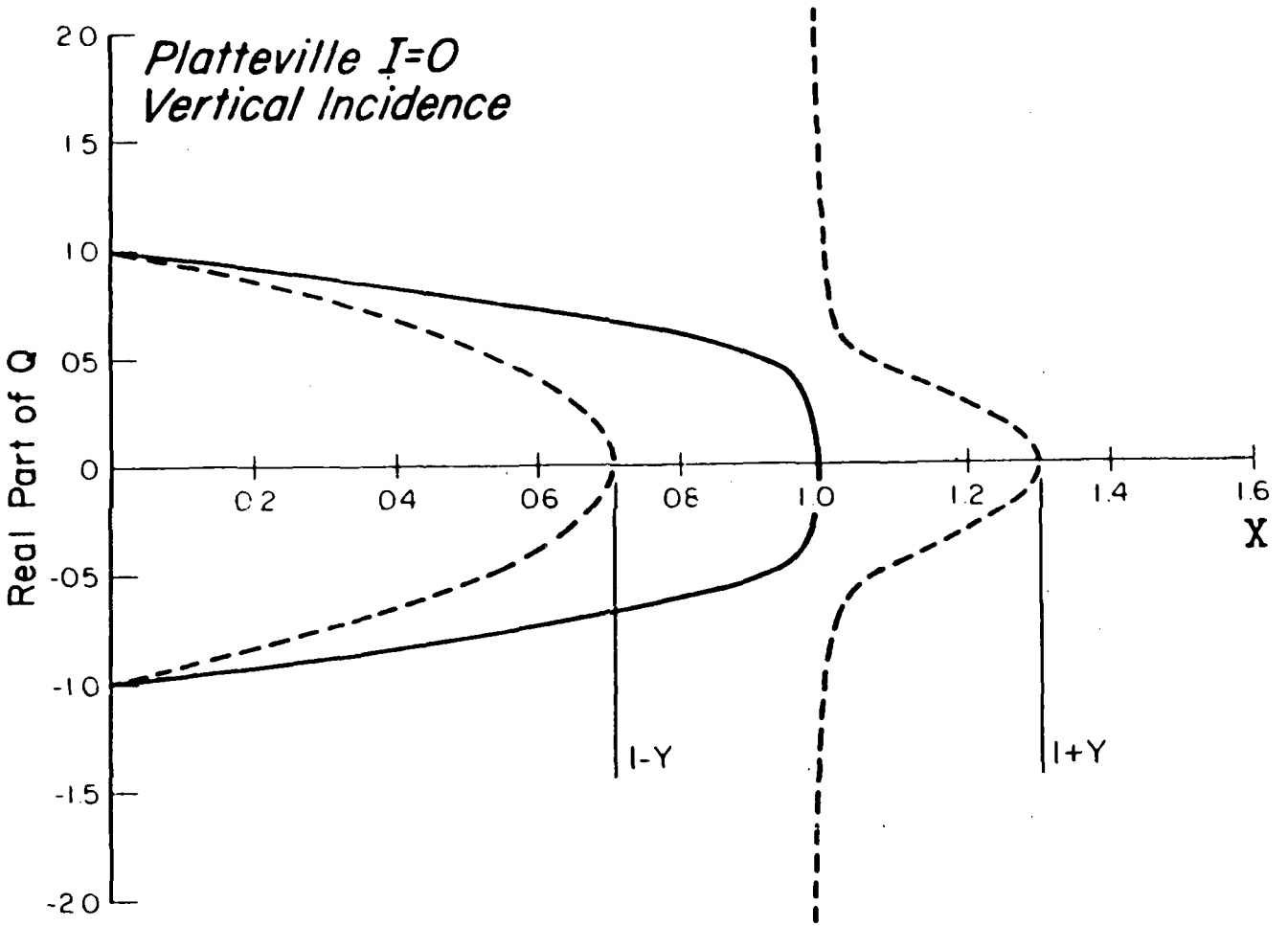

Fig. 2.6 Roots of the Booker quartic for the vertical incidence case

As discussed previously in Sect. 2.4, an o-wave may penetrate through a reflecting layer as a result of mode coupling to an x-wave. The terms radio window or holes are used to describe the occurrence of these possible penetrations [35,40,41].

The radio window of interest here occurs when the propagation is in the magnetic meridian at the critical angle of incidence

$$\theta_c = \pm \arcsin \left(\ell \sqrt{\frac{Y}{1 + Y}} \right) \qquad (2.39)$$

Figure 2.7 shows the sample behavior of the real part of the roots of the Booker quartic for $\theta_c < 0$. It is seen that the upgoing branch of the o-mode and x-mode is continuous at the X = 1 level. This suggests coupling from o- to x-waves. The energy coupled to the x-mode will propagate up to the X = 1 + Y level where it is reflected and eventually absorbed near the X_R level [25,28]. When the propagation is still in the magnetic meridian but incident at an angle $\theta_c > 0$, the real part of the roots become as shown in Fig 2.8. Note that this figure is symmetric to the previous figure about the x-axis. In this case the upgoing o-wave may also couple to an upgoing x-wave at the X=1

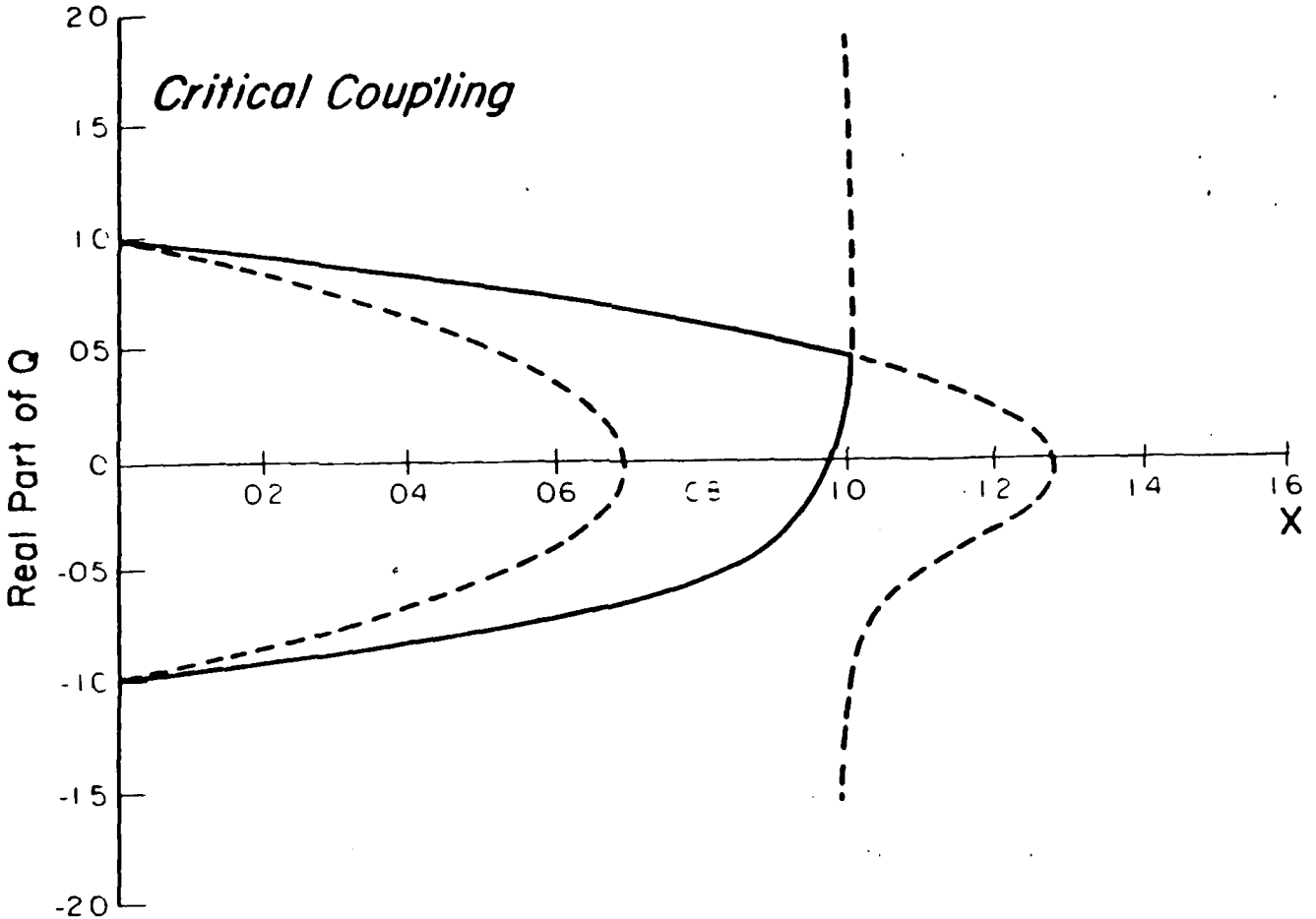

Fig. 2.7 Roots of the Booker quartic for the critical angle of incidence (propagation towards magnetic south)

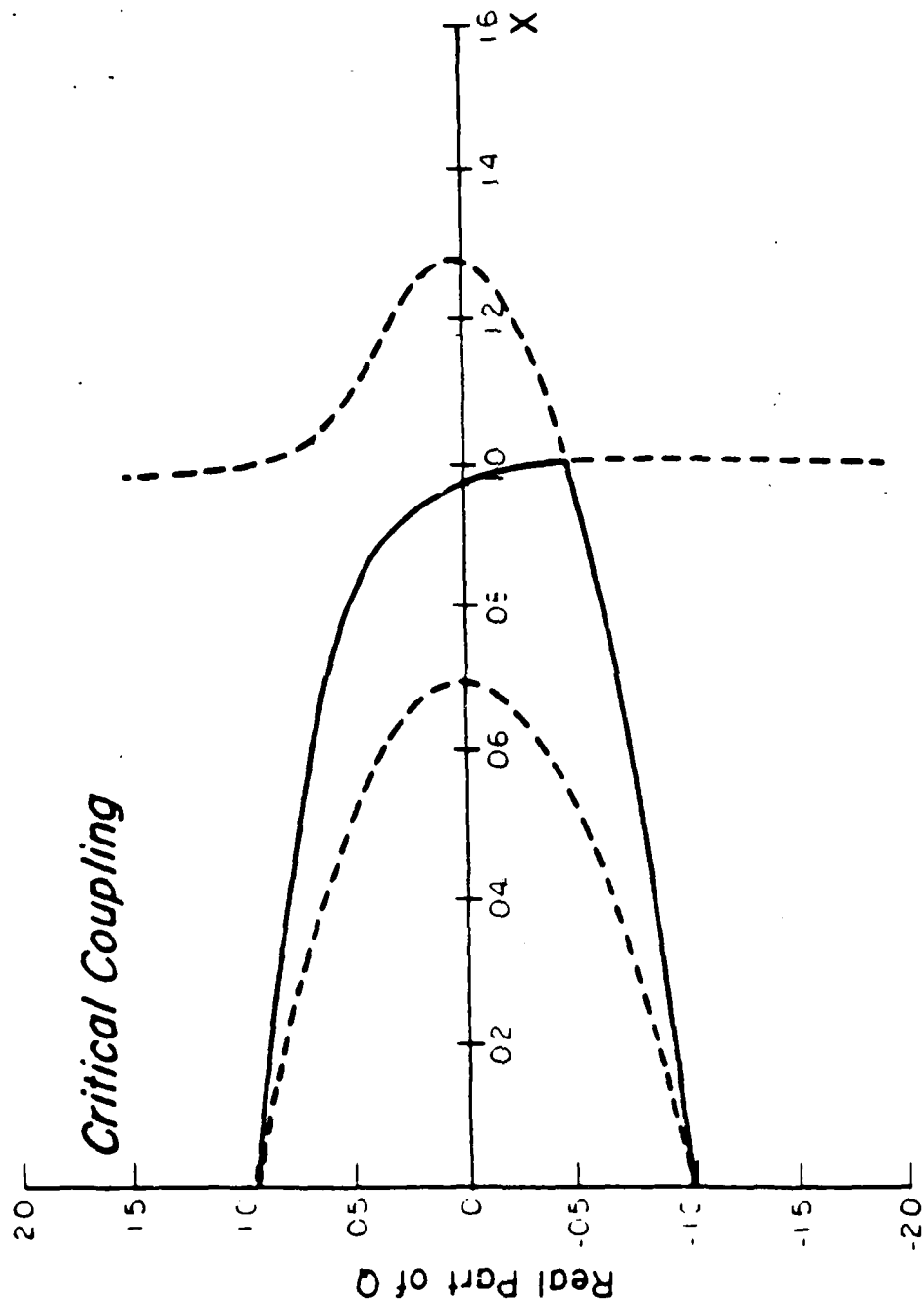

Fig. 2.8 Roots of the Booker quartic for the critical angle of incidence (propagation towards magnetic north)

level. However, this x-wave reflects just above $X = 1$ (rather than at $X = 1 + Y$) and is eventually absorbed in the absorption region near $X = X_R$ [25,28].

Throughout the text, the X_R level is assumed to be the absorption level for the x-wave. This occurs because of the fact that the imaginary part of q becomes large as this level is approached when collisions are present. Therefore, in this region propagation over a small height range will result in absorption of large amounts of energy by conversion to heat. For high power radio waves, this heating may significantly modify the plasma.

An important related equation is what happens to the flow of energy of an x-wave near the X_R level when there is no physical mechanism for absorption? This happens when there are no collisions, in which the non-evanescent imaginary part of q is always zero throughout the magnetoionic medium. It has been found that as the x-wave approaches the X_R level, the direction of energy flow becomes horizontal. This phenomenon is true both with and without collisions, provided the collision frequency is not very great [42,43].

Blachier and Bouchet computed ray paths or equivalently the direction of energy flow in the magnetic meridian for the two critical angles of incidence [42,43]. According to their results, coupled x-mode rays turn towards the south and propagate horizontally as they approach the X_R level. Figure 2.9 shows these ray paths for both critical incidence angles $\pm \theta_c$ (indicated by the dashed lines) along with several other ray paths at different angles. Additional information on this subject is given by Ginzburg [28].

2.8 - DIFFERENTIAL EQUATIONS GOVERNING RADIO-WAVE PROPAGATION IN THE IONOSPHERE

The differential equations governing radio wave propagation in the ionosphere are found by combining Maxwell's curl equations

$$\nabla \times E = ik H$$

$$\nabla \times H = \frac{ik}{\varepsilon_o} D \qquad (2.40)$$

with the constitutive relations

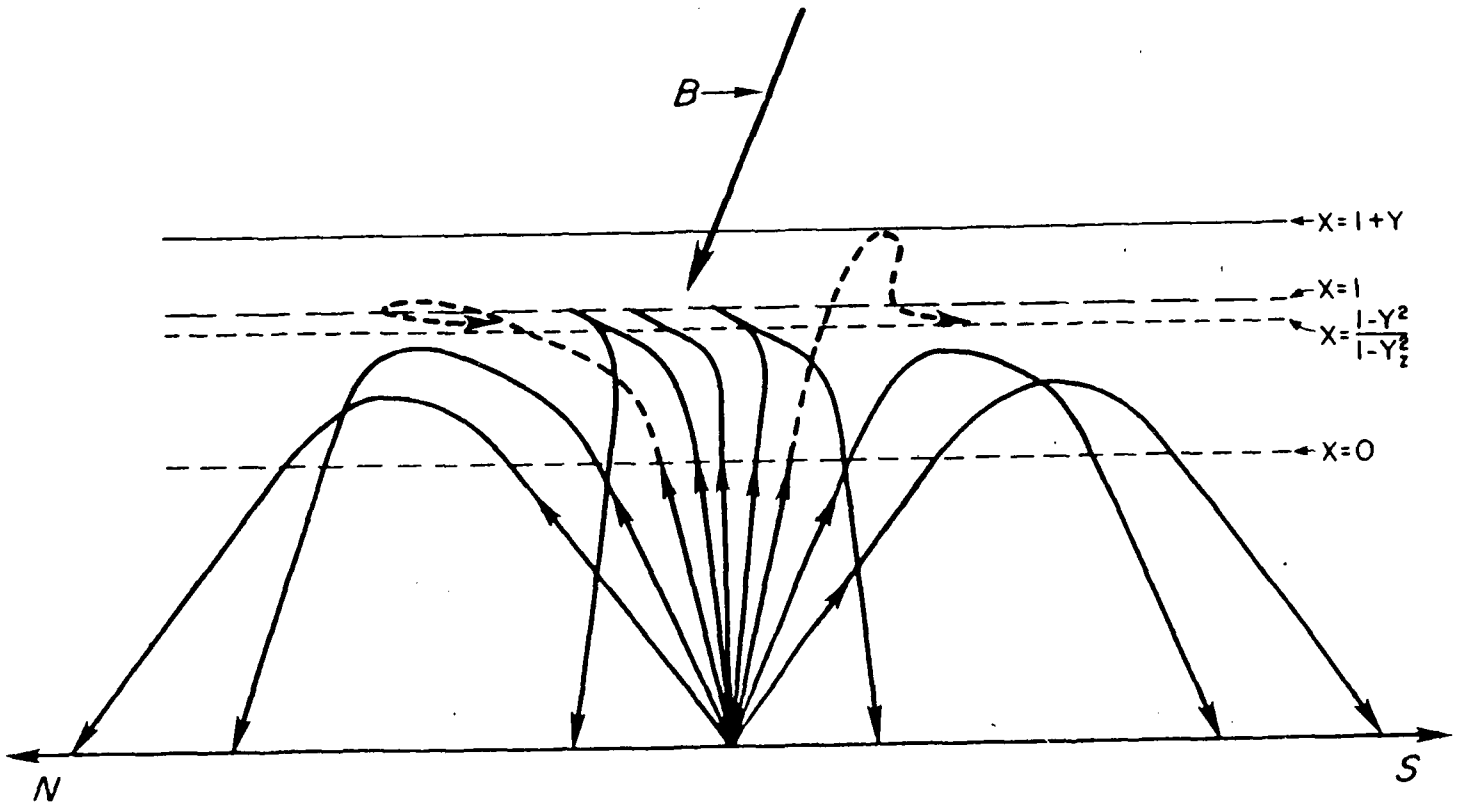

Fig. 2.9 Ray paths in the magnetic meridian; Critical coupling rays are indicated by dashed lines [42,43]

$$\vec{P} - \epsilon_0 M \vec{E} \qquad (2.41)$$

The x-z plane is chosen to be the plane of incidence, and plasma stratification is assumed to be in the z-direction. The incident plane wave is taken to be inclined at an angle θ from the z-axis. The inhomogenous medium may be thought of as being made up of a very large number of discrete strata in each of which the electron density and the collision frequency are constant, that is, homogenous. Then, in each strata the field quantities vary with x as $\exp\{ikx\sin\theta\}$ and do not vary with y, thus the differential operators

$\frac{\partial}{\partial X}$, $\frac{\partial}{\partial Y}$, $\frac{\partial}{\partial Z}$ are equivalent to $-ik\sin\theta$, 0, d/dz. If the factor $\exp\{ikx\sin\theta\}$ is dropped as was done with $\exp\{i\omega t\}$, the equations are functions of z only and the problem becomes one dimensional.

Combining Maxwell's curl equations with the constitutive relations and eliminating E_z and H_z results in four simultaneous linear differential equations of first order with E_x, E_y, H_x, H_y as dependent variables [45,32].

$$\frac{d}{dz} E_x = ik\left\{-H_y + \frac{\sin\theta}{I+M_{zz}} (\sin\theta H_y + M_{zx}E_x + M_{zy}E_y)\right\}$$

$$\frac{d}{dz} E_y = ik\, H_x$$

$$\frac{d}{dz} H_x = ik\left\{M_{yx}E_x + (I+M_{yy})E_y - \frac{M_{yz}}{I+M_{zz}} (\sin\theta H_y - M_{zx}E_x + M_{zy}E_y) - \sin^2\theta E_y\right. \qquad (2.41)$$

$$\frac{d}{dz} H_y = ik\left\{-(I-M_{xx})E_x - M_{xy}E_y - \frac{M_{xz}}{I+M_{zz}} (\sin\theta H_y + M_{zx}E_x + M_{zy}E_y)\right\}$$

E_z and H_z are given as

$$E_z = \frac{-I}{I+M_{zz}} \left\{\sin\theta\ y + M_{zx}E_x + M_{zy}E_y\right\} \qquad (2.42)$$

$$H_z = \sin\theta\ E_y$$

In general, in an homogenous medium these four simultaneous linear differential equations result in four independent solutions for the field quantities E_x, E_y, H_x, H_y. These four independent solutions correspond to the upgoing ordinary, downgoing ordinary, upgoing extraordinary and downgoing extraordinary waves, propagating independently. Under most

circumstances, separation of the wave fields in this manner is also applicable in inhomogenous media. Exceptions to this occur at the levels of reflection and/or coupling where the independence of the solutions are lost.

Eqs. 2.41 may be written in matrix form as:

$$\frac{d}{dz}\,(\underline{e}) = ikT\,(\underline{e}) \tag{2.43}$$

where $\underline{e}$ is a 4 x 1 column vector

$$\underline{e} = (E_x\ E_y\ H_x\ H_y)^T \tag{2.44}$$

and T is a 4 x 4 matrix given by

$$\begin{matrix}
\frac{\sin\theta M_{zx}}{1 + M_{zz}} & \frac{\sin_1 M_{zy}}{1 + M_{zz}} & 0 & \frac{-(\cos^2_1 + M_{zz})}{1 + M_{zz}} \\
0 & 0 & 1 & 0 \\
M_{yx} - \frac{M_{yz}M_{zx}}{1 + M_{zz}} & \cos^2\theta + M_{yy} - \frac{M_{yz}M_{zy}}{1 + M_{zz}} & 0 & \frac{-\sin\theta M_{yz}}{1 + M_{zz}} \\
\frac{M_{xz}\cdot_{zx}}{1 + M_{zz}} - (M_{xx}+1) & \frac{M_{xz}M_{zy}}{1 + M_{zz}} & 0 & \frac{\sin_2 M_{xz}}{1 + M_{zz}}
\end{matrix} \tag{2.45}$$

In each stratum the field components depend on z only through the factor exp{-ikqz} which gives $\frac{d}{dz} \equiv -ikq$. Eq. 2.43 then can be written as

$$T\underline{e} = -q\underline{e} \tag{2.46}$$

The nontrivial solutions for q are the eigenvalues of the T matrix or, equivalently, the solution to Eq. 2.47

$$\det(T+qI) = 0 \tag{2.47}$$

which is another form of the Booker quartic. Expanding the determinant gives the coefficients of the quartic

$$\alpha = 1$$

$$\beta = T_{11} + T_{44}$$

$$\gamma = T_{11}T_{44} - T_{14}T_{41} + T_{32}$$

$$\delta = -T_{32}(T_{11} + T_{44}) + T_{34}T_{42} + T_{12}T_{31}$$

$$\varepsilon = T_{11}(T_{34}T_{42} - T_{44}T_{32}) + T_{12}(T_{31}T_{44} - T_{34}T_{41}) + T_{14}(T_{32}T_{41} - T_{31}T_{42})$$

For each eigenvalue there is an eigenvector $\underline{e}_i$ which satisfies the equation

$$(T + q_i I)\, \underline{e}_i = 0 \qquad i = 1, 2, 3, 4 \qquad (2.49)$$

The elements of $\underline{e}_i$ are proportional to the field quantities E_x, E_y, H_x, H_y of the i-th wave component and define the polarization state of the i-th wave.

2.9 - FULL WAVE SOLUTION TECHNIQUE

There are several approximate solutions available for finding the field components in the ionosphere [26, 28]. The W.K.B. solutions of the form

$$F = F_0(z) \exp\{-ik \int^z q\, dz\} \qquad (2.50)$$

are considered to be a good approximation for many ionospheric applications. These solutions fail to represent the true field components when they lose their independence. The regions where they lose their independence occur near the reflection and coupling levels where two or more of the quartic roots become equal. Also, the medium must be slowly varying so that the refractive indices do not change significantly within one local wavelength.

Since this study is concerned with the regions where reflection and coupling occur, the W.K.B.

solutions are not considered. Rather, the exact solution of the field components is required necessitating use of the full wave solution technique.

The full wave problem is to find the exact solution to the differential Eqs. 2.41 either analytically or numerically. Analytical solutions are limited to special kinds of electron density profiles and magnetic field conditions [26]. Numerical solutions, on the other hand, are more general and are therefore used here [32,44].

The differential equations 2.41 have four sets of independent solutions and require four sets of boundary conditions for their complete solution. At the bottom level where the transmitter is located the upgoing incident wave, which gives two of the boundary conditions, is assumed to be known. However, the other two resulting from downgoing waves are not known, which implies that boundary conditions at the bottom level are insufficient. Above the highest reflection level only upgoing waves, which supply the other two boundary conditions, can exist. Here upgoing waves are defined to be waves travelling in the positive z-direction, or are evanescent with decreasing amplitudes in the positive z-direction. The downgoing wave components

above the highest reflection level must be zero; this completes the required four boundary conditions. Two sets of solutions are obtained from these upper boundary conditions by separately integrating them down through the ionospheric model. Since these two solutions are independent, the total wave field is then a linear combination of them. The coefficients relating the two solutions to the total wave field is found by extracting their upgoing components and matching them to the known incident wave at the bottom level where the integration is ended.

2.10 - DERIVING THE BOUNDARY CONDITIONS

At the highest level where integration is started the initial values of the upgoing field components E_x, E_y, H_x, H_y are required as boundary conditions. The medium above the highest level is considered homogenous so that the field quantities vary with z as -ikq as before. Substituting this into the Eqs. 2.41 gives the wave polarizations for each field component [32]

$$E_x = \frac{-M_{xy}(\cos^2\theta+M_{zz})+M_{zy}(q\sin\theta+M_{xz})}{(1-q^2+M_{xx})(\cos^2\theta+M_{zz})-(q\sin\theta+M_{zx})(q\sin\theta+M_{xz})} E_y \quad (2.51)$$

$$H_x = -q\, E_y$$

$$H_y = \frac{E_x\{q(1+M_{zz})+\sin\theta M_{zx}\} + E_y\{\sin M_{zy}\}}{M_{zz} + \cos^2\theta}$$

$$E_z = \frac{-1}{I+M_{zz}} (\sin\theta H_y + M_{zx}E_x + M_{zy}) \qquad (2.52)$$

$$H_z = \sin\theta E_y$$

The two boundary conditions correspond to the quartic roots with negative imaginary parts which denote upgoing waves. Solving the quartic and substituting appropriate roots into Eq. 2.51 results in two sets of initial solutions.

$$\underline{e}_1 = (E^1_x\ E^1_y\ H^1_x\ H^1_y)^T \qquad (2.53)$$

$$\underline{e}_2 = (E^2_x\ E^2_y\ H^2_x\ H^2_y)^T \qquad (2.54)$$

2.11 - INTEGRATION

Numerical integration is done by the fourth-order Runge-Kutta method. Integration starts with initial solutions (1) and (2) at the maximum height and proceeds downwards in the medium with h meter decrements. At selected intervals of h, solutions (1) and (2) are stored; they will be used later to

reconstruct the total field components by forming their appropriate linear combination. The Runge-Kutta scheme is outlined below.

The simultaneous differential equations can be represented as

$$y'_i = f_i (y_1, y_2, y_3, y_4, z) \qquad i = 1, , 3, 4 \tag{2.55}$$

where

$$y_1 = E_x \qquad y_2 = E_y \qquad y_3 = H_x \qquad y_4 = H_y \tag{2.56}$$

Then the integration coefficients become

$$k_{i0} = -h\, f_i\,(y_1,\ y_2,\ y_3,\ y_4,\ z)$$

$$k_{i1} = -h\, f_i\,(y_1+1/2k_{10},\ y_2+1/2k_{20},\ y_3+1/2k_{30},\ y_4+1/2k_{40},\ z-1/2h)$$

$$k_{i2} = -h\, f_i\,(y_1+1/2k_{11},\ y_2+1/2k_{21},\ y_3+1/2k_{31},\ y_4+1/2k_{41},\ z-1/2h)$$

$$k_{i3} = -h\, f_i\,(y_1+1/2k_{12},\ y_2+1/2k_{22},\ y_3+1/2k_{32},\ y_4+1/2k_{42},\ z-1/2h)$$

$$k_{i4} = -h\, f_i\,(y_1+k_{13},\ y_2+k_{23},\ y_3+k_{33},\ y_4+k_{43},\ z-h)$$

$$y_i(z-h) = y_i(z) + \frac{1}{6}\,(k_{i0} + 2k_{i1} + 2k_{i2} + k_{i3})$$

2.12 - NUMERICAL SWAMPING

It has been observed that during integration numerical swamping might cause problems because of the limited accuracy of the computations. For example, at the beginning of integration when the initial solutions are calculated, or during integration, numerical errors such as roundoff may introduce a small fraction of an evanescent wave into the travelling wave solution. This evanescent wave, which is very insignificant at the beginning, may eventually dominate the travelling solution and lead to incorrect results.

Several methods have been devised to overcome this problem. One method is to change dependent variables

and transform the differential Eq. 2.43 to a different form. Instead of E_x, E_y, $_x$, $_y$, four elements of the admittance matrix A may be used [40]

$$A = \begin{pmatrix} E^1_x & E^2_x \\ H^1_x & H^2_x \end{pmatrix} \begin{pmatrix} H^1_y & H^2_y \\ -E^1_y & -E^2_y \end{pmatrix}^{-1} \qquad (2.58)$$

Alternatively, elements of the variable ρ are also possible [40]

$$\rho = (A - I)(A + I)^{-1} \qquad (2.59)$$

Since solutions (1) and (21) are both contained in the wave admittance matrix A, these two methods require only one integration. However, they yield only the ratios of field components rather than the true field amplitudes, and are employed primarily for calculating reflection coefficients. If the field variation with height is required, the choice of independent variables must in each case yield E_x, E_y, H_x, H_y and the differential Eq. 2.43 must retain their original form.

The numerical swamping problem has been overcome by a different method suggested by Pitteway [44]. The

method is based on constraining solutions at regular intervals during integration and forcing them to remain independent. This is accomplished by adding a fraction of one solution to the other one. This is possible because the differential equations are linear. In practice, these modifications are recorded along with the field components during integration and can be accounted for later, during the reconstruction of the total field.

The fraction of one solution added to the other solution must satisfy certain conditions. Let $\underline{e}_2$ represent the solution to be constrained

$$\underline{e}_2 = (E^2_x \; E^2_y \; H^2_x \; H^2_y)^T \tag{2.60}$$

and $\underline{e}'_2$ the solution to replace $\underline{e}_2$

$$\underline{e}'_2 = \underline{e}_2 + \alpha \underline{e}_1 \tag{2.61}$$

where α is a complex constant such that $\underline{e}'_2$ is Hermitian orthogonal to $\underline{e}_1$. That is, the dot product

$$\underline{e}'_2 \cdot \underline{e}^*_1 = 0 \tag{2.62}$$

where * denotes the complex conjugate. This requires that

$$\alpha = - \frac{\underline{e}^* \cdot \underline{e}_2}{\underline{e}^*_1 \cdot \underline{e}_1} \tag{2.63}$$

2.13 - MATCHING SOLUTIONS TO THE INCIDENT WAVE

Below the ionosphere where the medium is assumed to be homogenous, the known incident wave must be matched to the upgoing wave components of both solutions through an appropriate linear combination. If the incident wave components are E_x^{inc}, E_y^{inc} and the upgoing field solutions are E_x^1, E_y^1, E_x^2, E_y^2, then

$$E_x^{inc} = \alpha E^1_x + \beta E^2_x \tag{2.64}$$

$$E_y^{inc} = \alpha E^1_y + \beta E^2_y \tag{2.65}$$

Solving for α and β gives

$$\alpha = \frac{E_x^{inc} E^2_y - E_y^{inc} E^2_x}{E^1_x E^2_y - E^1_y E^2_x} \tag{2.66}$$

$$\beta = \frac{E_y^{inc} E^1_x - E_x^{inc} E^1_y}{E^1_x E^2_y - E^1_y E^2_x} \tag{2.67}$$

Another method of matching exists when the incident wave has only o- or x-wave polarization. Let $E_{y,o}^{inc}$, $E_{y,x}^{inc}$ denote the o- and x-wave components, respectively. Then,

$$E_{y,o}^{inc} = \alpha E^1_{y,o} + \beta E^2_{y,o} \tag{2.68}$$

$$E_{y,x}^{inc} = \alpha E^1_{y,x} + \beta E^2_{y,x} \tag{2.69}$$

If there is only an upgoing o-wave, then $E_{y,x}^{inc} = 0$ and the coefficients α and β become

$$\alpha = -\beta \frac{E^2_{y,x}}{E^1_{y,x}} \tag{2.70}$$

$$\beta = \frac{E_{y,o}^{inc} E^1_{y,x}}{E^2_{y,o} E^1_{y,x} - E^2_{y,o} E^1_{y,x}} \tag{2.71}$$

The coefficients for the x-wave can be derived in a similar manner.

After the coefficients α and β are determined, the total fields anywhere in the ionosphere can be found by taking the linear combination of the two solutions which were stored during integration.

2.14 - DECOMPOSING TOTAL FIELD COMPONENTS IN THE LOWER BOUNDARY

The full wave solution technique gives the total fields. One would also want to know the upgoing and downgoing o- and x-wave fields for determining the reflection properties of the ionospheric model. Decomposing the total fields into their magnetoionic modes in an homogenous medium is possible using the method described below.

Let subscripts i=1,2,3,4 refer to the upgoing o-, downgoing o-, upgoing x-, downgoing x-waves, respectively. The total field may then be written as a sum of these four waves such that

$$\vec{E} \sum \vec{E}_i \tag{2.72}$$

$$\vec{H} \sum \vec{H}_i \tag{2.73}$$

where only the total fields $\vec{E}$ and $\vec{H}$ are known. These equations may be written in terms of the polarization states ρ of each wave component (Eqs. 2.75-2.76) where ρ's are defined as

$$\rho_{1i} = E_{xi}/E_{yi} \qquad \rho_{\omega i} = E_{yi}/E_{yi} \qquad \rho_{3i} = H_{xi}/E_{yi}$$

$$\rho_{4i} = H_{yi}/E_{yi} \qquad \rho_{5i} = E_{zi}/E_{yi} \qquad \rho_{6i} = H_{zi}/E_{yi} \tag{2.74}$$

$$\begin{bmatrix} E_x \\ E_y \\ H_x \\ H_y \end{bmatrix} = \begin{bmatrix} \rho_{11} & \rho_{12} & \rho_{13} & \rho_{14} \\ 1 & 1 & 1 & 1 \\ \rho_{31} & \rho_{32} & \rho_{33} & \rho_{34} \\ \rho_{41} & \rho_{42} & \rho_{43} & \rho_{44} \end{bmatrix} \begin{bmatrix} E_{y1} \\ E_{y2} \\ E_{y3} \\ E_{y4} \end{bmatrix} \tag{2.75}$$

$$\begin{bmatrix} E_z \\ H_z \end{bmatrix} = \begin{bmatrix} \rho_{51} & \rho_{52} & \rho_{53} & \rho_{54} \\ \rho_{61} & \rho_{62} & \rho_{63} & \rho_{64} \end{bmatrix} \begin{bmatrix} E_{y1} \\ E_{y2} \\ E_{y3} \\ E_{y4} \end{bmatrix} \tag{2.76}$$

Each polarization state ρ is determined from Eqs. 2.51-2.52 with its respective root q. Now, the total fields $(E_x\ E_y\ H_x\ H_y)^T$ on the left of Eq. 2.75 and the 4 x 4 polarization matrix are known. Solving Eq. 2.75 for $(E_{y1}\ E_{y2}\ E_{y3}\ E_{y4})^T$ gives the upgoing o-, downgoing o-, upgoing x-, downgoing x-wave components of E_y, respectively. The other cartesian components may then be found from

$$
\begin{aligned}
E_{xi} &= \rho_{1i} E_{yi} \\
H_{xi} &= \rho_{3i} E_{yi} \\
H_{yi} &= \rho_{4i} E_{yi} \\
E_{zi} &= \rho_{5i} E_{yi} \\
H_{zi} &= \rho_{6i} E_{yi}
\end{aligned}
\qquad (2.77)
$$

$$(i = 1, 2, 3, 4)$$

CHAPTER 3

MODEL COMPUTATIONS

In this chapter field solutions for simple ionospheric models are performed using the full wave solution program developed by Seliga [32]. The solutions give the wave fields for an incident o-wave for different electron density profiles, collision frequencies and angles of incidence. With the aid of the corresponding Booker quartic solutions, the behavior of electromagnetic waves in the plasma are determined. The reflection coefficients for several propagation directions are also calculated to determine the shape and angular width of the radio windows. The results demonstrate the importance of o- to x-mode wave coupling which occurs when propagation is near the critical angle in the magnetic meridian.

3.1 - PARAMETERS OF THE IONOSPHERIC MODEL

Three different models are chosen which approximate the increasing electron density of the F region of the ionosphere.

Electron Density Profile:

Each profile has a linearly increasing electron density with height given by the equation

$$N(z) = N_B + N_S \left(\frac{z}{H}\right) \qquad (3.1)$$

where $N_B(m^{-3})$ is the initial electron density at the reference height

$z = 0$

N_S/H (m^{-4}) is the rate of change of electrons density with height

z (m) is the height relative to the reference level.

The three models chosen are shown in Table 3.1

Table 3.1 - Parameters of the selected ionospheric models

	Model 1	Model 2 & 3
N_B (m^{-3})	1.8×10^{11}	1.8×10^{11}
N_S (m^{-3})	2.7×10^{11}	2.7×10^{11}
H (m)	10^4	10^3

Frequency:

All computations are performed at a wave frequency f = 5 MHz

Collision Frequency:

A constant collision frequency is used throughout the medium. For each model, $\nu_m << |\omega - \omega_H|$ so that the effective collision frequency ν_e is given by Eq. 2.19. Table 3.2 gives the collision frequency values for each model.

Table 3.2 - Collision frequencies for the ionospheric models

	Model 1	Model 2	Model 3
ν_m (s^{-1})	10^3	10^3	200
ν_e (s^{-1})	2.5×10^3	$2,5 \times 10^3$	500

Geomagnetic Field:

The geomagnetic field conditions at Platteville, Colorado (Fig. 3.1) are chosen, since a major heating facility was located there and much experimental data exists at this location.

Flux Density B_o: 5.64260×10^{-5} Wbm^{-2}

Magnetic Dip θ_B: 67.74

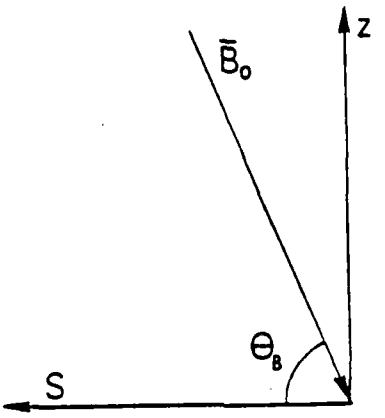

Fig. 3.1 Geomagnetic field conditions at Platteville, Colorado

Using Eq. 2.11 one obtains

f_H = 1.58 MHz

Y = 0.316

Based on these parameters, the X = 1, 1 + Y, 1 - Y and X_R levels occur at heights listed in Table 3.3.

Table 3.3 - Critical level heights for the ionospheric models

	Model 1	Models 2 & 3
$X = 1$	4818 m.	481.8 m.
$X = 1 + Y$	8447 m.	844.7 m.
$X = 1 - Y$	1190 m.	119.0 m.
$X = X_R$	4639 m.	463.9 m.

Critical Angle of Incidence:

The critical coupling angles for each model are same

$$\theta_c = \pm 10.696°$$

3.2 - PARAMETERS OF THE FULL WAVE SOLUTION PROGRAM

Cartesian components of the E and H fields are outputted by the full wave solution program. Field magnitudes are relative to the incident wave amplitude. Note that since propagation is in the x-z plane, E_y and H_y are the components perpendicular to the plane of propagation.

Integration Increment:

The integration increment h is determined by a computational procedure. Three arbitrary angles are chosen for each model, one in the S-N direction near the critical coupling angle, one in the vertical direction and one in the N-S direction near the critical coupling angle. For each of these angles the program is run several times, each with decreasing integration increments until the reflection coefficients and fields converge. Then the program is run for the rest of the angles using the resulting integration increment. Table 3.4 shows the integration increments used for the models.

Table 3.4 - Integration increments used for each ionospheric model

Model 3	10^3 m.	200 s^{-1}	0	10^3 m.	0.02 m.
Model 2	10^3 m.	10^3 s^{-1}	0	10^3 m.	0.1 m.
Model 1 (N-S)	10^4 m.	10^3 s^{-1}	10^3	6×10^3 m.	0.05 m.
Model 1 (S-N)	10^4 m.	10^3 s^{-1}	10^3	9×10^3 m.	0.05 m.

Hermitian Orthogonal Constraint:

Constraining of the solutions is done at every 20 to 50 integration steps, depending on the storage requirements of the computer program.

Computation Time:

The program was run on an IBM 3081 with the VS FORTRAN compiler. The average run times for the models are given in Table 3.5

Table 3.5 - Average execution times for the ionospheric models

	Execution Time	Number of Angles	Total Time
Model 1 (S-N)	9 min/angle	22	198 min.
Model 1 (N-S)	6 min/angle	22	132 min.
Model 2	1 min/angle	60	60 min.
Model 3	3 in/angle	60	180 min.

3.3 - INTERPRETATION OF THE RESULTS

In this section the field solutions for Model 1 at $\theta = 0$ and $\theta = \pm \theta_c$ in the magnetic meridian are presented along with the corresponding roots of the Booker quartic. The levels $X = 1$, $1 + Y$, $1 - Y$, X_R are indicated on the full wave solutions as vertical lines numbered 1, 2, 3, 4, respectively. On top of the

figures are the parameters of the ionospheric model, including N_B, N_S, H, ν_m which are denoted by CON(1), CON(2), CON(4), CON(5), respectively. The solutions for other models and magnetic fields are given in Appendix A.

Case 1: Model 1, Vertical incidence ($\theta = 0$)

Figures 3.2, 3.3 and 3.4 show the E_x, E_y, E_z components of the vertical incidence solution, respectively. The upgoing incident wave has ordinary polarization. The standing waves below X = 1 are due to interference between the incident upgoing o-wave and reflected o-wave. The reflection coefficients for E and H are

$$R(E) = 0.889$$

$$R(H) = 0.889$$

which indicate that most of the incident energy is reflected back at vertical incidence.

The roots of the Booker quartic are useful for understanding the observed reflection mechanism. Figs. 3.5-3.6 show the real and imaginary parts of the roots. The roots corresponding to the upgoing o-wave and

Wave Frequency	: 5.0	E 6	Angle of Incidence	: 0.000	E 0
Magnetic Y Vector	: 3.150	E-1	Con (1)	: 2.700	E 11
Tot. Geomag. Field	: 5.643	E-5	Con (2)	: 1.800	E 11
X-Dir Cosine of Y	:-3.789	E-1	Con (3)	: 0.000	E 0
Y-Dir Cosine of Y	: 0.000	E-0	Con (4)	: 1.000	E 4
Z-Dir Cosine of Y	: 9.255	E-1	Con (5)	: 1.000	E 3

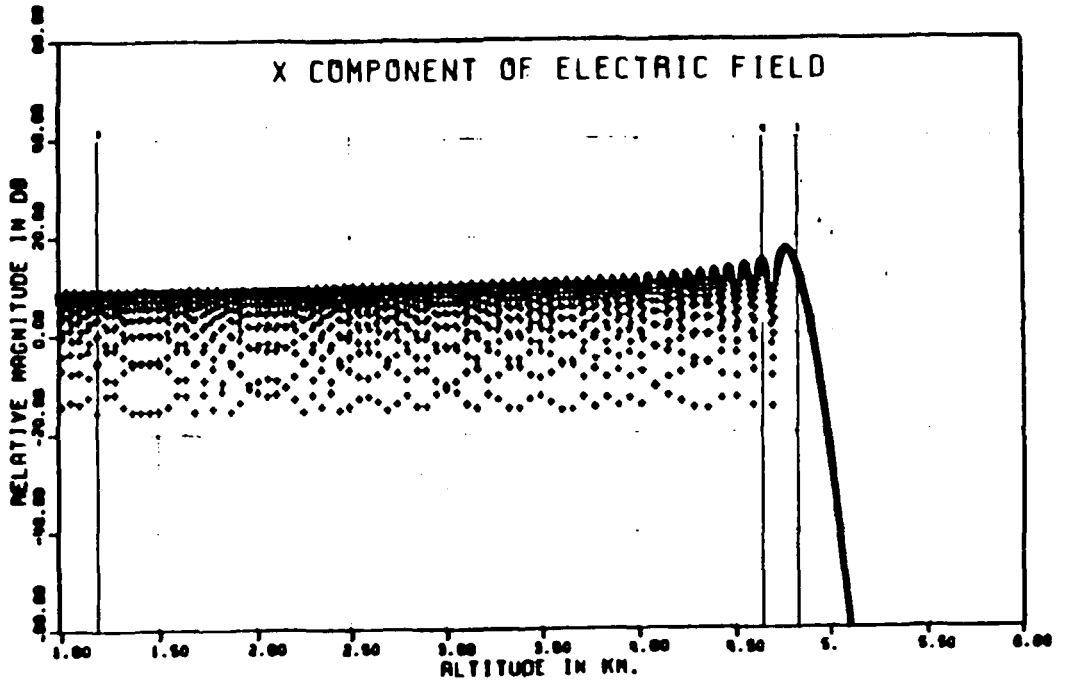

Fig. 3.2 x-component of electric field intensity; vertical incidence case

Wave Frequency	: 5.0	E 6	Angle of Incidence	: 0.000	E 0
Magnetic Y Vector	: 3.150	E-1	Con (1)	: 2.700	E 11
Tot. Geomag. Field	: 5.643	E-5	Con (2)	: 1.800	E 11
X-Dir Cosine of Y	:-3.789	E-1	Con (3)	: 0.000	E 0
Y-Dir Cosine of Y	: 0.000	E-0	Con (4)	: 1.000	E 4
Z-Dir Cosine of Y	: 9.255	E-1	Con (5)	: 1.000	E 3

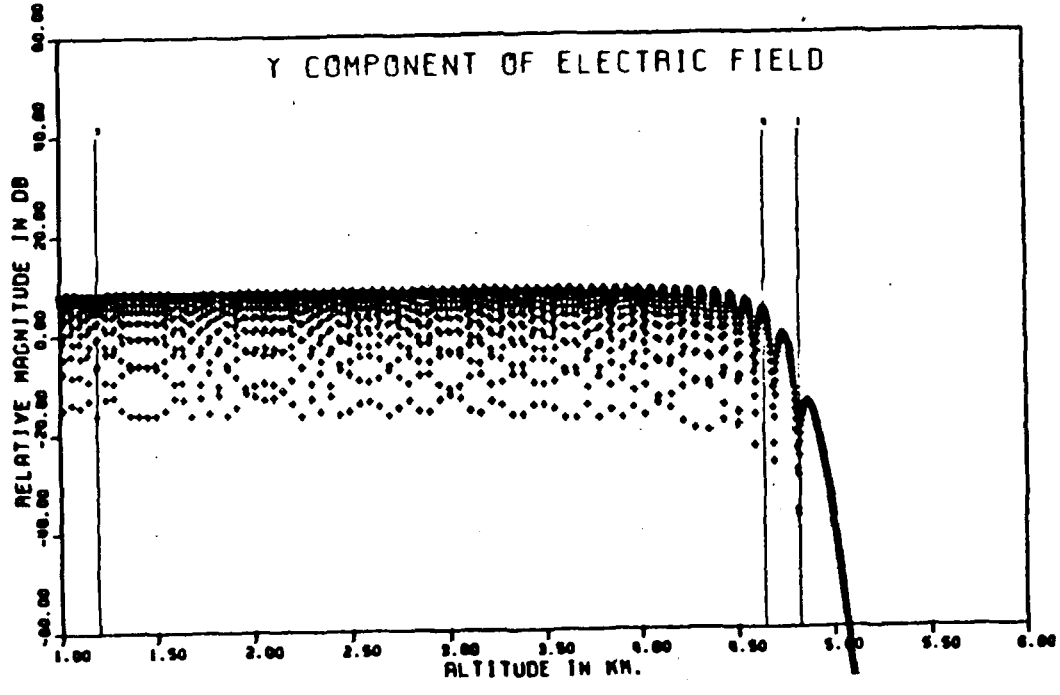

Fig. 3.3 y-component of electric field intensity; vertical incidence case

Wave Frequency	: 5.0	E 6	Angle of Incidence	: 0.000	E 0
Magnetic Y Vector	: 3.150	E-1	Con (1)	: 2.700	E 11
Tot. Geomag. Field	: 5.643	E-5	Con (2)	: 1.800	E 11
X-Dir Cosine of Y	:-3.789	E-1	Con (3)	: 0.000	E 0
Y-Dir Cosine of Y	: 0.000	E-0	Con (4)	: 1.000	E 4
Z-Dir Cosine of Y	: 9.255	E-1	Con (5)	: 1.000	E 3

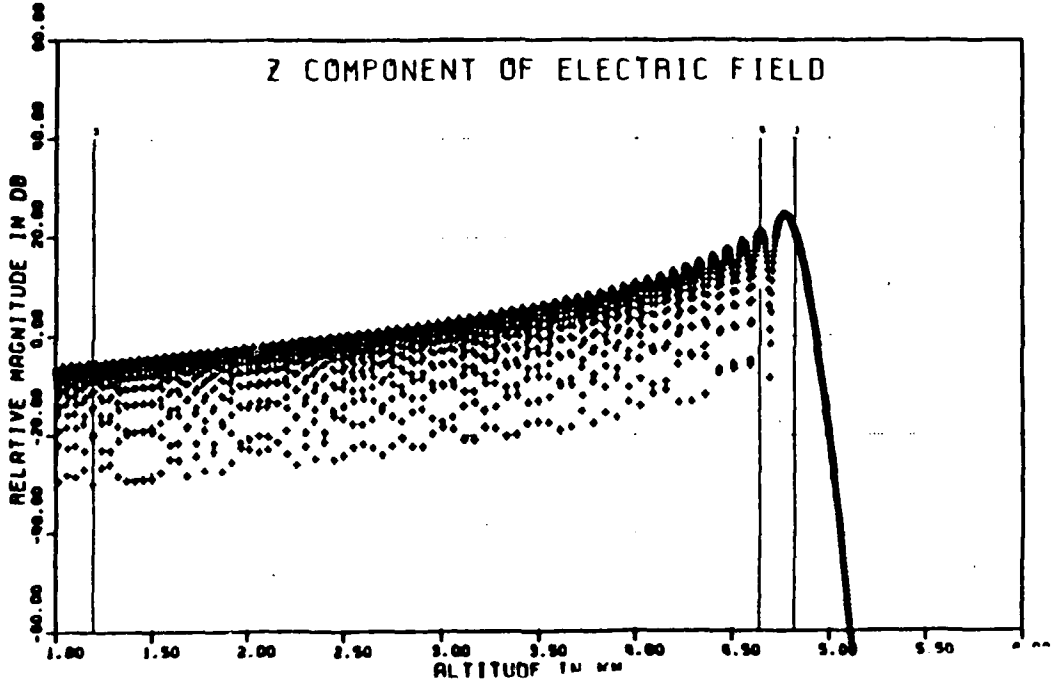

Fig. 3.4 z-component of electric field intensity; vertical incidence case

Solution Increment	: 0.005000	Critical Coupling Angle	: 10.70086
Wave Frequency	: 5.00000E+06	X-Direction Cosine of Y	: - 3.78972E-01
Angle of Incidence	: 0.00000E+00	Y-Direction Cosine of Y	: 0.00000E+00
Geomagnetic Field	: 5.64260E-05	Z-Direction Cosine of Y	: 9.25408E-01
Magnetic Y Vector	: 3.15898E-01	Collision Frequency	: 1.00000E+03
Electron Gyrofreq	: 1.57949E+06	Resonance Condition	: 0.964328

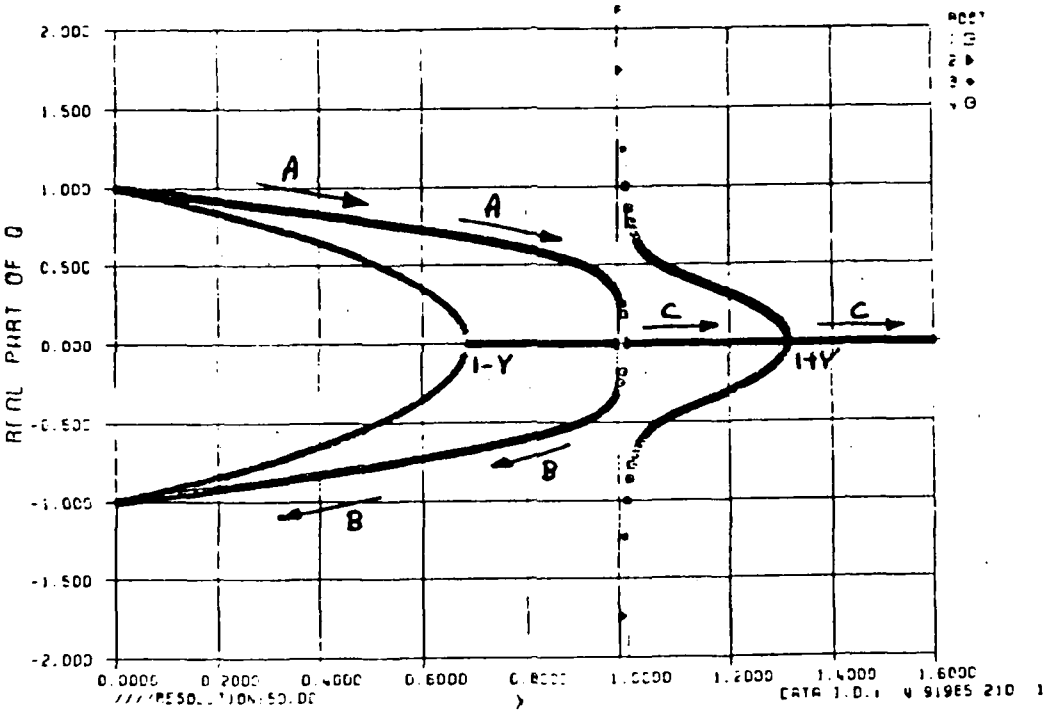

Fig. 3.5 Real part of q; vertical incidence case

Solution Increment	: 0.005000	Critical Coupling Angle	: 10.70086
Wave Frequency	: 5.00000E+06	X-Direction Cosine of Y	: - 3.78972E-01
Angle of Incidence	: 0.00000E+00	Y-Direction Cosine of Y	: 0.00000E+00
Geomagnetic Field	: 5.64260E-05	Z-Direction Cosine of Y	: 9.25408E-01
Magnetic Y Vector	: 3.15898E-01	Collision Frequency	: 1.00000E+03
Electron Gyrofreq	: 1.57949E+06	Resonance Condition	: 0.964328

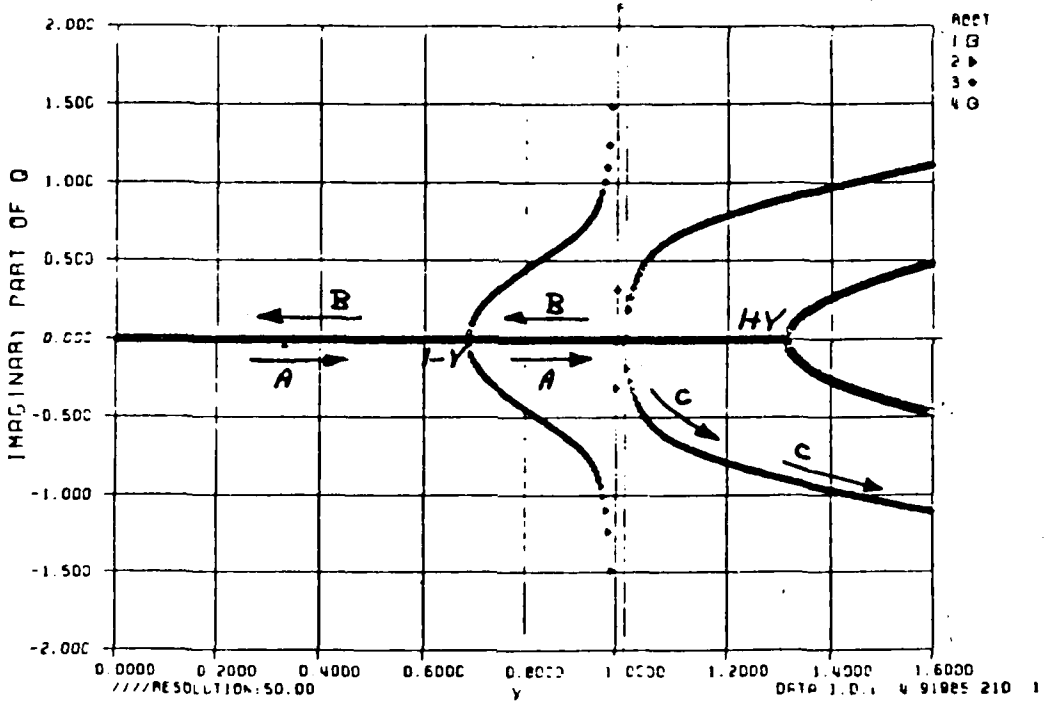

Fig. 3.6 Imaginary part of q; vertical incidence case

downgoing o-wave are denoted by A and B, respectively. The reflection level for the o-wave occurs where the two roots become equal, which is X = 1 in this case. The imaginary part of the roots corresponding to A and B appears to be zero, indicating that there is no energy lost during this process. Actually, q has a small imaginary part. A detailed plot would reveal that Im(q) for A is negative, indicating that direction of energy flow is upwards; Im(q) for B is positive, indicating that direction of energy flow is downwards.

A sketch of the ray path for the vertical incidence case is shown in Fig. 3.7. The rays bend towards the north as the X = 1 level is reached, and become perpendicular to B_o at that level. More detailed information on these ray paths may be found in [26,42,43].

Beyond X = 1, Re(Q) = 0 and Im(q) < 0 for the o-wave as denoted by C in Fig. 3.6. This indicates that the o-wave is evanescent and does not propagate in this region. In the full wave solutions this effect is seen as a sharp decrease of the field amplitudes beyond X = 1.

Another interesting property is the existence of an E_z component, although the propagation vector is in the

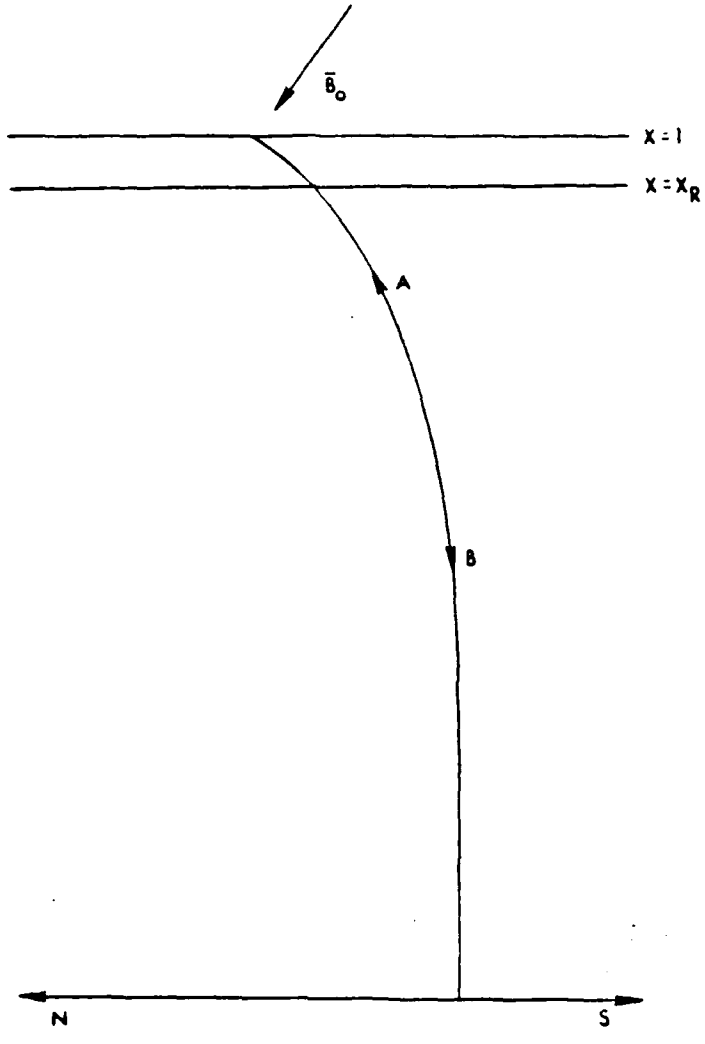

Fig. 3.7 Ray path for the vertical incidence case

z-direction. This is common to anisotropic media. The magnitude of E_z is quite insignificant at the bottom level (Fig. 3.4), but as the waves progress up to the $X = 1$ level it grows larger.

Another observation of interest is the changing wavelength of the fields, decreasing with height. This is in agreement with the roots of the quartic (equal to the refractive index in this case) which indicate that $\eta \to 0$ as $X \to 1$.

Case 2: Model 1, Critical Angle of incidence (S-N): Propagation Towards Magnetic North

Figures 3.8, 3.9 and 3.10 show the E_x, E_y, E_z components of the fields, respectively. The field magnitudes in this case are nearly constant at the bottom level. The absence of any standing wave peaks below X_R indicate the absence of significant reflected downgoing waves. The reflection coefficients for E and H are

$$R(E) = 6.4450 \times 10^{-3}$$

$$R(H) = 6.9295 \times 10^{-3}$$

Wave Frequency	: 5.0	E 6	Angle of Incidence	: 1.070	E 1
Magnetic Y Vector	: 3.150	E-1	Con (1)	: 2.700	E 11
Tot. Geomag. Field	: 5.643	E-5	Con (2)	: 1.800	E 11
X-Dir Cosine of Y	3.789	E-1	Con (3)	: 0.000	E 0
Y-Dir Cosine of Y	: 0.000	E-0	Con (4)	: 1.000	E 4
Z-Dir Cosine of Y	: 9.255	E-1	Con (5)	: 1.000	E 3

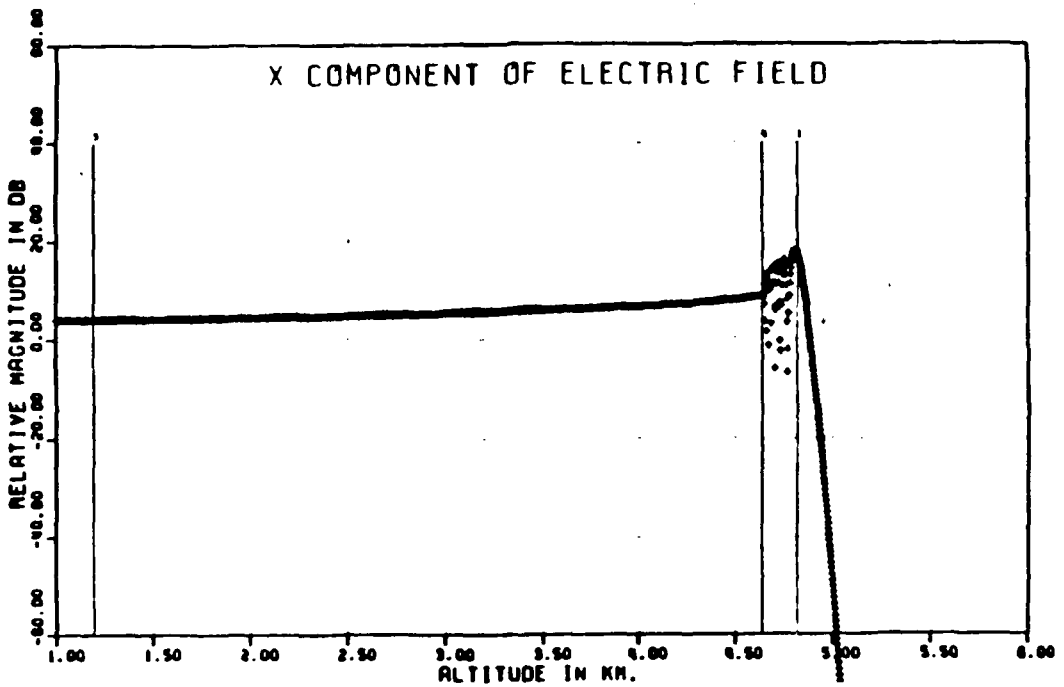

Fig. 3.8 x-component of electric field intensity; critical angle of incidence case (towards magnetic north)

Wave Frequency	: 5.0	E 6	Angle of Incidence	: 1.070	E 1
Magnetic Y Vector	: 3.150	E-1	Con (1)	: 2.700	E 11
Tot. Geomag. Field	: 5.643	E-5	Con (2)	: 1.800	E 11
X-Dir Cosine of Y	:-3.789	E-1	Con (3)	: 0.000	E 0
Y-Dir Cosine of Y	: 0.000	E-0	Con (4)	: 1.000	E 4
Z-Dir Cosine of Y	: 9.255	E-1	Con (5)	: 1.000	E 3

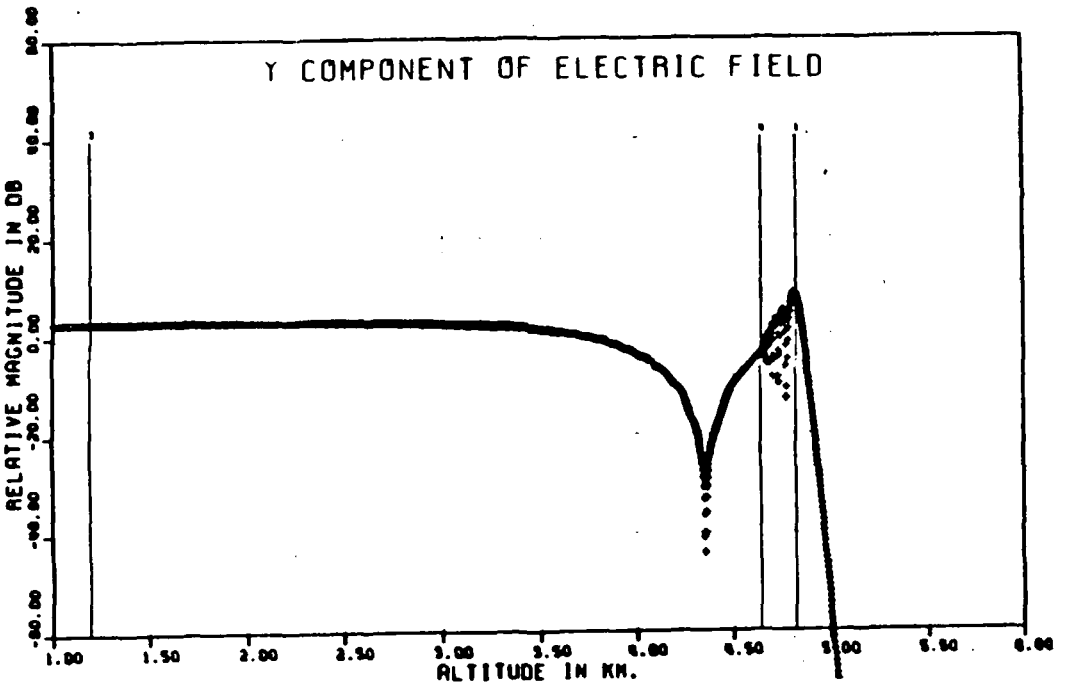

Fig. 3.9 y-component of electric field intensity; critical angle of incidence case (towards magnetic north)

Wave Frequency	: 5.0	E 6	Angle of Incidence	: 1.070	E 1
Magnetic Y Vector	: 3.150	E-1	Con (1)	: 2.700	E 11
Tot. Geomag. Field	: 5.643	E-5	Con (2)	: 1.800	E 11
X-Dir Cosine of Y	:-3.789	E-1	Con (3)	: 0.000	E 0
Y-Dir Cosine of Y	: 0.000	E-0	Con (4)	: 1.000	E 4
Z-Dir Cosine of Y	: 9.255	E-1	Con (5)	: 1.000	E 3

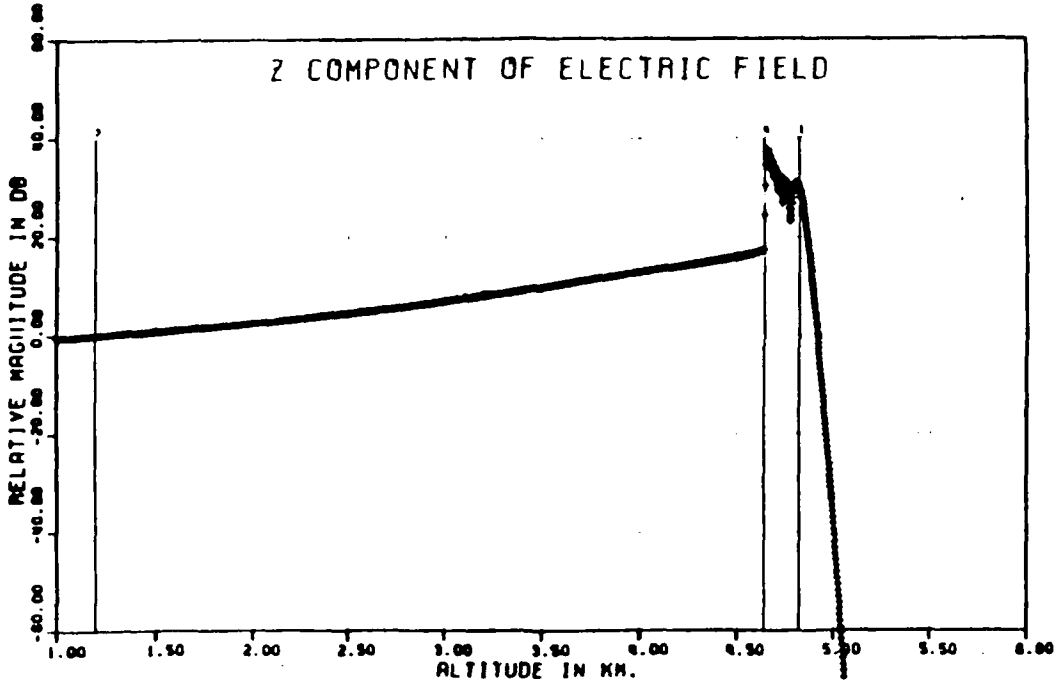

Figure 3.10 z-component of electric field intensity; critical angle of incidence case (towards magnetic north)

which implies that practically all of the incident wave is absorbed in the medium.

Figs. 3.11 and 3.12 show the real and imaginary parts of the Booker quartic roots. The upgoing o-wave path is denoted by A. Unlike the vertical incidence case, the roots do not follow path B corresponding to the downgoing o-wave, but progress up to just above $X = 1$ where the two roots are equal, then become very large at the X_R level. This is more clearly seen in Figs. 3.13 and 3.14.

The roots of the Booker quartic show that upgoing o-waves (branch A) propagate up to just above $X = 1$ ($X = 1.0015$ for this case), reflect back and approach X_R. The corresponding ray path for this case is sketched in Fig. 3.15. The phenomenon described above is seen in the field solutions as standing waves above the X_R level. Above $X = 1.0015$ the waves exhibit evanescent behavior and decay rapidly as expected from the quartic roots.

The imaginary part of q (Fig. 3.14) shows that Im(q) is zero or almost zero for the upgoing o-wave (branch A). On the way back, after reflection as an x-wave, IM(q) becomes large near X_R. This increase becomes significant in the region between $X = 0.9981$ and X_R, as

Solution Increment	: 0.005000	Critical Coupling Angle	: 10.70086
Wave Frequency	: 5.00000E+06	X-Direction Cosine of Y	: - 3.78972E-01
Angle of Incidence	: 0.00000E+00	Y-Direction Cosine of Y	: 0.00000E+00
Geomagnetic Field	: 5.64260E-05	Z-Direction Cosine of Y	: 9.25408E-01
Magnetic Y Vector	: 3.15898E-01	Collision Frequency	: 1.00000E+03
Electron Gyrofreq	: 1.57949E+06	Resonance Condition	: 0.964328

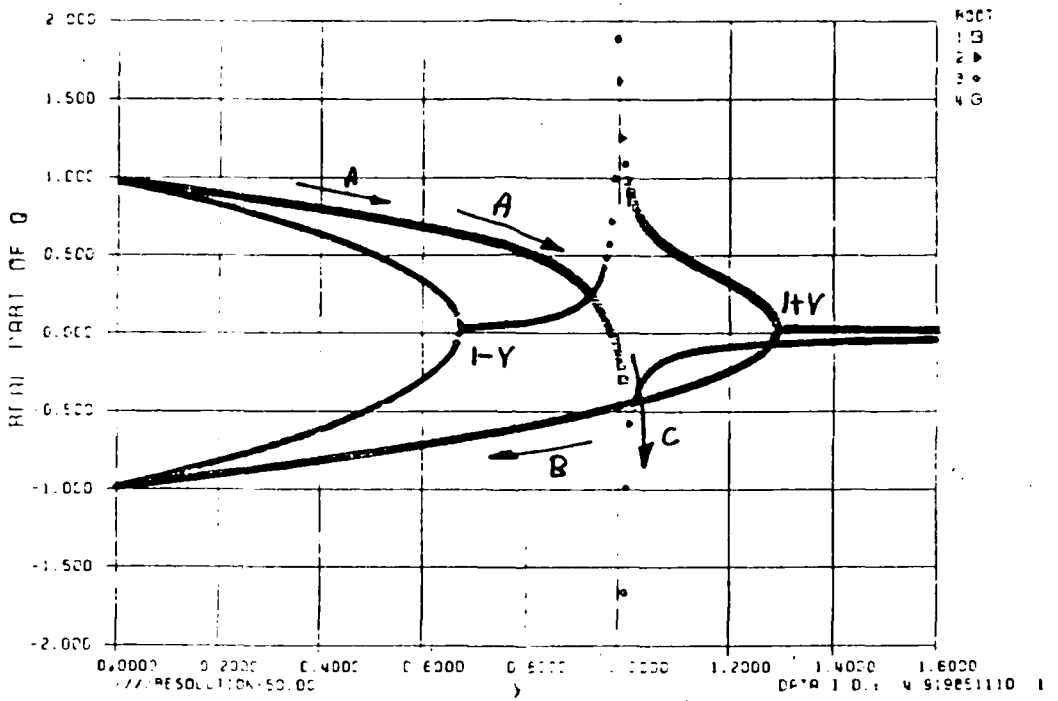

Fig. 3.11 Real part of q; critical angle of incidence case (towards magnetic north)

Solution Increment	: 0.005000	Critical Coupling Angle	: 10.70086
Wave Frequency	: 5.00000E+06	X-Direction Cosine of Y	: - 3.78972E-01
Angle of Incidence	: 0.00000E+00	Y-Direction Cosine of Y	: 0.00000E+00
Geomagnetic Field	: 5.64260E-05	Z-Direction Cosine of Y	: 9.25408E-01
Magnetic Y Vector	: 3.15898E-01	Collision Frequency	: 1.00000E+03
Electron Gyrofreq	: 1.57949E+06	Resonance Condition	: 0.964328

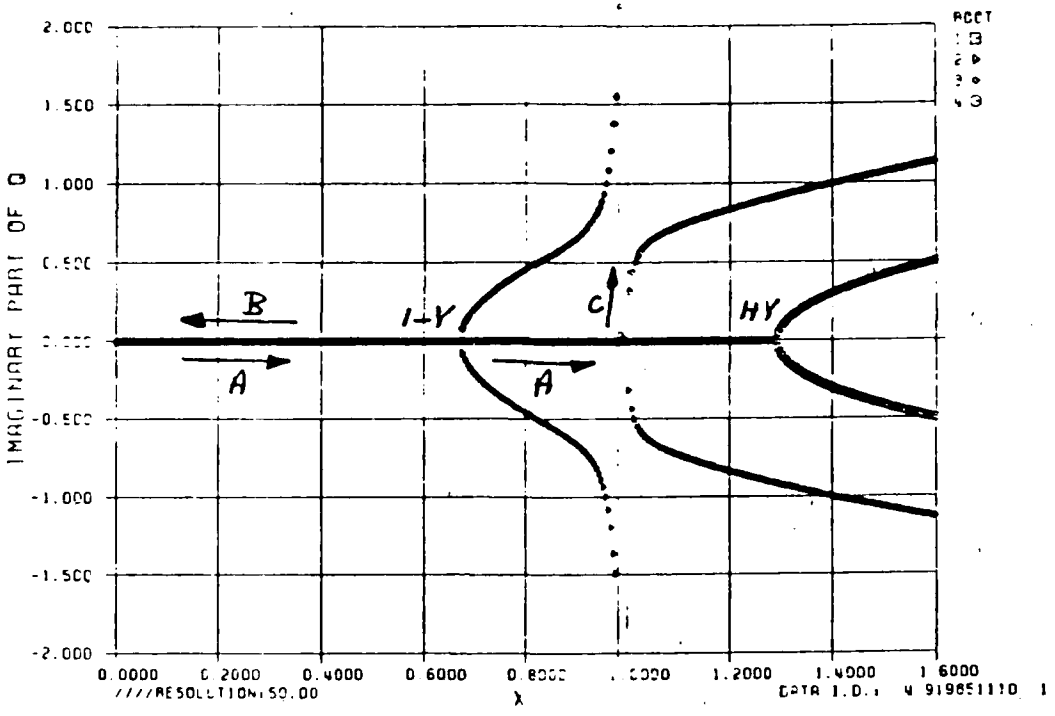

Fig. 3.12 Imaginary part of q; critical angle of incidence case (towards magnetic north)

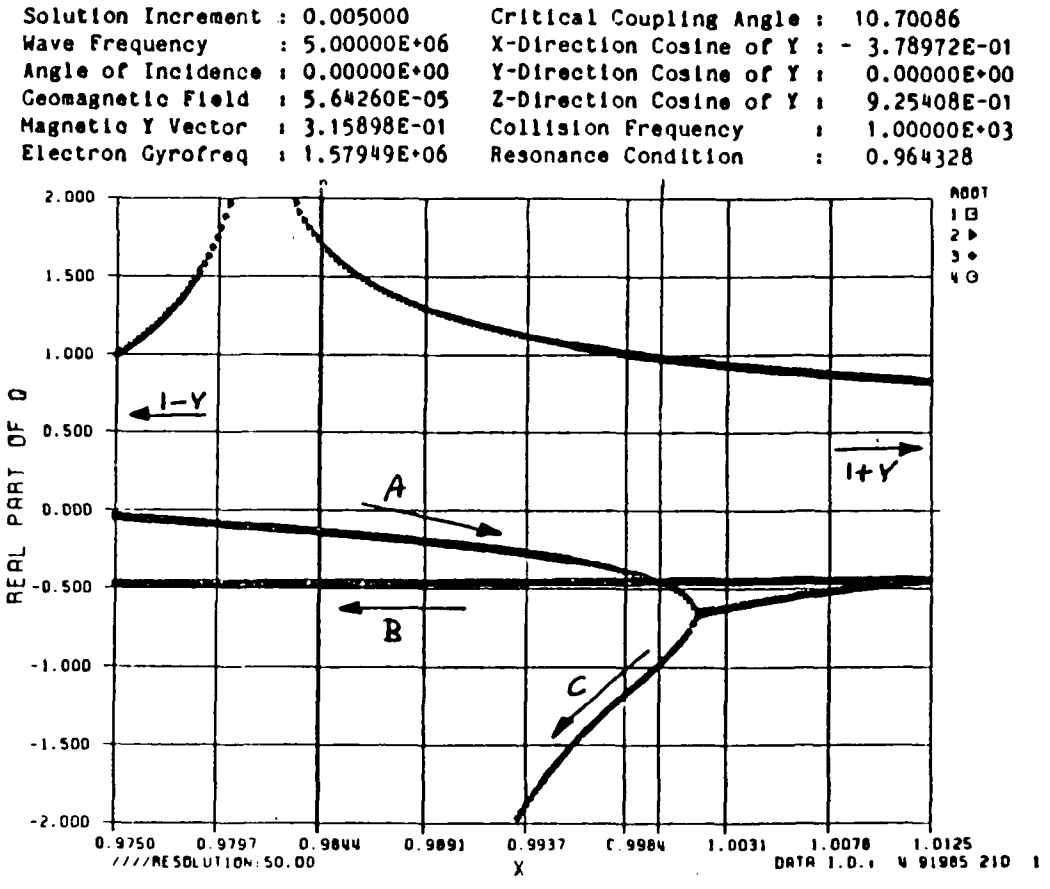

Fig. 3.13 Real part of q near the X = 1 level; critical angle of incidence case (towards magnetic north)

This high resolution behavior of q (Figure 3.11) shows the transition of the upgoing o-wave along path A to the downgoing X-wave along path C.

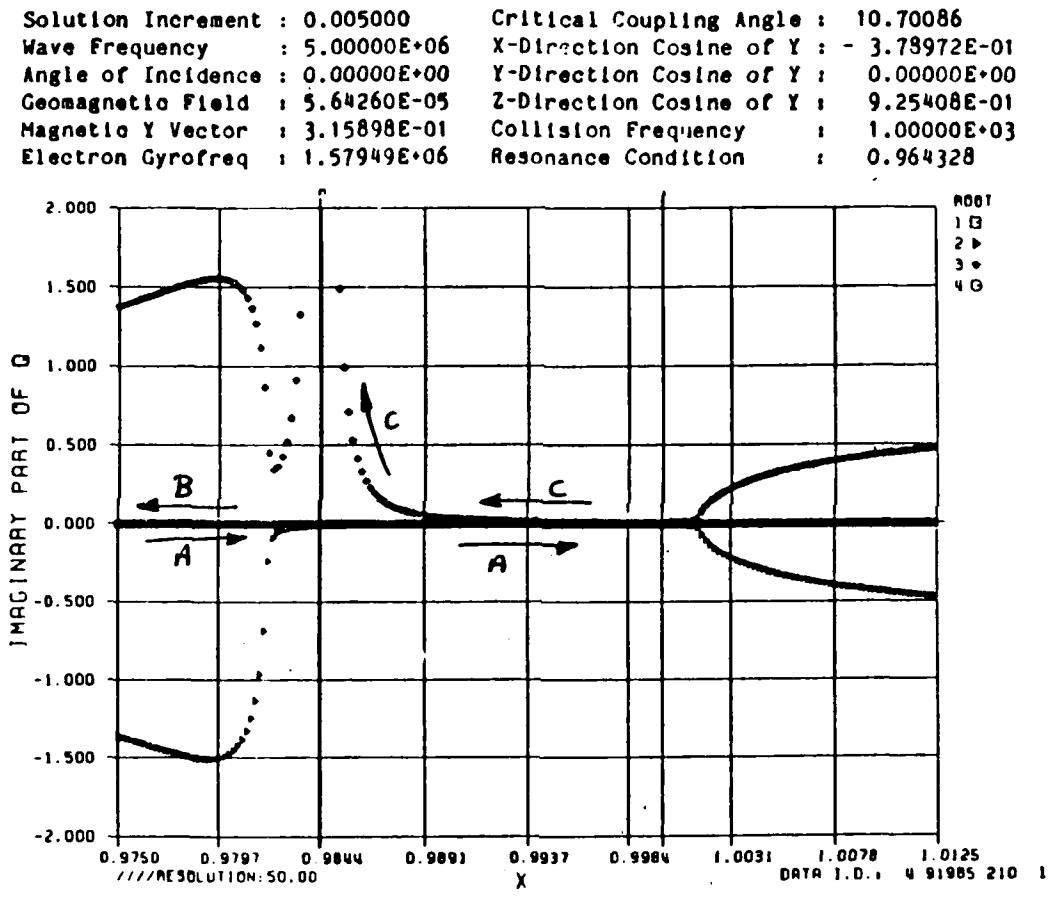

Fig. 3.14 Imaginary part of q near the X = 1 level; critical angle of incidence case (towards magnetic north)

Note that large attenuation of the downgoing X-wave along path C will occur near the resonance level X_R.

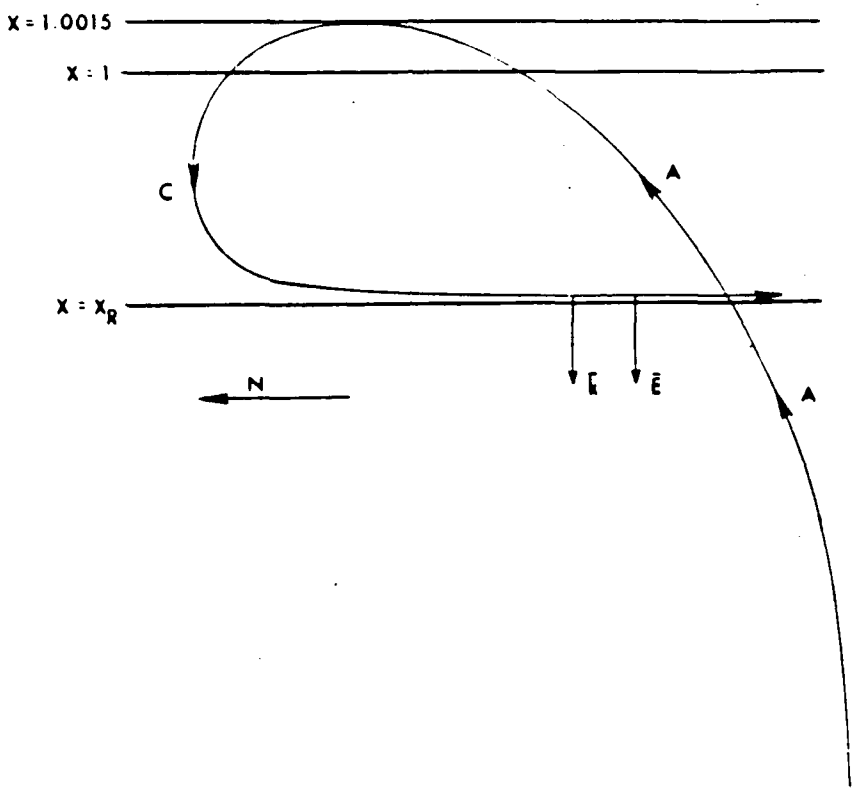

Fig. 3.15 Ray path in the magnetic meridian; critical angle of incidence case (towards magnetic north)

seen by the following branch C in Fig. 3.14. The results show that for this critical incidence case (S-N), most of the incident energy is focused and absorbed in a very narrow region just below the X = 1 level.

Near the X_R level the real part of q along C becomes very large and E_z exhibits a peak of 40dB compared to an incident wave intensity of around 5dB. This indicates that E and k become almost vertical at X_R while the direction of energy flow is horizontal.

Case 3: Model 1, Critical Angle of incidence (N-S): Propagation Towards Magnetic South

Figures 3.16, 3.17, and 3.18 show the E_x, E_y, E_z components of the fields, respectively. The field magnitudes in this case are also nearly constant at the bottom level. The absence of standing waves below X_R indicates the absence of significant reflected downgoing waves. The reflection coefficients for E and H are

$$R(E) = 6.3 \times 10^{-3}$$

$$R(H) = 6.3 \times 10^{-3}$$

Wave Frequency	: 5.0	E 6	Angle of Incidence	:-1.070	E 1
Magnetic Y Vector	: 3.150	E-1	Con (1)	: 2.700	E 11
Tot. Geomag. Field	: 5.643	E-5	Con (2)	: 1.800	E 11
X-Dir Cosine of Y	:-3.789	E-1	Con (3)	: 0.000	E 0
Y-Dir Cosine of Y	: 0.000	E-0	Con (4)	: 1.000	E 4
Z-Dir Cosine of Y	: 9.255	E-1	Con (5)	: 1.000	E 3

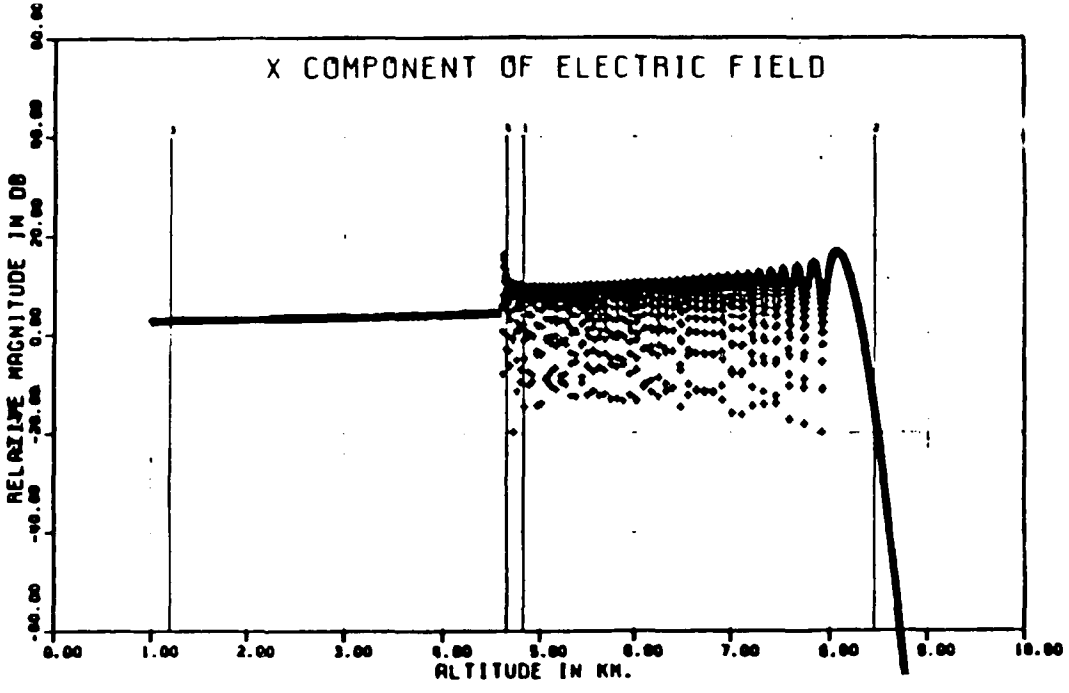

Fig. 3.16 x-component of electric field; critical angle of incidence case (towards magnetic south)

Wave Frequency	: 5.0	E 6	Angle of Incidence	:-1.070	E 1
Magnetic Y Vector	: 3.150	E-1	Con (1)	: 2.700	E 11
Tot. Geomag. Field	: 5.643	E-5	Con (2)	: 1.800	E 11
X-Dir Cosine of Y	:-3.789	E-1	Con (3)	: 0.000	E 0
Y-Dir Cosine of Y	: 0.000	E-0	Con (4)	: 1.000	E 4
Z-Dir Cosine of Y	: 9.255	E-1	Con (5)	: 1.000	E 3

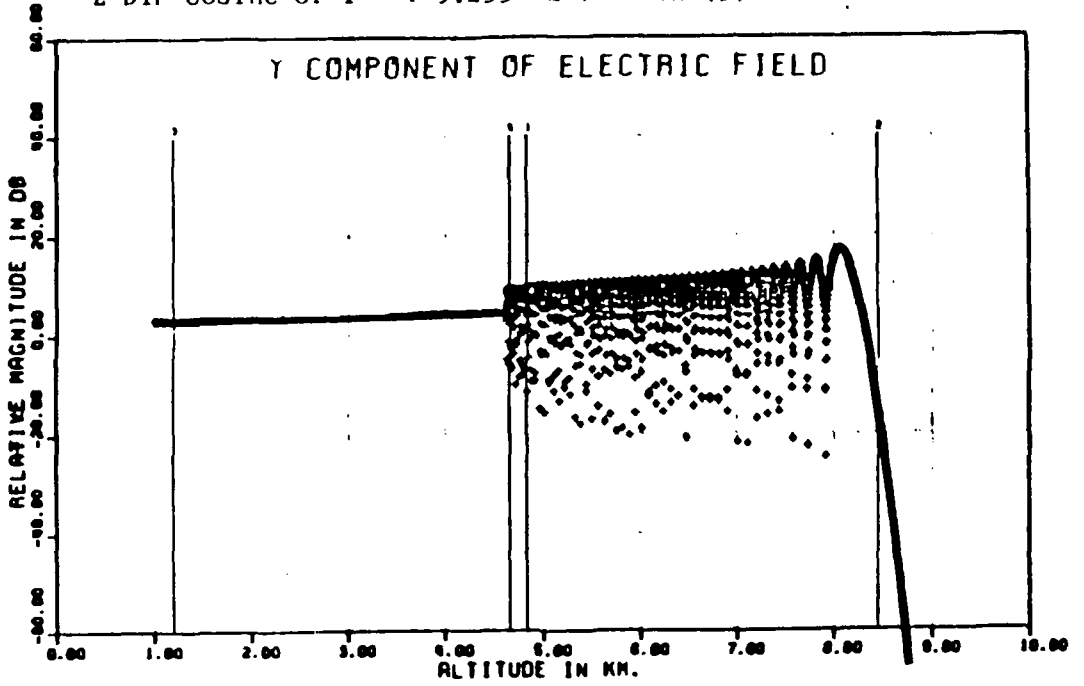

Fig. 3.17 y-component of electric field; critical angle of incidence case (towards magnetic south)

Wave Frequency	: 5.0	E 6	Angle of Incidence	:-1.070	E 1
Magnetic Y Vector	: 3.150	E-1	Con (1)	: 2.700	E 11
Tot. Geomag. Field	: 5.643	E-5	Con (2)	: 1.800	E 11
X-Dir Cosine of Y	:-3.789	E-1	Con (3)	: 0.000	E 0
Y-Dir Cosine of Y	: 0.000	E-0	Con (4)	: 1.000	E 4
Z-Dir Cosine of Y	: 9.255	E-1	Con (5)	: 1.000	E 3

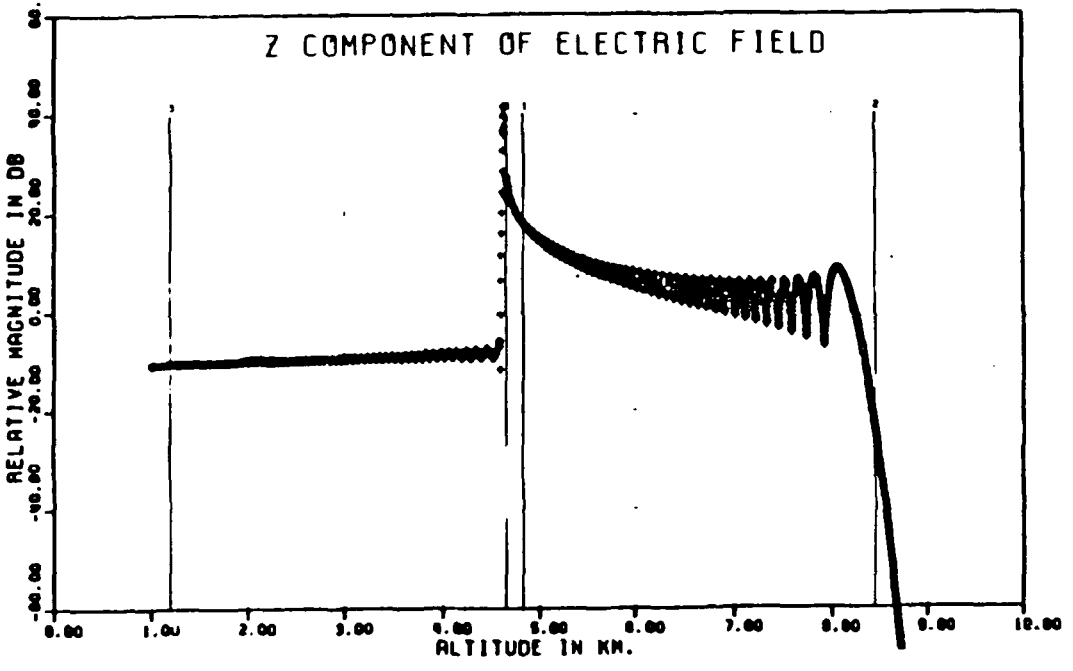

Fig. 3.18 z-component of electric field; critical angle of incidence case (towards magnetic south)

which indicate that almost 100% of the incident energy is absorbed in the medium.

The roots of the Booker quartic (Figs. 3.19-3.20), corresponding to the upgoing o-wave, is continuous at the X = 1 level. The roots continue (branch B) up to the 1 + Y level, return back, with the real part getting large as the X_R level is approached (branch C). These indicate that the upgoing o-wave progresses up to the X = 1 level, couples to the upgoing x-wave and is reflected back from the 1 + Y level. This is seen on the field solutions as standing waves between X_R and 1 + Y. The reflected x-waves do not attenuate significantly until the X_R level is reached; this is observed on the roots of the Booker quartic as imaginary parts being zero (Figs. 3.20, 3.22, branches A, B, C). Figures 3.20 and 3.21 show that the roots cross the X_R level (branch D), contrary to the S-N propagation case in which the roots reach their maximum at the X_R level.

The imaginary part of q (Fig. 3.22, branch D) is large between X_R and 1 - Y. The waves attenuate significantly and the energy is absorbed in this region, most of it localized near X_R. Fig. 3.23 shows the sketch of the ray path for this case. Note that

Solution Increment	: 0.005000	Critical Coupling Angle	: 10.70086
Wave Frequency	: 5.00000E+06	X-Direction Cosine of Y	: - 3.78972E-01
Angle of Incidence	: 0.00000E+00	Y-Direction Cosine of Y	: 0.00000E+00
Geomagnetic Field	: 5.64260E-05	Z-Direction Cosine of Y	: 9.25408E-01
Magnetic Y Vector	: 3.15898E-01	Collision Frequency	: 1.00000E+03
Electron Cyrofreq	: 1.57949E+06	Resonance Condition	: 0.964328

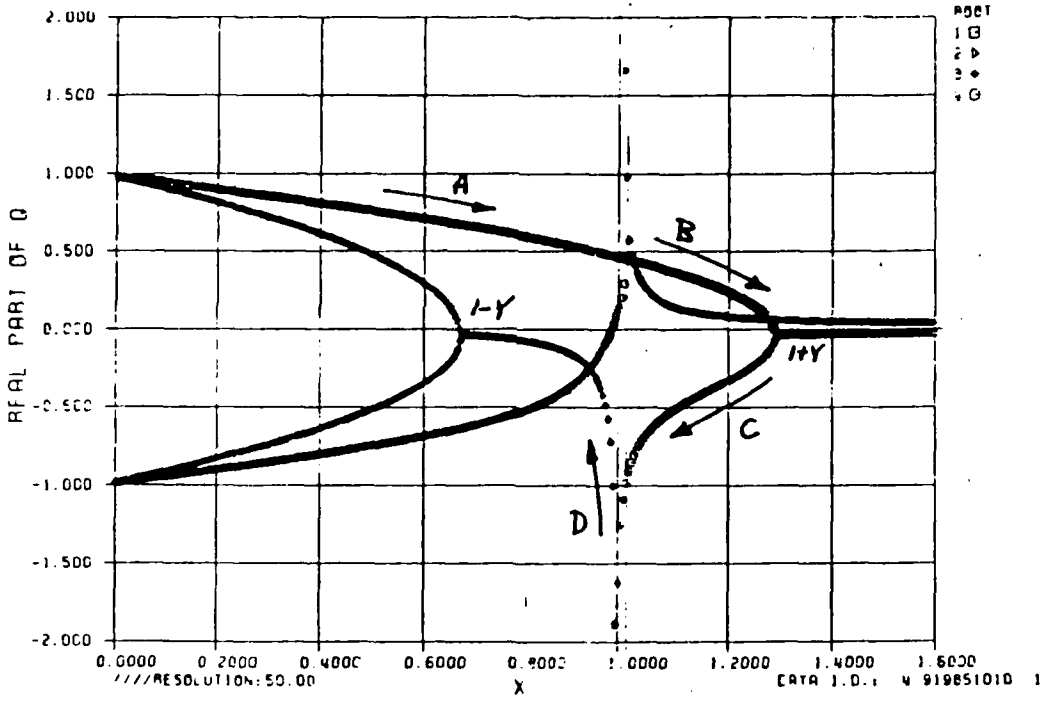

Fig. 3.19 Real part of q; critical angle of incidence case (towards magnetic south)

This high resolution behavior of q (Figure 3.19) shows the transition of the upgoing o-wave along path A to the upgoing X-wave along path B.

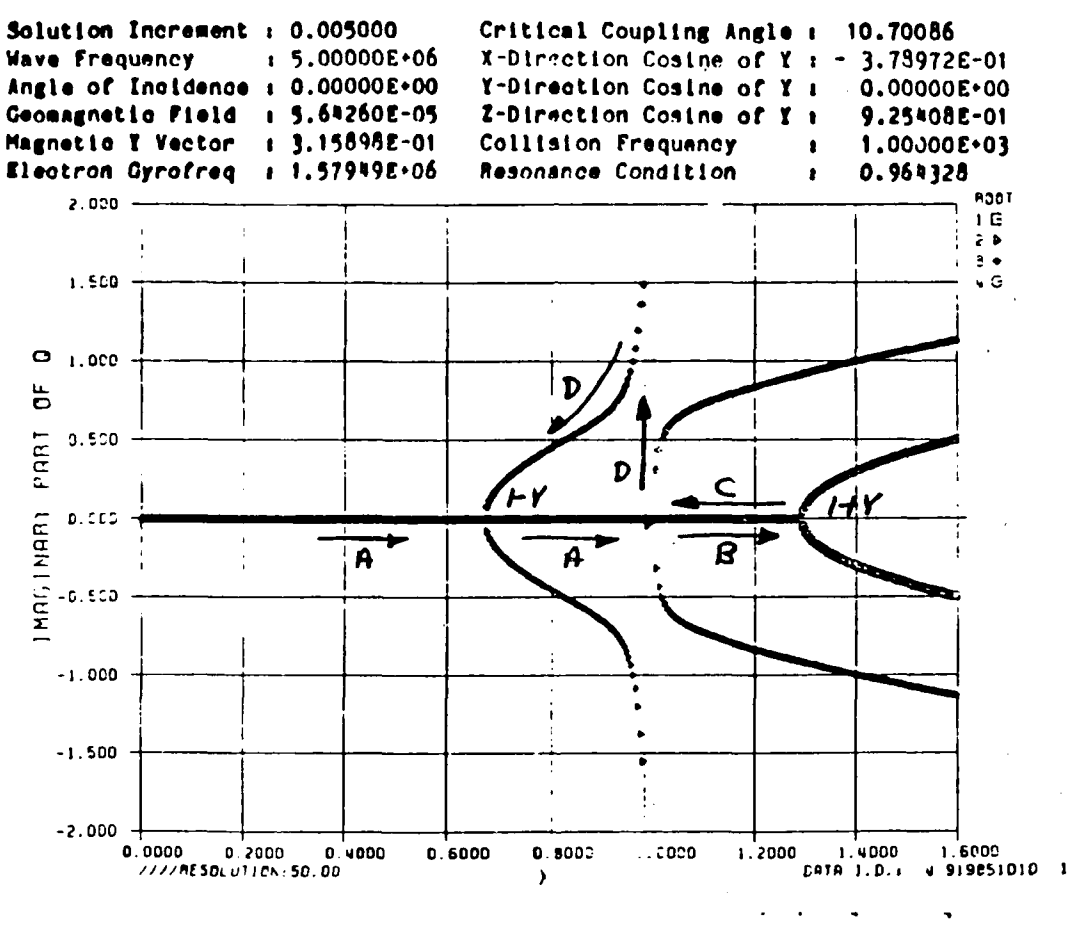

Fig. 3.20 Imaginary part of q; critical angle of incidence case (towards magnetic south)

AD-A195 335 ROLE OF ORDINARY TO EXTRAORDINARY MODE WAVE COUPLING IN 2/2
IONOSPHERIC HEATI..(U) OHIO STATE UNIV RESEARCH
FOUNDATION COLUMBUS B ABALI ET AL. MAR 88 AS-S-121
UNCLASSIFIED RADC-TR-88-22 F19628-83-K-0005 F/G 12/3 NL

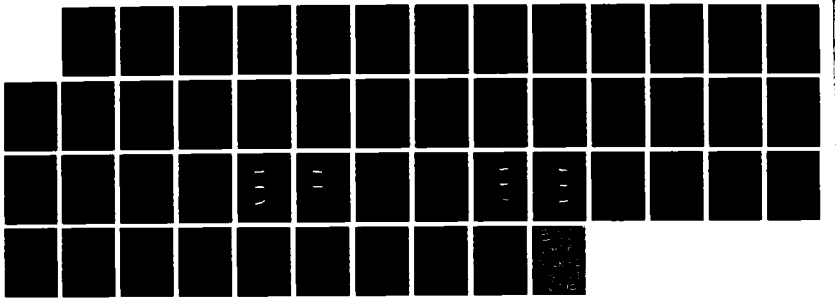

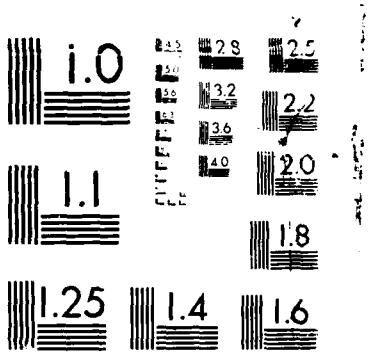

MICROCOPY RESOLUTION TEST CHA
NATIONAL BUREAU OF STANDARDS 1963

Solution Increment	: 0.005000	Critical Coupling Angle	: 10.70086
Wave Frequency	: 5.00000E+06	X-Direction Cosine of Y	: - 3.78972E-01
Angle of Incidence	: 0.00000E+00	Y-Direction Cosine of Y	: 0.00000E+00
Geomagnetic Field	: 5.64260E-05	Z-Direction Cosine of Y	: 9.25408E-01
Magnetic Y Vector	: 3.15898E-01	Collision Frequency	: 1.00000E+03
Electron Gyrofreq	: 1.57949E+06	Resonance Condition	: 0.964328

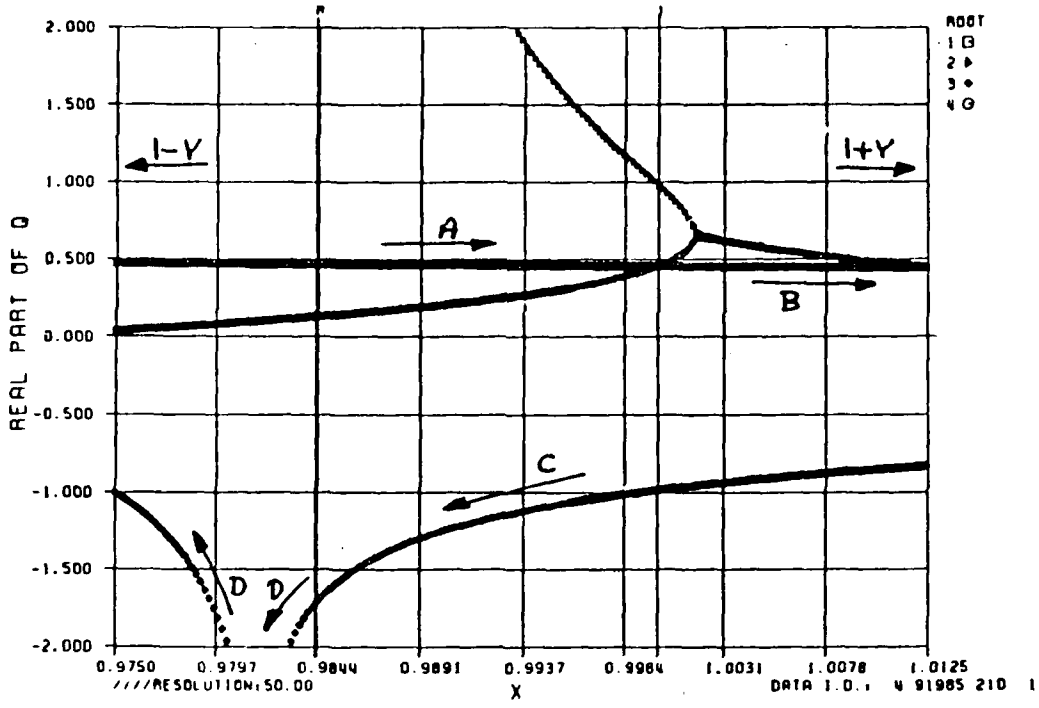

Fig. 3.21 Real part of q near the X = 1 level; critical angle of incidence case (towards magnetic south)

This high resolution behavior of q (Figure 3.19) shows the transition of the upgoing o-wave along path A to the upgoing X-wave along path B.

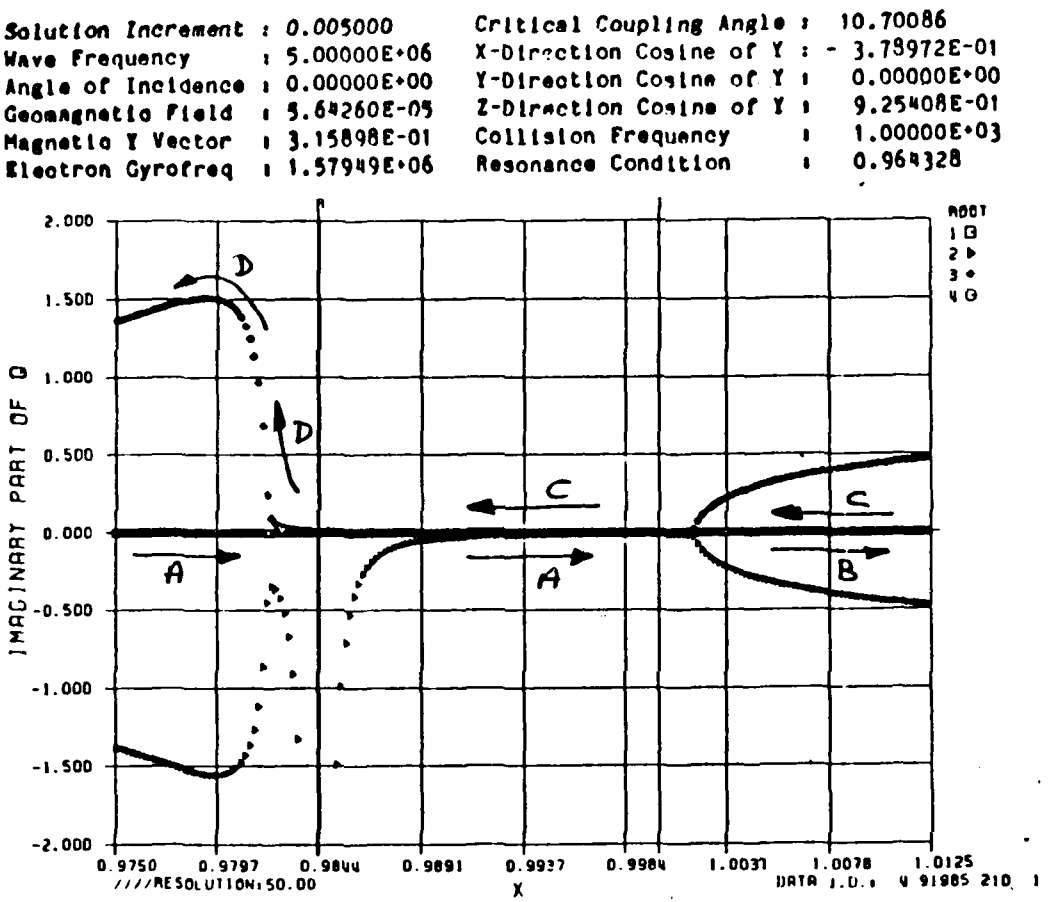

Fig. 3.22 Imaginary part of q near the X = 1 level; critical angle of incidence case (towards magnetic south)

Note that large attenuation of the downgoing X-wave along path C→D will occur just below the resonance level Y_R.

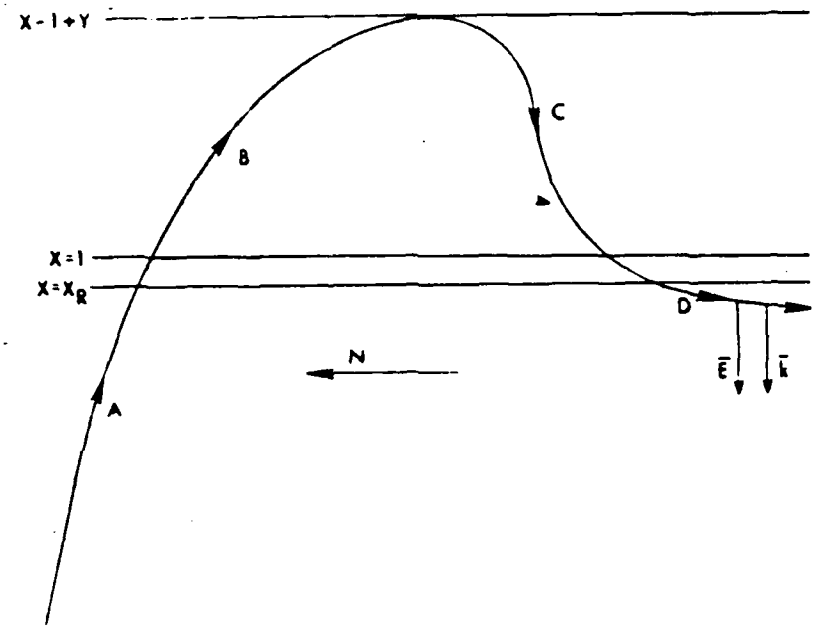

Fig. 3.23 Ray path in the magnetic meridian; critical angle of incidence case (towards magnetic south)

near X_R, the real part of q and E_z component is very large. This indicates that E and k are almost vertical while the energy flow is horizontal.

3.4 - WIDTH OF THE COUPLING WINDOW

There is a region around the critical coupling angle at which the o-wave to x-wave coupling is most effective. The width of this region, which is referred to as the coupling window, is determined by performing a series of full wave solutions near the critical angle of incidence. The incidence angle is varied around the coupling angle in two planes: (i) in the magnetic meridian (N-s), and (ii) perpendicular to the magnetic meridian (E-W). The -3dB points are used to define the edges of the coupling window. Table 3.6 lists the angular widths for the E field. Figures 3.24-3.29 and 3.30-3.35 show the variation of the reflection coefficients with the angle of incidence, in the magnetic meridian and off the magnetic meridian, respectively. The rest of the reflection coefficients are listed in Appendix B.

The results show that the angular shape of the coupling windows is approximately circular around the critical coupling angle. The gradient of the electron

Table 3.6 - Angular Widths of the Coupling Windows

		N-S and S-N			E-W	
Model	Angle	-3dB(low)	-3dB(high)	Width	-3dB	Width
1	+10.7	8.7	12.8	4.1	2.0	4.0
1	-10.7	-9.1	-12.6	3.5	1.7	3.7
2	+10.7	5.5	16.0	10.5	5.5	11.0
2	-10.7	-6.0	-15.0	9.0	5.0	10.0
3	+10.7	5.6	16.0	10.4	5.5	11.0
3	-10.7	-6.0	-15.0	9.0	5.0	9.0

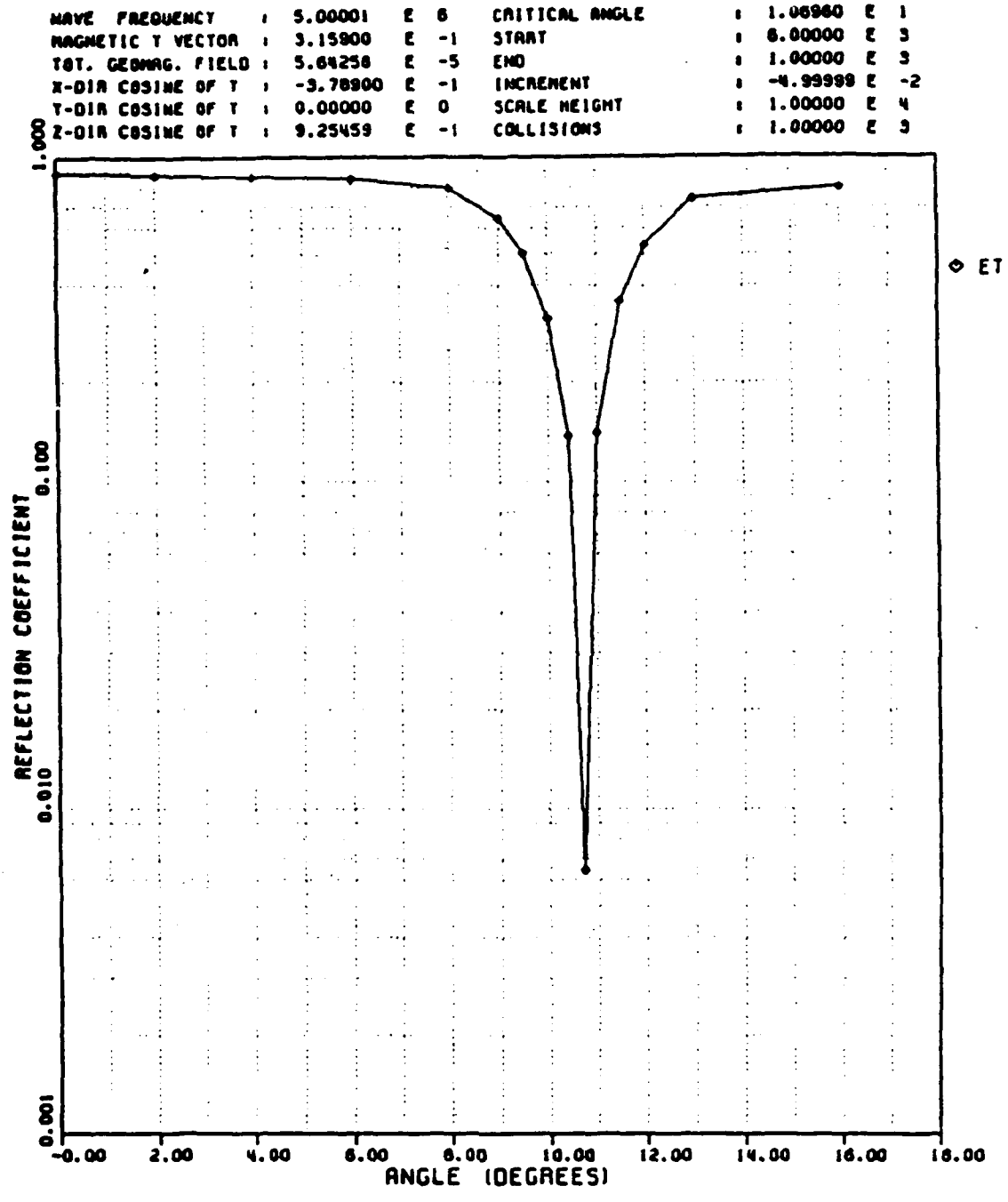

Fig. 3.24 Reflection coefficient vs. angle of incidence: Model 1, in the magnetic meridian, towards magnetic north

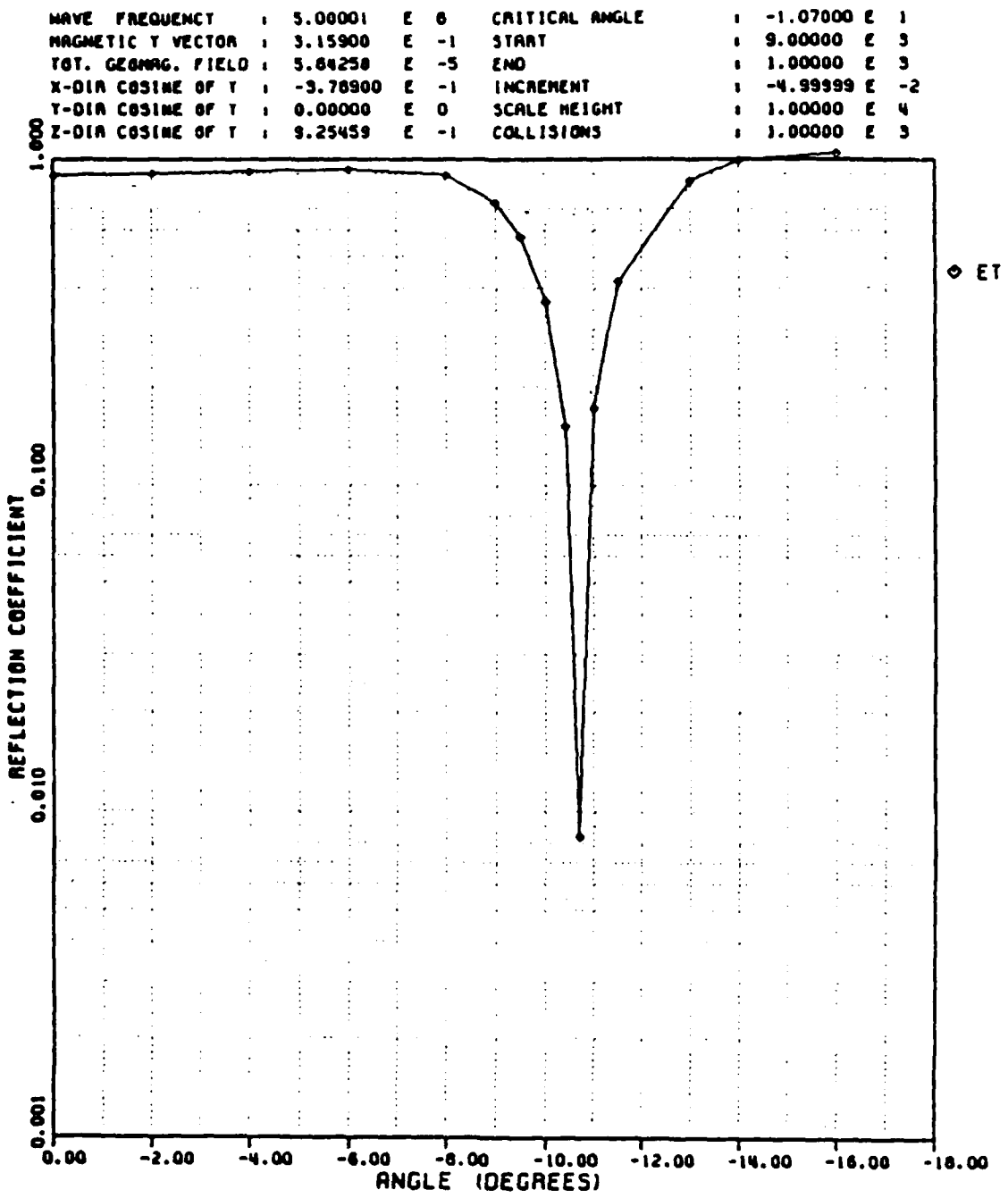

Fig. 3.25 Reflection coefficient vs. angle of incidence: Model 1, in the magnetic meridian, towards magnetic south

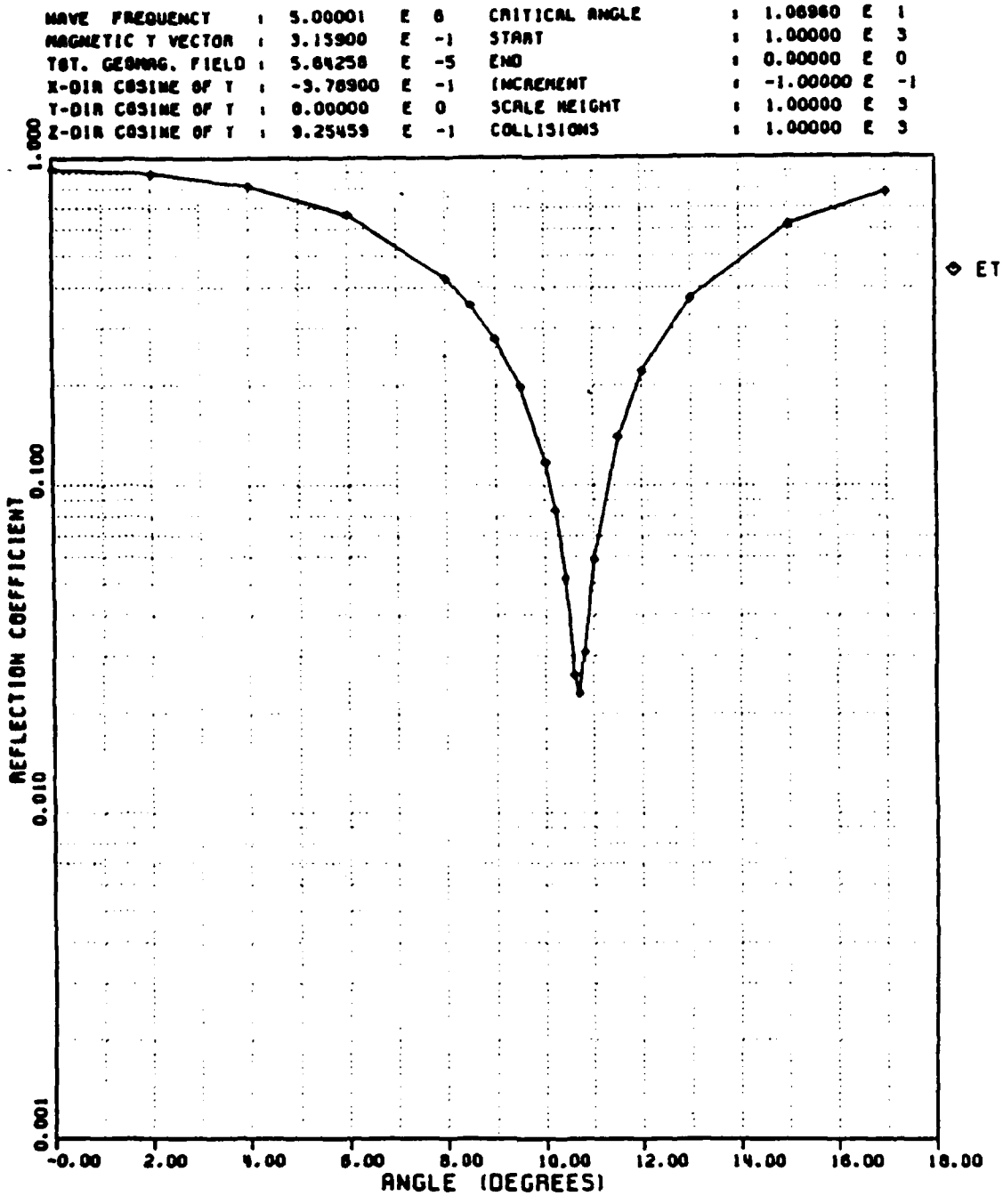

Fig. 3.26 Reflection coefficient vs. angle of incidence: Model 2, in the magnetic meridian, towards magnetic north

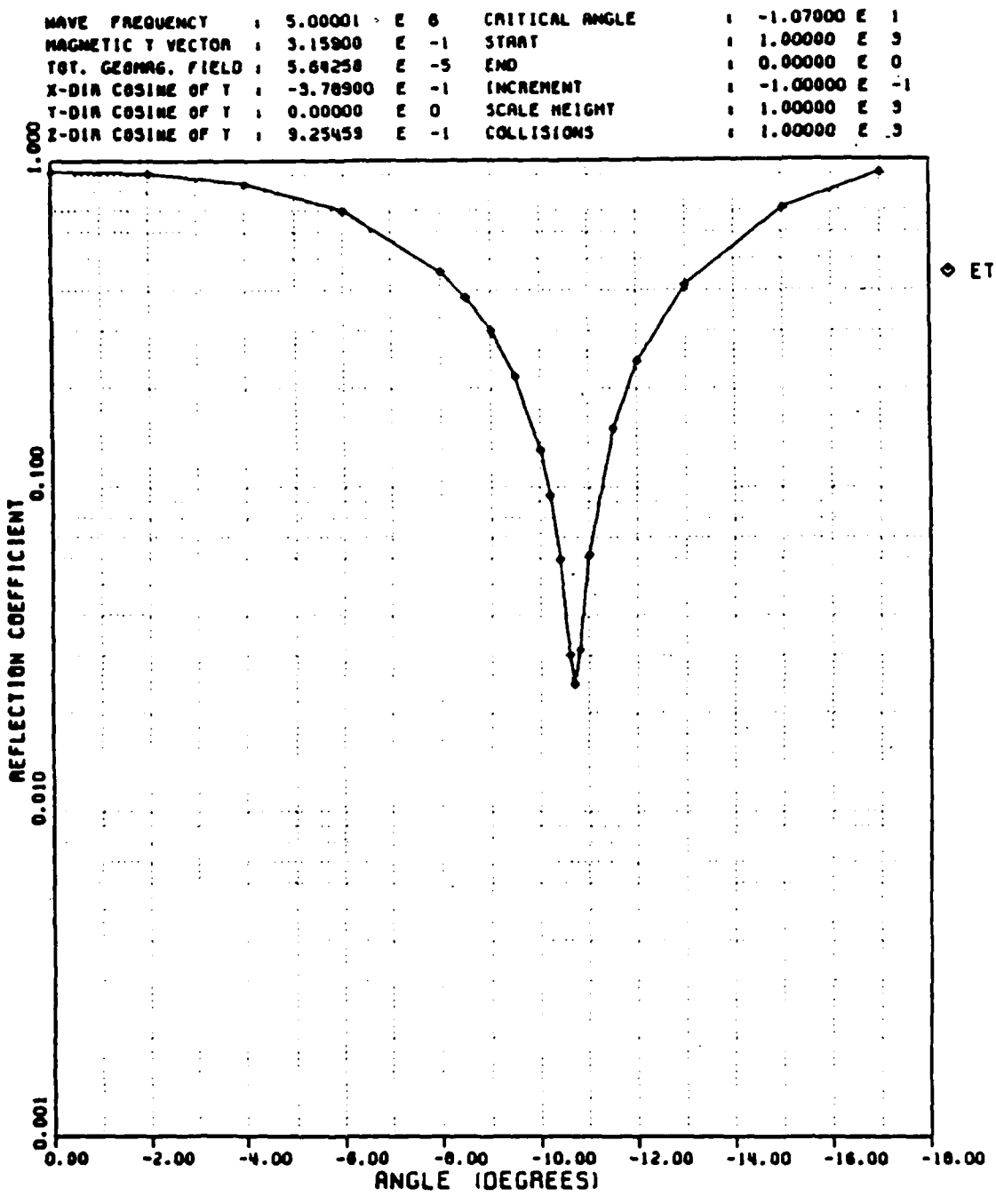

Fig. 3.27 Reflection coefficient vs. angle of incidence: Model 2, in the magnetic meridian, towards magnetic south

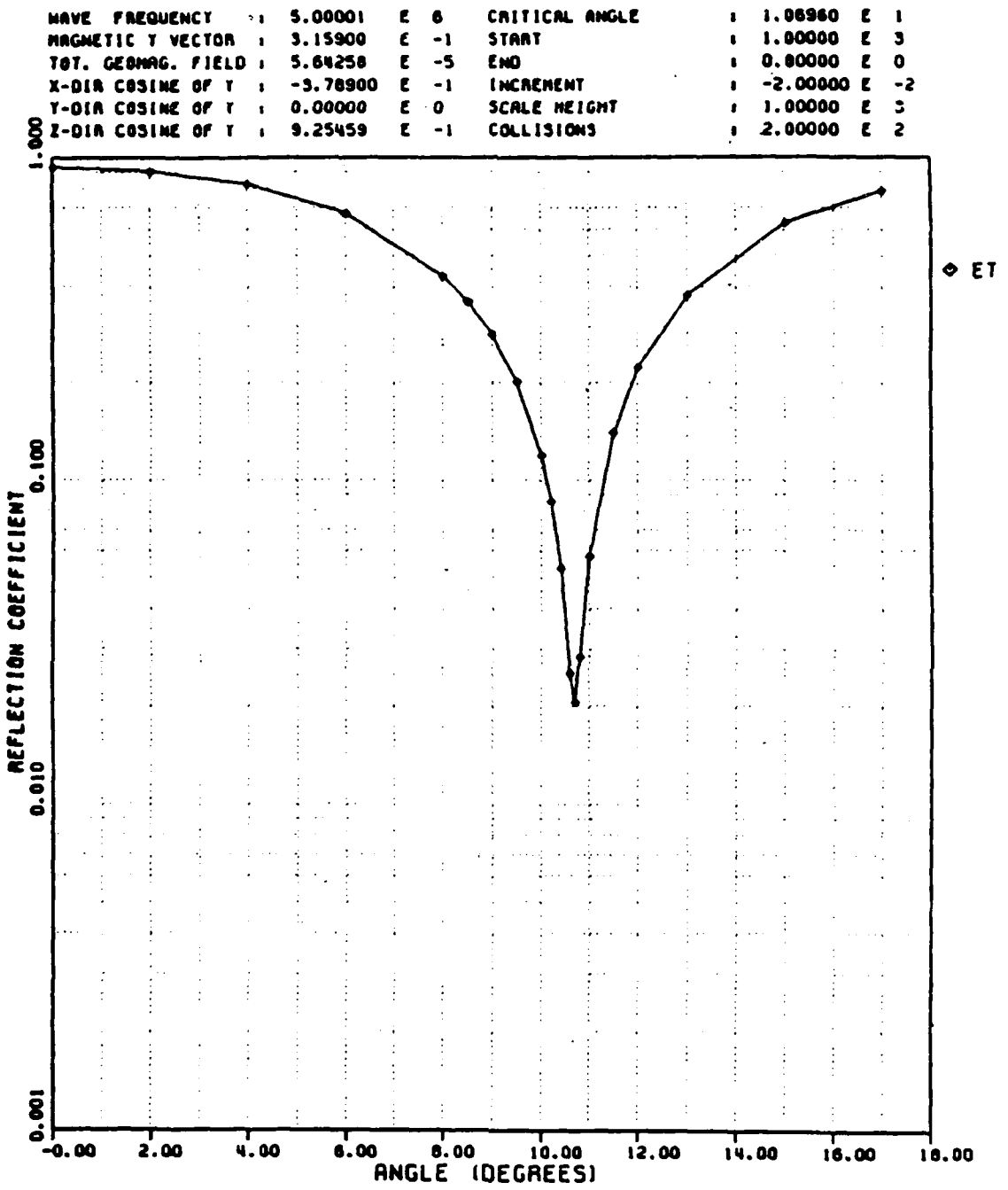

Fig. 3.28 Reflection coefficient vs. angle of incidence: Model 3, in the magnetic meridian, towards magnetic north

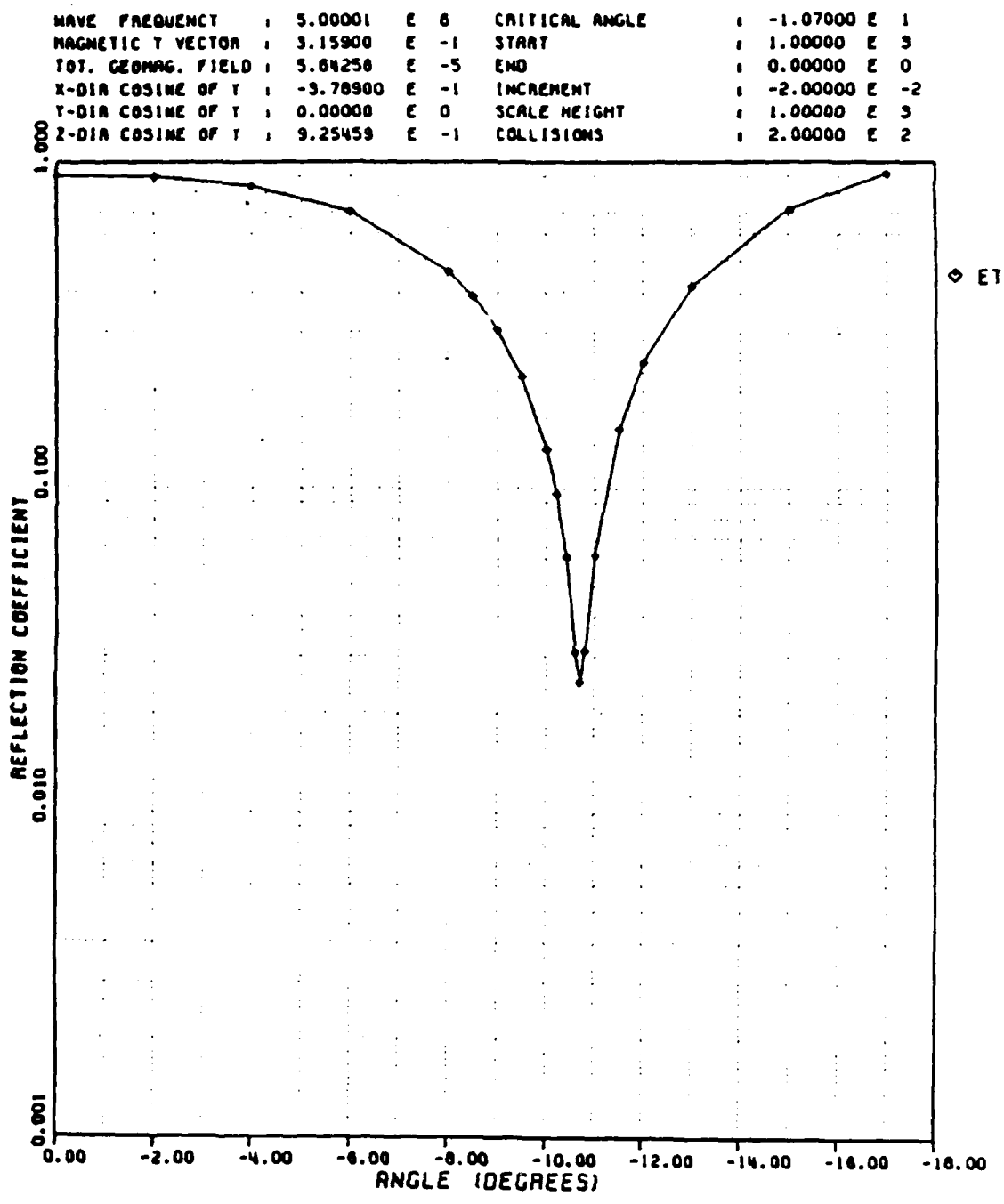

Fig. 3.29 Reflection coefficient vs. angle of incidence: Model 3, in the magnetic meridian, towards magnetic south

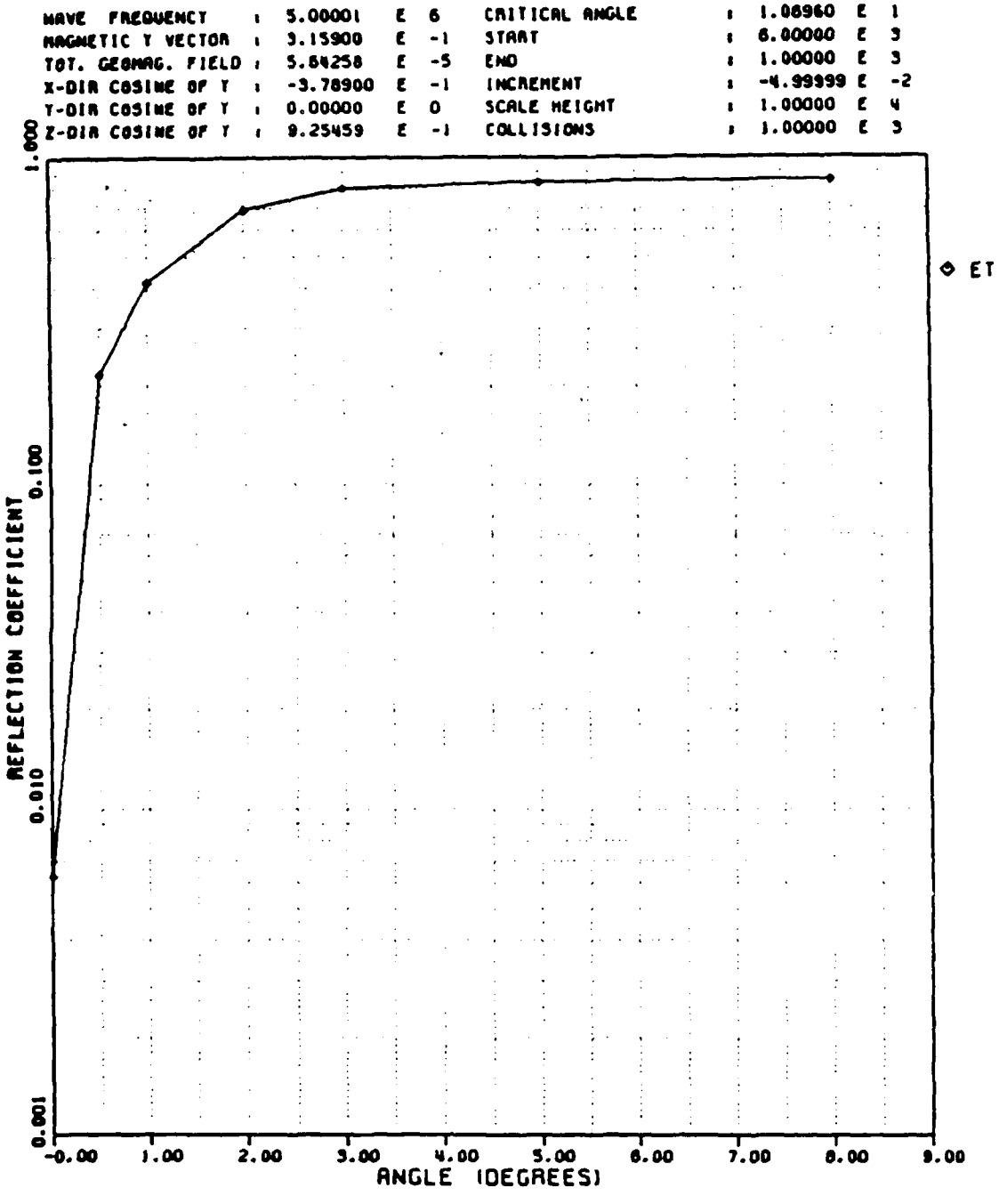

Fig. 3.30 Reflection coefficient vs. angle of incidence: Model 1, off the magnetic meridian, towards magnetic north

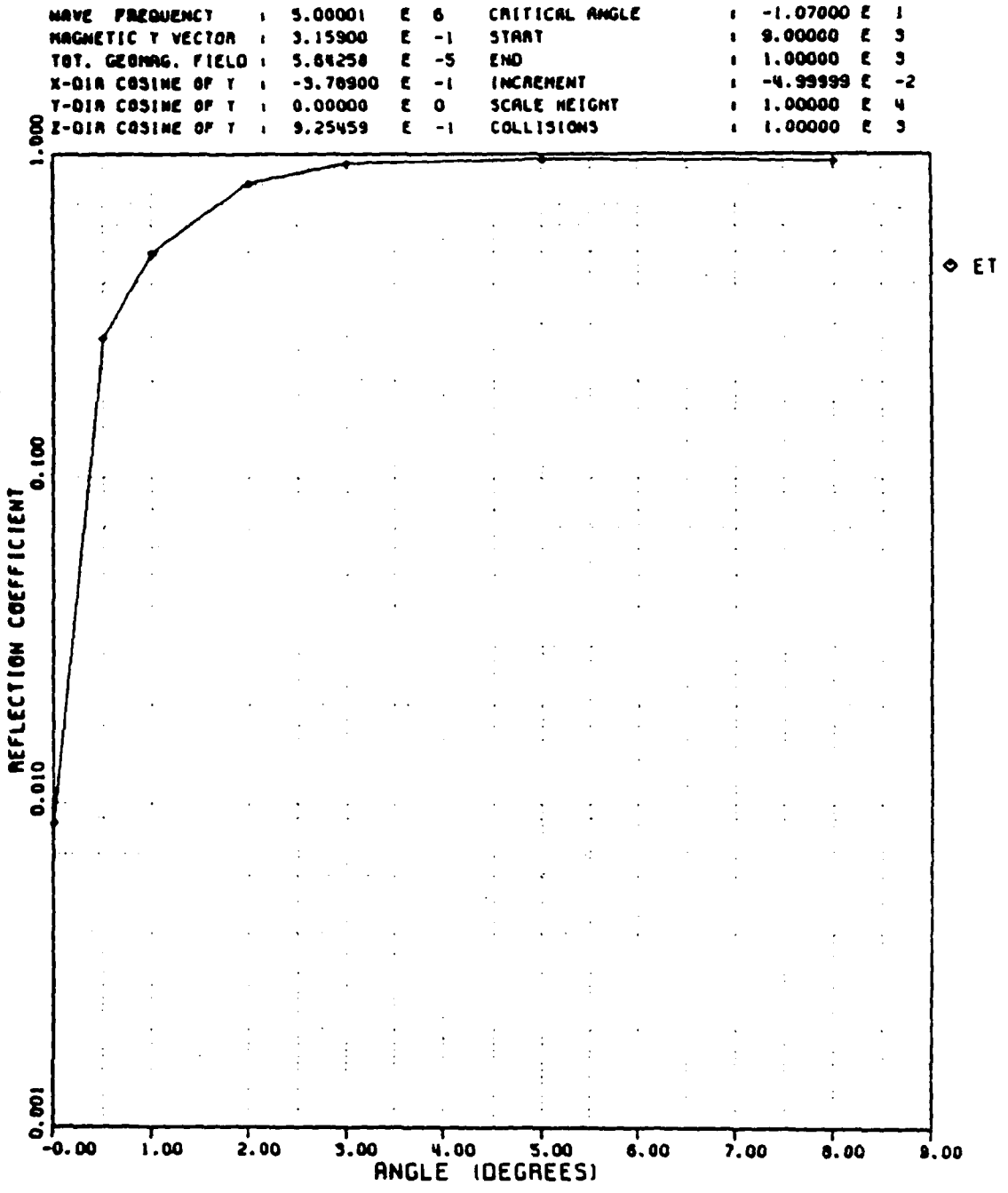

Fig. 3.31 Reflection coefficient vs. angle of incidence: Model 1, off the magnetic meridian, towards magnetic south

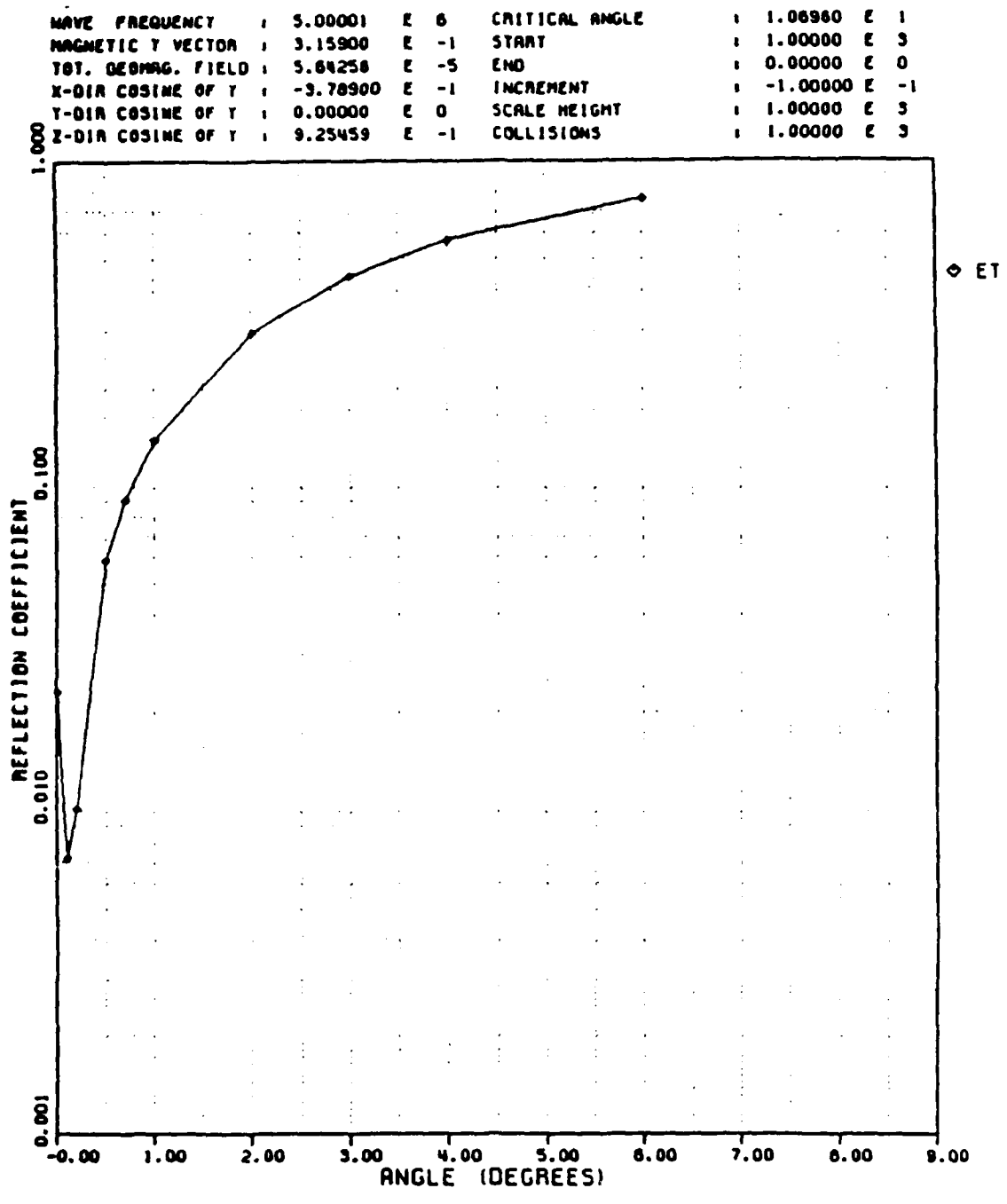

Fig. 3.32 Reflection coefficient vs. angle of incidence: Model 2, off the magnetic meridian, towards magnetic north

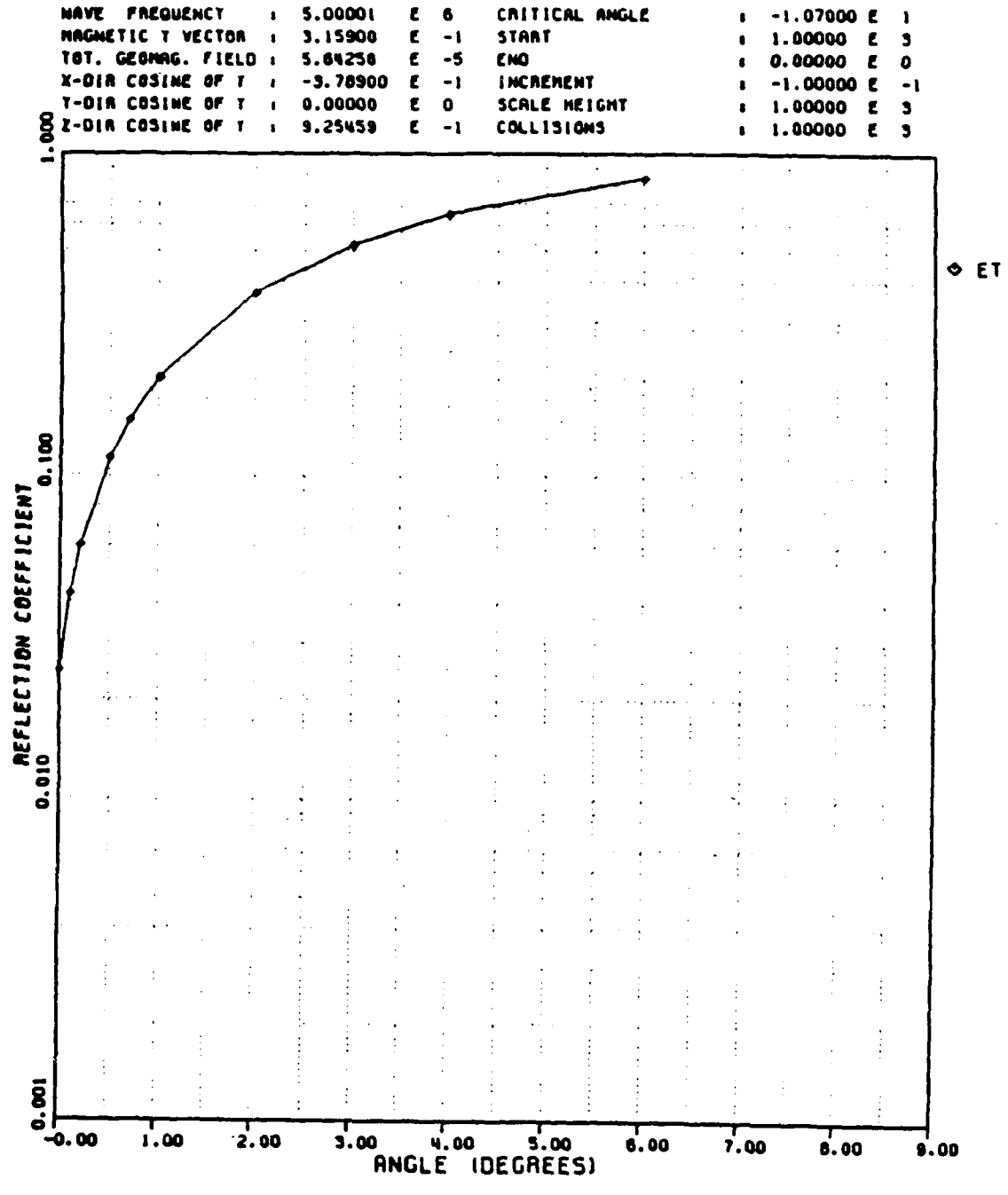

Fig. 3.33 Reflection coefficient vs. angle of incidence: Model 2, off the magnetic meridian, towards magnetic south

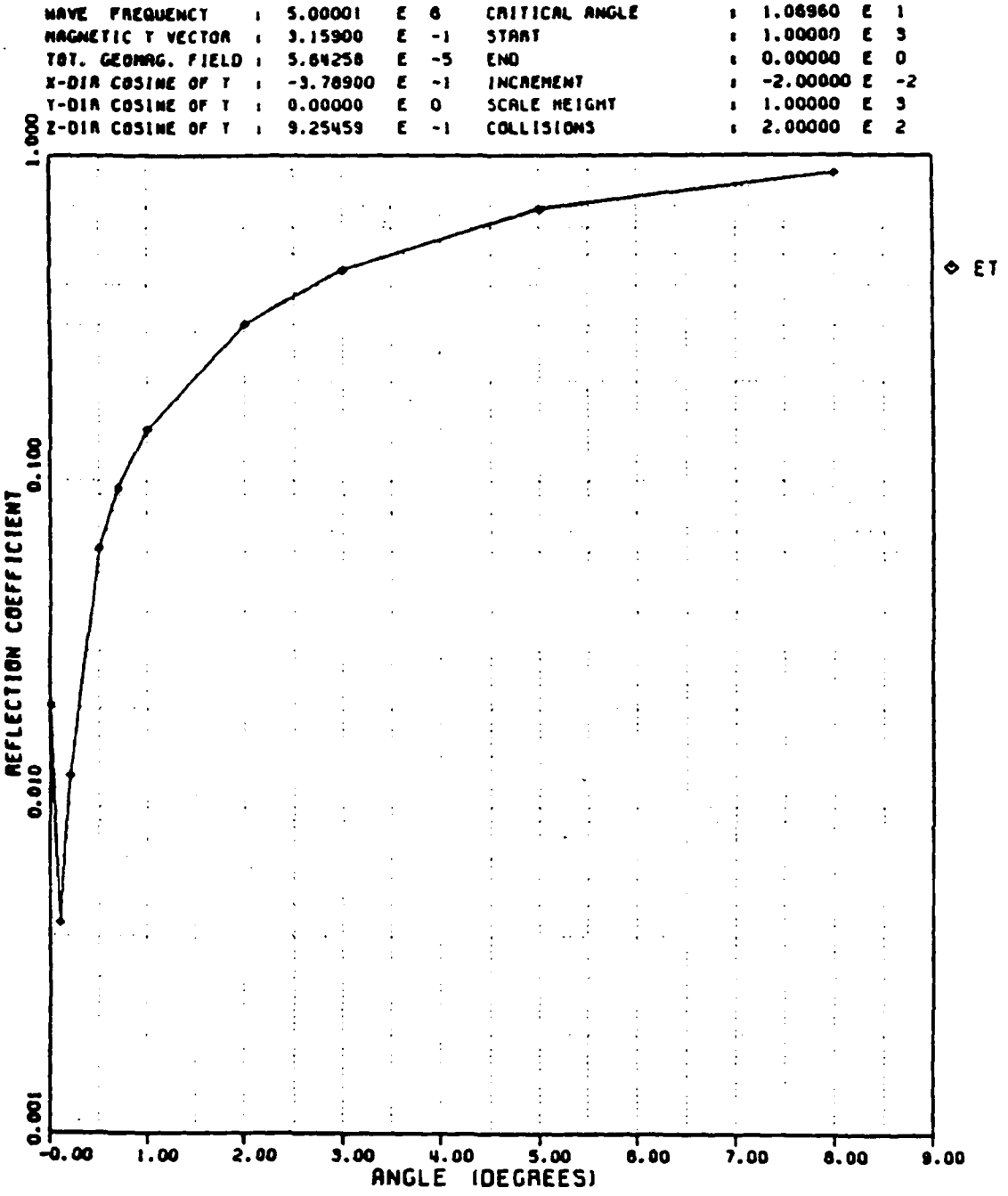

Fig. 3.34 Reflection coefficient vs. angle of incidence: Model 3, off the magnetic meridian, towards magnetic north

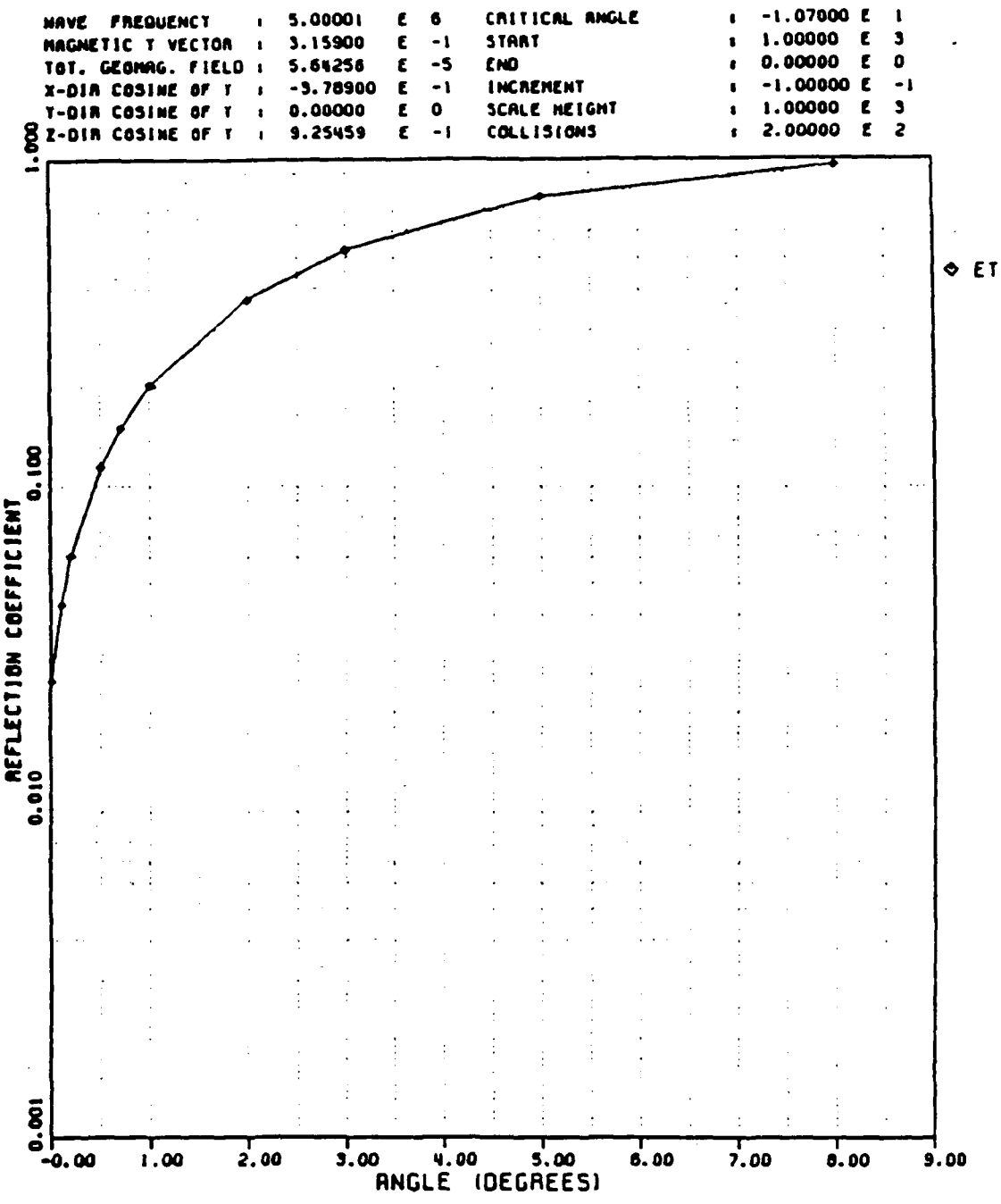

Fig. 3.35 Reflection coefficient vs. angle of incidence: Model 3, off the magnetic meridian, towards magnetic south

density appears to be a major determining factor affecting the width of the coupling window. The angular width of Model 1 is about 3.5-4° and Model 2 is about 10-11°. The parameters of Model 1 and Model 2 differ only in the gradient of the electron density H (H Model 1 H = 10^4, Model 2 H = 10^3). This indicates that steep gradients are more favorable for effective coupling. Also, for a given ionospheric model, the coupling window in the S-N direction (+10.7°) appears to be wider than the window in the N-S direction (-10.7°) by about 0.5 - 1°.

No significant difference is found between Model 2 and Model 3 which differ only by the collision frequency. The collision frequencies in these models do not seem to be a determining factor affecting the width of the coupling window, or are of secondary importance compared to the gradient of electron density.

CHAPTER 4

CONCLUSIONS AND RECOMMENDATIONS

The objective of this research was to demonstrate the possible role of o- to x- mode coupling in ionospheric radiowave heating experiments. Most previous related studies and experiments have not considered the importance of o- to x-mode coupling near the plasma frequency, which may result in intense radiowave energy absorption in the ionospheric plasma [41,46]. Theory and simulations in this report indicate that mode coupling may provide a viable explanation for many experimental observations and should be an efficient heating mechanism for enhancement of future experiments. The approach, conclusions and recommendations regarding mode coupling and its relationship to high power HF modification experiments are reviewed here.

In Chapter 1 the complex nature of the ionosphere due to the Earth's magnetic field and the importance of high-power HF ionospheric modification and its possible application to over-the-horizon communications were briefly discussed. In Chapter 2 the relevant theory of electromagnetic wave propagation in the ionosphere was reviewed as a basis for understanding the coupling

phenomenon. This chapter considered the differential equations governing electromagnetic wave propagation, the full wave solution technique and the method of extracting wave components from the total field to determine the reflection coefficients. In Chapter 3 parameters of the three ionospheric models chosen for study, demonstration of the theory with sample full wave solutions and roots of the Booker quartic and reflection coefficients were presented. The major results are briefly summarized below:

- For the vertical incidence case standing waves below X = 1 indicated the presence of strongly reflected downgoing waves. The reflection coefficients for the sample model were R(E) = 0.889 and R(H) = 0.889. The imaginary part of q was very small throughout the propagation path, indicating small energy loss; this is also supported by the large reflection coefficients. In this case vertical incidence ionospheric heating is seen to be very inefficient.

- For propagation at the critical angle of incidence in the S-N direction, there were no

standing waves below X_R, indicating the absence of any strongly reflected wave. The reflection coefficients for the sample model (Model 1) were R(E) = 6.4450 x 10^{-3} and R( ) = 6.9295 x 10^{-3}. The roots of the quartic indicated that the upgoing o-wave couples to the upgoing x-wave which then reflects just above the X = 1 level. This x-wave travels downwards, approaching the plasma resonance region X_R. The imaginary part of q is very small throughout the propagation path except in a narrow region near the X_R level for the x-wave. This results in attenuation of wave fields and absorption of the incident energy by conversion to heat. Peaking of the E_z component was observed near the plasma resonance region. This implies that the absorption of energy, combined with the large E_z field, should be capable of significantly modifying the ionosphere near the X_R level.

- For propagation at the critical angle of incidence in the N-S direction, just like the S-N case, there were no standing waves below

the X_R level, indicating absence of a strongly reflected wave. The reflection coefficients for the sample model were $R(E) = 2.4455 \times 10^{-2}$ and $R(H) = 2.3433 \times 10^{-2}$. In contrast to the S-N results, there were standing waves between the X_R and 1 + Y levels. The roots of the Booker quartic indicated that the upgoing o-wave couples to the upgoing x-wave near the X = 1 level. This x-wave then reflects from the 1 + Y level and approaches the plasma resonance region X_R. The imaginary part of q was very small throughout the propagation path, except near the X_R level which results in attenuation of the fields and absorption of the incident energy through conversion to heat. This absorption is expected to modify the ionosphere significantly near the X_R level.

- The effective coupling region around the critical angle of incidence was determined for the three models considered. The results revealed that the coupling window is approximately circular, and that the determining factor affecting its angular width

or its diameter is the gradient of the electron density. Among three models, the one with the steepest gradient had the widest coupling window. Therefore, as expected from theory, steeper gradients are most favorable for effective coupling of incident energy into the ionospheric plasma.

A general conclusion deduced from the results of this study is that oblique propagation in the magnetic meridian near critical coupling angles should play a significant role in ionospheric radiowave modification and, therefore, help explain many of the observed experimental phenomena. A number of recommendations regarding future investigations about the mode coupling phenomenon follow:

- The models used here were simple representations of the ionosphere. Further computations are required for numerous other models having different electron density profiles and collision frequency profiles at different geomagnetic locations throughout the world.

- Experiments need to be performed to validate the findings. These should consist of ground-based ionospheric soundings as well as in situ probing of the electromagnetic wave fields with rockets and satellites.

- Existing experimental data, obtained at several locations of the Earth, should be examined with the emphasis placed on the o- to x-mode coupling phenomenon.

- The phenomenon of o- to x-wave mode coupling should be carefully considered in the context of future high-power HF radiowave heating experiments.

- The theoretical framework of the coupling phenomenon should be expanded to include nonlinear effects, such as plasma wave generation and irregularity scattering.

REFERENCES

[1] Utlaut, W. F. (1970), "An ionospheric modification experiment using very high power, high frequency transmission," J. Geophys. Res. 75, 6402-6405.

[2] Gordon, W. E., H. C. Carlson and R. L. Showen (1971), "Ionospheric heating at Arecibo: First tests," J. Geophys. Res., 76, 7808-7813.

[3] Utlaut, W. F. and R. Cohen (1971), "Modifying the ionosphere with intense radio waves," Science, 175, 245.

[4] Carlson, H. C., W. E., Gordon and R. L. Showen (1972), "High frequency induced enhancements of the incoherent scatter spectrum at Arecibo," J. Geophys. Res., 77, 1242-1250.

[5] Gordon, W. E. and H. C. Carlson (1974), "Arecibo heating experiments," Radio Sci., 9, 1041-1047.

[6] Utlaut, W. F. (1975), "Ionospheric modification induced by high power HF transmitters -- A potential for extended range VHF-UHF communications and plasma physics research," Proc. IEEE, 63, 1022-1043.

[7] Muldrew, D. B. and R. L. Showen (1977), "Height of the HF-enhanced plasma line at Aerecibo," J. Geophys. Res., 82, 4793.

[8] Carlson, H. C. and L. M. Duncan (1977), "HF excited instabilities in space plasma," Radio Sci., 12, 1001-1013.

[9] Walker, J. C. G. (1979), "Active experimentation with the ionospheric plasma," Rev. Geophys. Space Phys., 17, 534-544.

[10] Duncan, L. M. and W. E. Gordon (1982), "Ionospheric modification by high power radio waves," J. Atmos. Terr. Phys., 44, 1009-1013.

[11] Stubbe, P., H. Kopka, H. Lauche, M. T. Rietveld, A. Brekke, O. Holt, T. B. Jones, T. Robinson, A. Hedberg, B. Thide', M. Crochet and H. J. Lotz (1982), "Ionospheric modification experiments in northern Scandinavia," J. Atmos. Terr. Phys., 44, 1025-1042.

[12] Stubbe, P. and H. Kopka (1983), "Summary of results obtained with the Tromso heating facility," Radio Sci., 18, 831-834.

[13] Gurevich, A. V. and V. V. Migulin (1982), "Investigations in the U.S.S.R. of non-linear phenomena in the ionosphere," J. Atmos. Terr. Phys., 44, 1019-1024.

[14] Duncan, L. M. and R. A. Behnke (1978), "Observations of self-focusing electromagnetic waves in the ionosphere," Phys. Rev. Lett, 41, 998-1001.

[15] LaHoz, C. A. (1982), Ph.D. thesis, Cornell University, Ithaca, New York.

[16] Frey, A. (1982), Ph.D. thesis, Rice University, Houston, Texas.

[17] Allen, E. M., G. D. Thome and P. B. Rao (1974), "HF phased array observations of heater-induced spread-F," Radio Sci., 9, 905.

[18] Tushentsova, I. A., D. I. Fischuk, Ye. Ye. Tzedilina (1975), "Investigation of the global properties of the ionospheric wave ducts," Geomagn. Aeron., 15(1), 62-66.

[19] Toman, K., D. C. Miller (1977), "Computational study of long-range high frequency ionospheric ducting," Radio Sci. 12(3), 467-476.

[20] Gurevich, A. V. and Ye. Ye. Tzedilina (1976), "Trapping of radiation in the ionospheric duct during scattering on artificial inhomogeneties," Geomagn. Aeron. 15(6), 713-715.

[21] Vever, A. S., T. P. Danilova, A. G. Shlionsky (1978), "Possibility of the trapping of radio waves, scattered by meteor trails, by ionospheric ducts," Goemagn. Aeron., 18(3), 306-308.

[22] Toman, K. (1979), "High-frequency ionospheric ducting: A review," Radio Sci., 14(3) 447-453.

[23] Stubbe, P., H. Kopka, M. T. Rietveld (1982), "ELF and VLF wave generation by modulated HF heating of the current carrying lower ionosphere," J. Atmos. Terr. Phys., 44, 1123-1135.

[24] Ferraro, A. J., H.S. Lee, R. Allhouse, K. Carroll, A. A. Tomko, F. J. Kelly, R. G. Joiner (1982), "VLF/ELF radiation from the ionospheric dynamo current system modulated by powerful HF signals," J. Atmos. Terr. Phys., 44, 12.

[25] Budden, K. G. (1961), Radio Waves in the Ionosphere, Cambridge University Press, Cambridge, MA.

[26] Ratcliffe, J. A. (1959), The Magneto-ionic Theory and Its Applications to the Ionosphere, University Press, Cambridge, Great Britain.

[27] Yeh, K. C. and C. H Liu (1972), Theory of Ionospheric Waves, Academic Press, New York, NY.

[28] Ginzburg, V. L. (1964), The Propagation of Electromagnetic Waves in Plasmas, Pergamon Press, NY.

[29] Hartree, D. R. (1931), "The propagation of electromagnetic waves in a refracting medium in a magnetic field," Proc. Cambridge Phil. Soc., 27, 143-162.

[30] Appleton, E. V. (1932), "Wireless studies of the ionosphere," J. Inst. Elec. Engrs. Lond., 71, 642-650.

[31] Sen, H. K. and A. A. Wyller (1960), "On the Generalization of the Appleton-Hartree Magnetoionic Formulas," J. Geophys. Res., 65, 3931-3949.

[32] Seliga, T. A. (1966), "Numerical full wave solution techniques for the calculation of low frequency plane wave fields in the ionosphere," J. Inst. Telecom. Engrs., 12, 198-213.

[33] Fialer, P. A. (1974), "Field-aligned scattering from a heated region of the ionosphere - Observations at HF and VHF," Radio Sci., 9, 923.

[34] Minkoff, J., P. Kugelman and J. Weissman (1974), "Radio frequency scattering from a heated ionospheric volume, 1, VHF/UHF field-aligned and plasma-line backscatter measurements," Radio Sci., 9, 941.

[35] Ellis, G. R. (1956), "The Z propagation hole in the ionosphere," J. Atmos. Terr. Phys., 8, 43-54.

[36] Ellis, G. R. (1953), "Angle of arrival of z-echoes," Nature, Lond. 171, 258.

[37] Ellis, G. R. (1953), "F-region triple splitting," J. Atmos. Terr. Phys., 3,263.

[38] Booker, H. G. (1936), "Oblique propagation of electromagnetic waves in a slowly varying non-isotropic medium," Proc. Roy. Soc. A, 341, 1-30.

[39] Booker, H. G. (1938), "Propagation of wave-packets incident obliquely upon a stratified doubly refracting ionosphere," Phil. Trans. R. Soc. Lond. A237, 411-451.

[40] Budden, K. G. (1980), "The theory of radio windows in the ionosphere and magnetosphere," J. Atmos. Terr. Phys., 42, 287-298.

[41] Seliga, T. A. (1985), "Ionospheric heating via ordinary to extraordinary mode wave coupling," Radio Sci., 20, 565-574.

[42] Blachier, P. B. and P. Bouchet (1966), "Etude de l'interaction coherente de deux ondes dans um plasma: Application aux radiocommunications a grande distance," Annales de Radioelectricite, XXI, 171-194.

[43] Bouchet, P. (1971), "Accessibilite a la resonance plasma electronique dans la region-F d'une onde emise au sol," J. Atmos. Terr. Phys., 33, 89-100.

[44] Pitteway, M. L. V. (1965), "The numerical calculation of wave-fields, reflexion coefficients and polarizations for long radio waves in the lower ionosphere," II, Trans. Roy. Soc. A (London), 257, 219-241.

[45] Clemmow, P. C. and J. Heading (1954), "Coupled forms of the differential equations governing radio propagation in the ionosphere," Proc Cambridge Phil. Soc., 50, Part 2, 319-333.

[46] Seliga, T. A. (1972), "Phenomena associated with very high power, high frequency F-region modification below the critical frequency," J. Atmos. Terr. Phys, 34, 1827-1841.

APPENDIX A

Cartesian Components of Electric and Magnetic Fields
for the Ionospheric Models 1 and 2.

Wave Frequency	: 5.0	E 6	Angle of Incidence	: 0.000	E 0
Magnetic Y Vector	: 3.150	E-1	Con (1)	: 2.700	E 11
Tot. Geomag. Field	: 5.643	E-5	Con (2)	: 1.800	E 11
X-Dir Cosine of Y	:-3.789	E-1	Con (3)	: 0.000	E 0
Y-Dir Cosine of Y	: 0.000	E-0	Con (4)	: 1.000	E 3
Z-Dir Cosine of Y	: 9.255	E-1	Con (5)	: 1.000	E 3

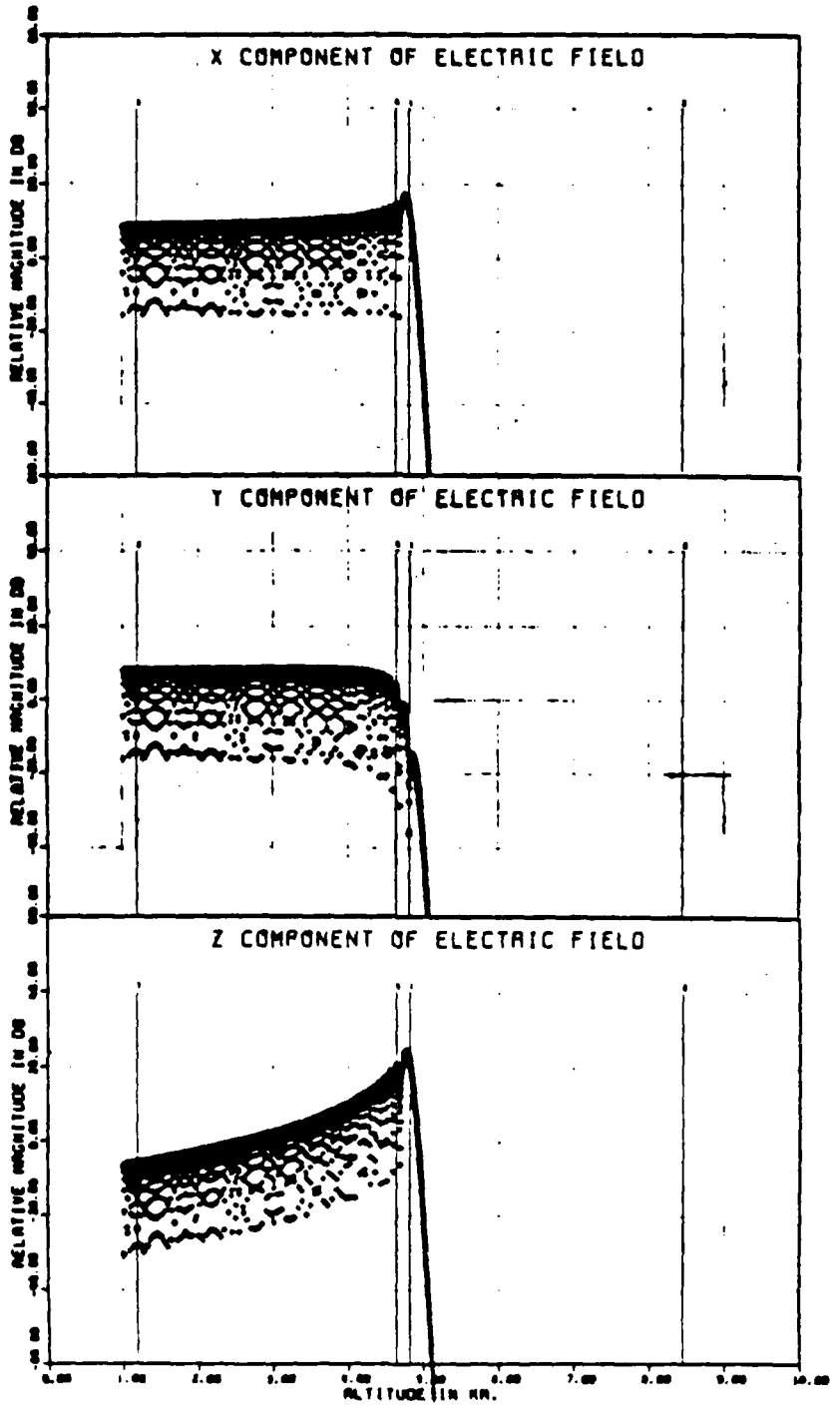

Fig. A.1 Model 1, x, y, z components of electric field for the vertical incidence case

Wave Frequency	: 5.0	E 6	Angle of Incidence	: 1.070	E 1
Magnetic Y Vector	: 3.150	E-1	Con (1)	: 2.700	E 11
Tot. Geomag. Field	: 5.643	E-5	Con (2)	: 1.800	E 11
X-Dir Cosine of Y	:-3.789	E-1	Con (3)	: 1.000	E 3
Y-Dir Cosine of Y	: 0.000	E-0	Con (4)	: 1.000	E 4
Z-Dir Cosine of Y	: 9.255	E-1	Con (5)	: 1.000	E 3

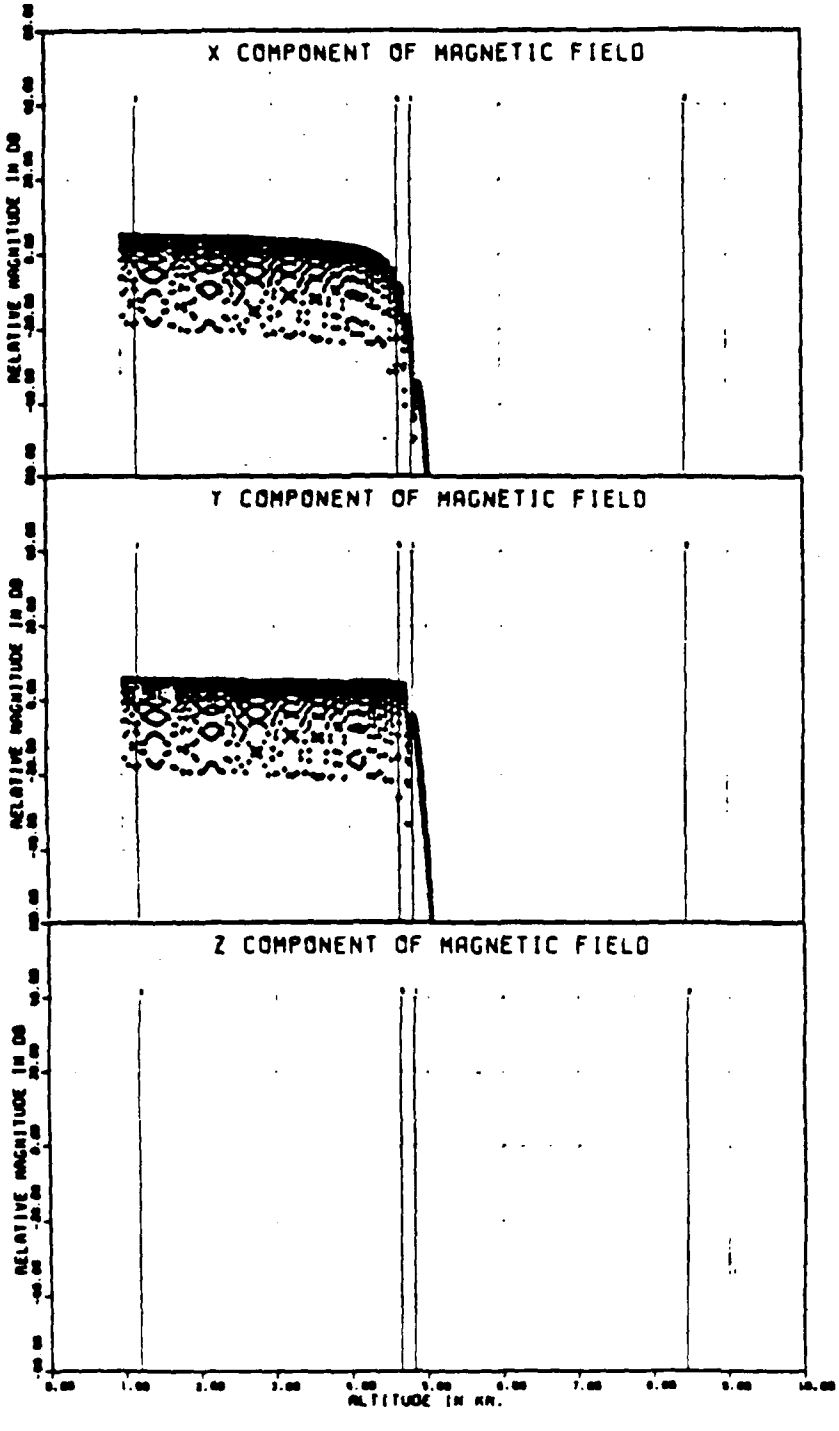

Fig. A.2 Model 1, x, y, z components of magnetic field for the vertical incidence case

Wave Frequency	: 5.0	E 6	Angle of Incidence	:-1.070	E 1
Magnetic Y Vector	: 3.150	E-1	Con (1)	: 2.700	E 11
Tot. Geomag. Field	: 5.643	E-5	Con (2)	: 1.800	E 11
X-Dir Cosine of Y	:-3.789	E-1	Con (3)	: 0.000	E 0
Y-Dir Cosine of Y	: 0.000	E-0	Con (4)	: 1.000	E 3
Z-Dir Cosine of Y	: 9.255	E-1	Con (5)	: 1.000	E 3

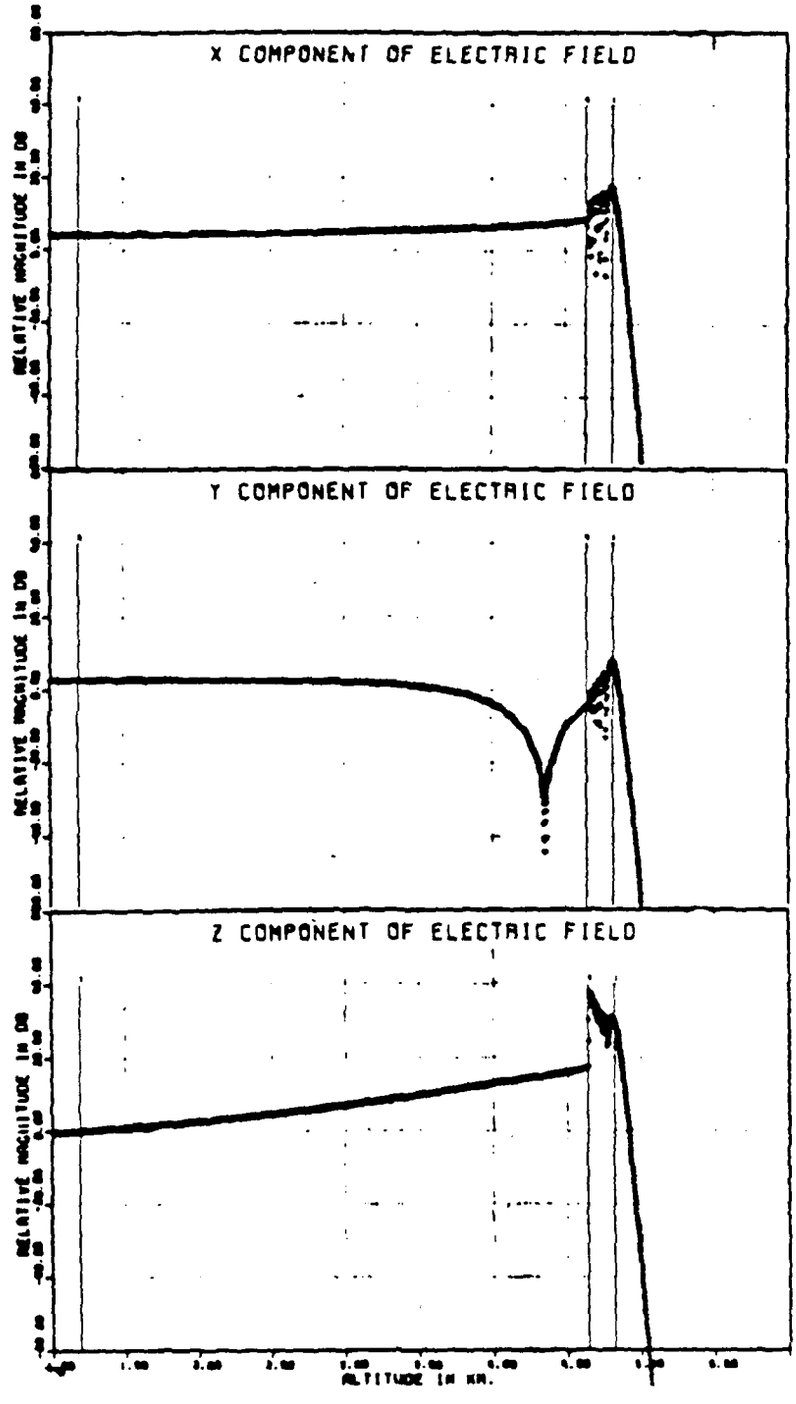

Fig. 4.3 Model 1, x, y, z components of electric field for the critical angle case

Wave Frequency	: 5.0	E 6	Angle of Incidence	: 0.000	E 0
Magnetic Y Vector	: 3.150	E-1	Con (1)	: 2.700	E 11
Tot. Geomag. Field	: 5.643	E-5	Con (2)	: 1.800	E 11
X-Dir Cosine of Y	:-3.789	E-1	Con (3)	: 0.000	E 0
Y-Dir Cosine of Y	: 0.000	E-0	Con (4)	: 1.000	E 3
Z-Dir Cosine of Y	: 9.255	E-1	Con (5)	: 1.000	E 3

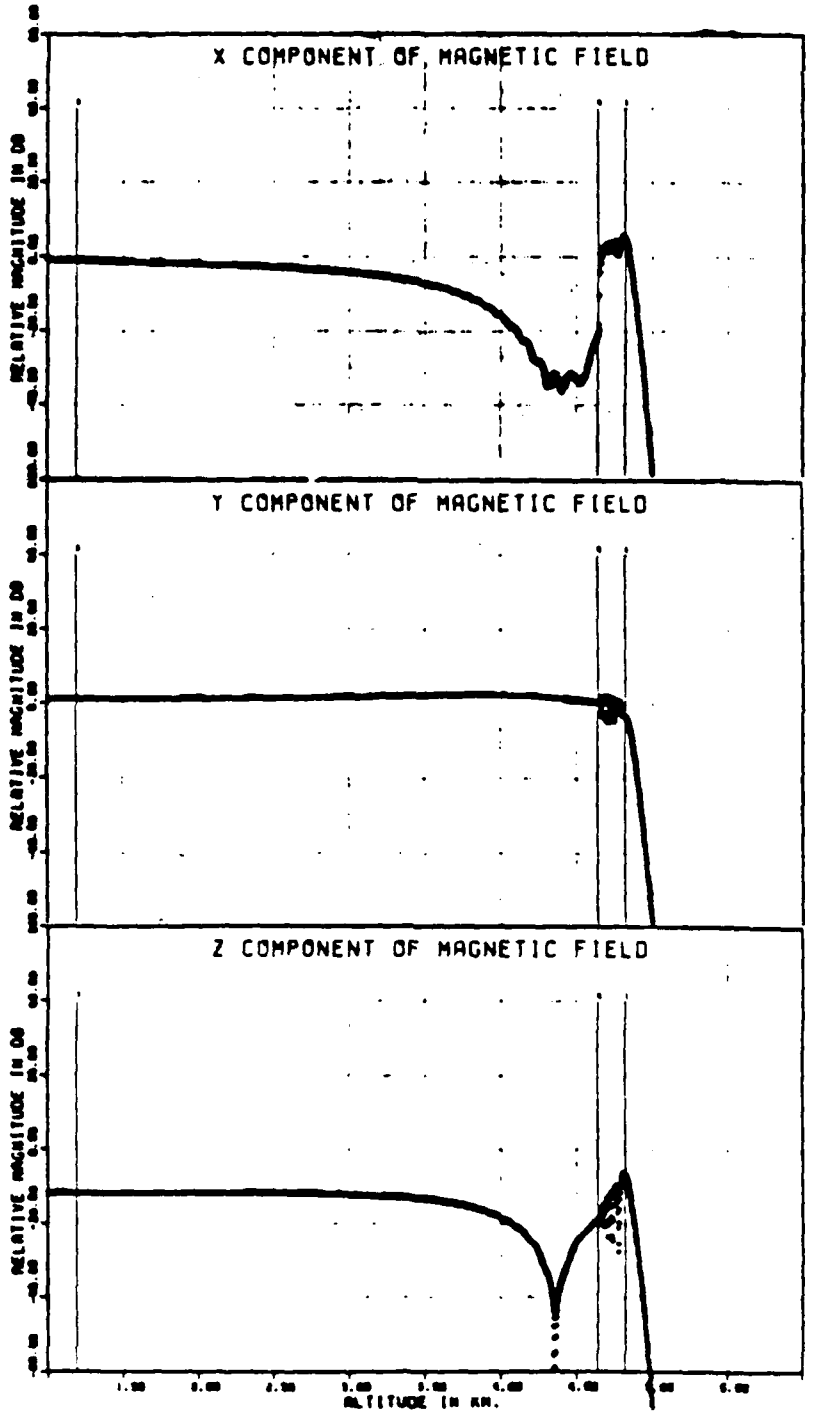

Fig. A.4 Model 1, x,y,z components of magnetic field for the critical angle case

Wave Frequency	: 5.0	E 6	Angle of Incidence	: 1.070	E 1
Magnetic Y Vector	: 3.150	E-1	Con (1)	: 2.700	E 11
Tot. Geomag. Field	: 5.643	E-5	Con (2)	: 1.800	E 11
X-Dir Cosine of Y	:-3.789	E-1	Con (3)	: 1.000	E 3
Y-Dir Cosine of Y	: 0.000	E-0	Con (4)	: 1.000	E 4
Z-Dir Cosine of Y	: 9.255	E-1	Con (5)	: 1.000	E 3

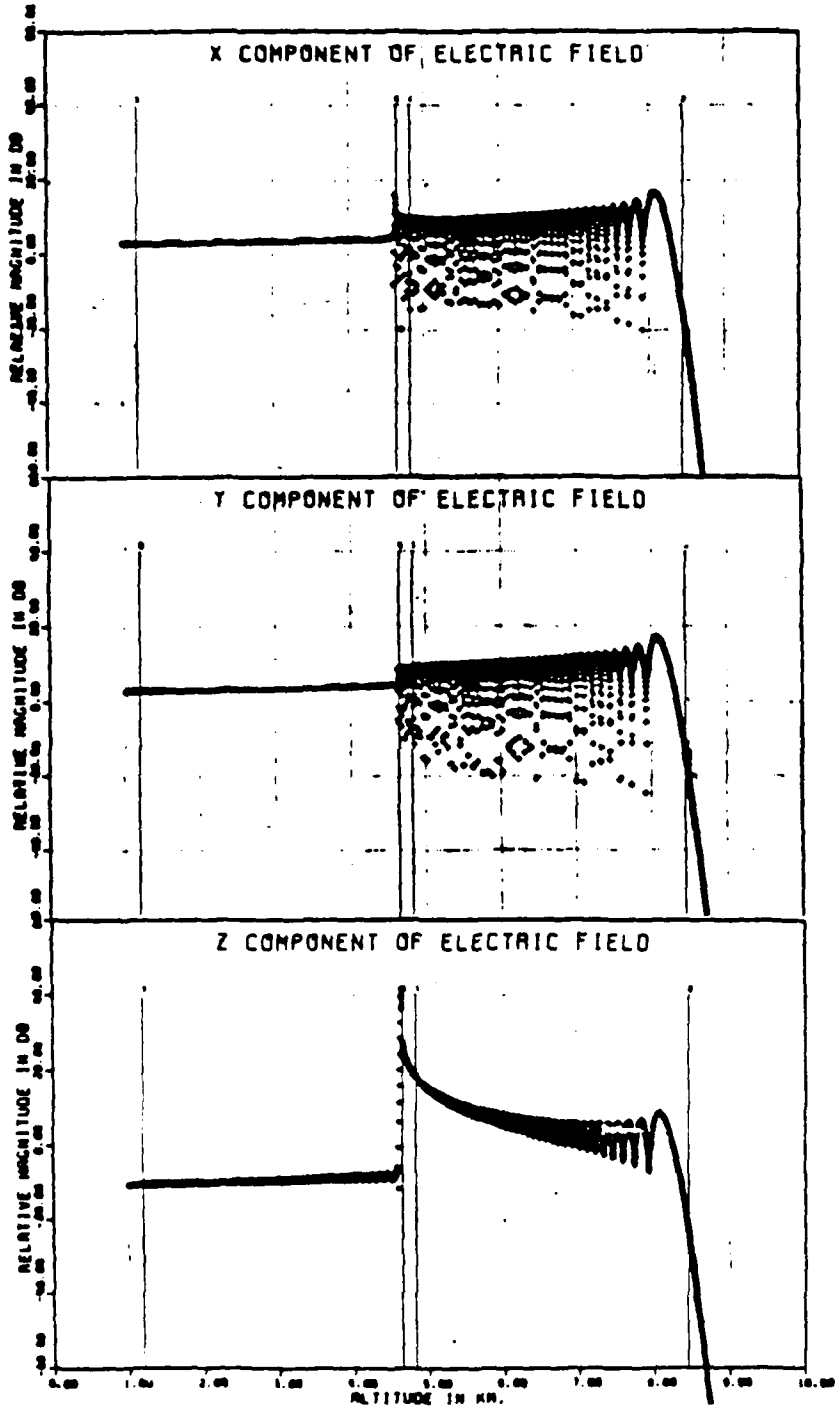

Fig. A.5 Model 1, x, y, z components of electric field for the critical incidence case

Wave Frequency	: 5.0	E 6	Angle of Incidence	:-1.070	E 1
Magnetic Y Vector	: 3.150	E-1	Con (1)	: 2.700	E 11
Tot. Geomag. Field	: 5.643	E-5	Con (2)	: 1.800	E 11
X-Dir Cosine of Y	:-3.789	E-1	Con (3)	: 0.000	E 0
Y-Dir Cosine of Y	: 0.000	E-0	Con (4)	: 1.000	E 3
Z-Dir Cosine of Y	: 9.255	E-1	Con (5)	: 1.000	E 3

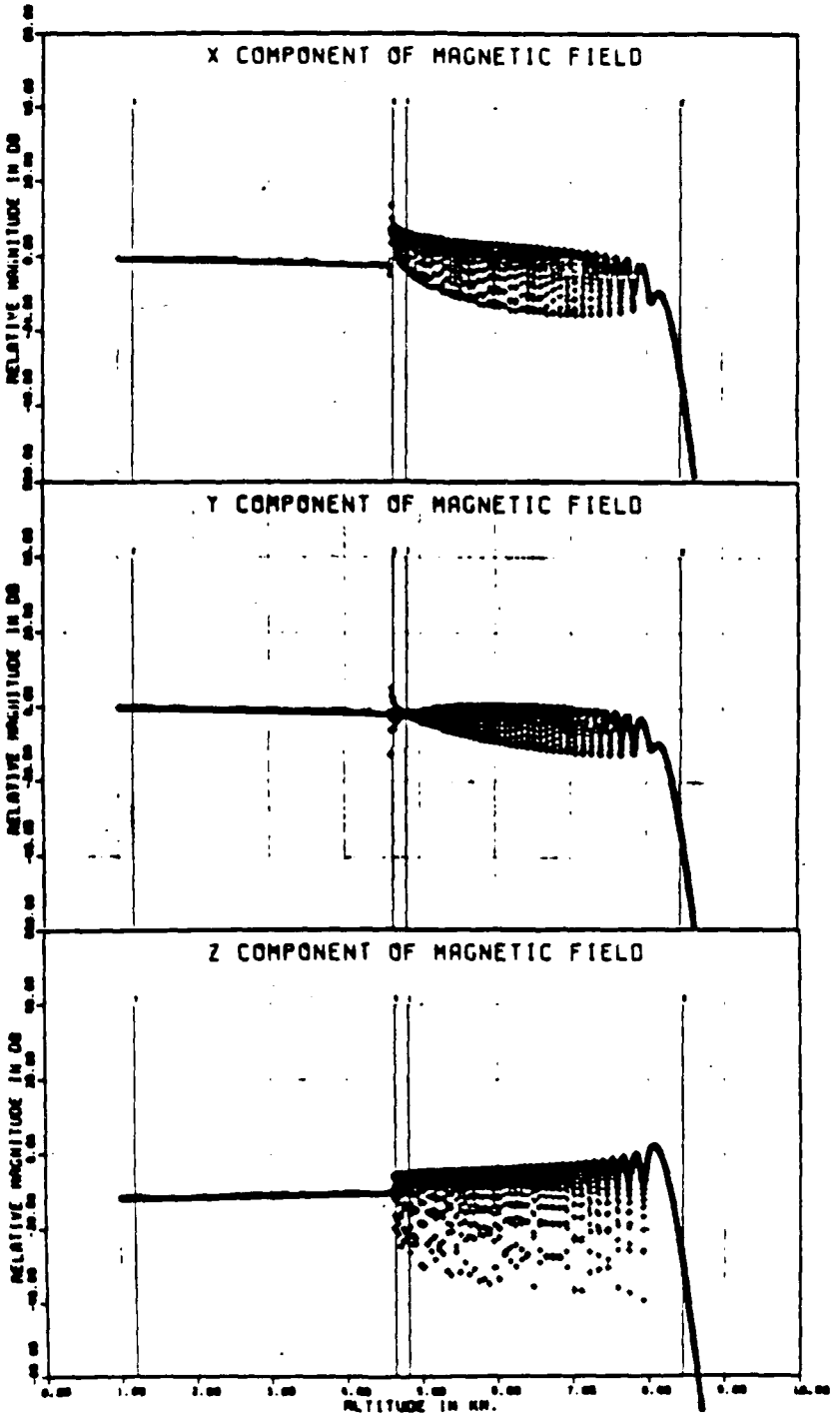

Fig. A.6 Model 1, x, y, z components of magnetic field for the critical incidence case

Wave Frequency	: 5.0	E 6	Angle of Incidence	: 0.000	E 0
Magnetic Y Vector	: -3.150	E-1	Con (1)	: 2.700	E 11
Tot. Geomag. Field	: 5.643	E-5	Con (2)	: 1.800	E 11
X-Dir Cosine of Y	: -3.789	E-1	Con (3)	: 0.000	E 0
Y-Dir Cosine of Y	: 0.000	E-0	Con (4)	: 1.000	E 3
Z-Dir Cosine of Y	: 9.255	E-1	Con (5)	: 1.000	E 3

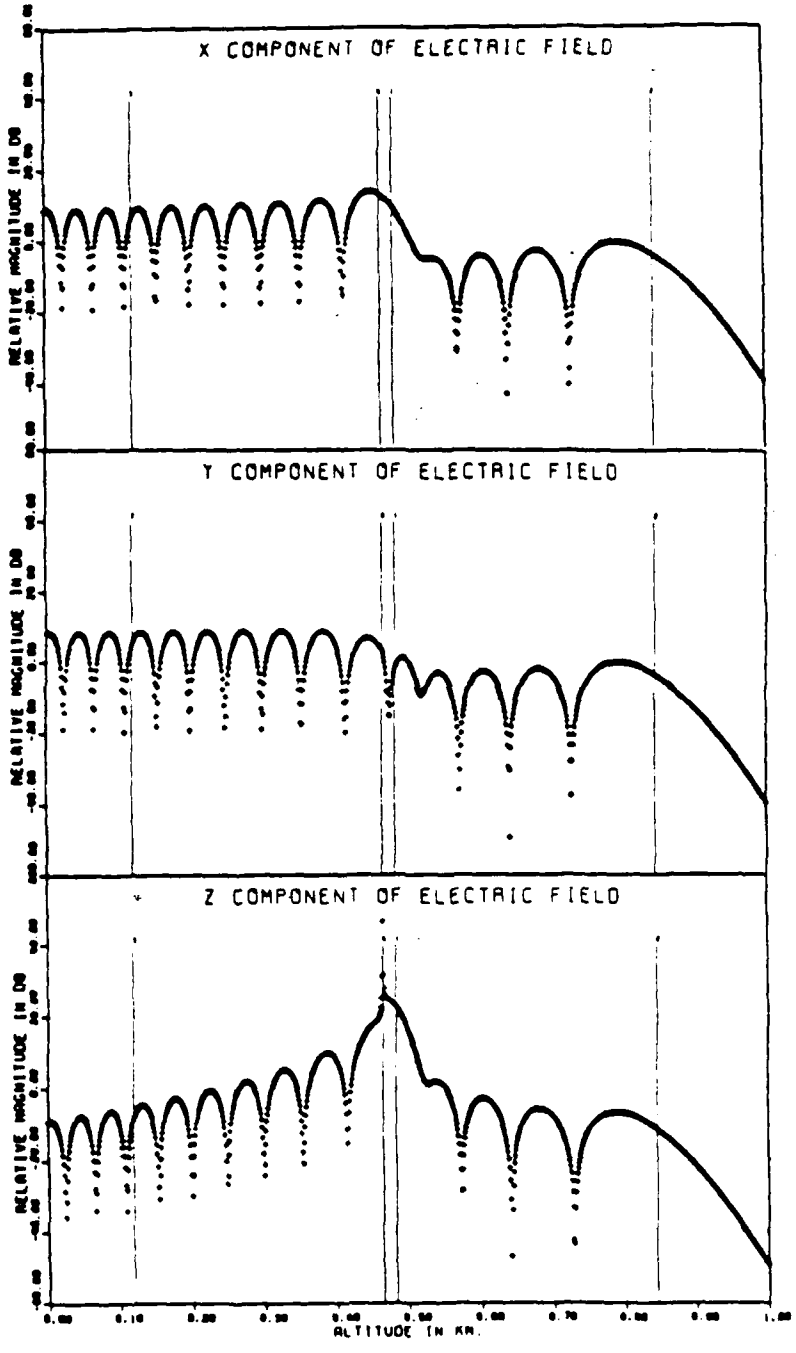

Fig. A.7 Model 2, x, y, z components of electric field for the vertical incidence case

Wave Frequency	: 5.0	E 6	Angle of Incidence	: 0.000	E 0
Magnetic Y Vector	: 3.150	E-1	Con (1)	: 2.700	E 11
Tot. Geomag. Field	: 5.643	E-5	Con (2)	: 1.800	E 11
X-Dir Cosine of Y	:-3.789	E-1	Con (3)	: 0.000	E 0
Y-Dir Cosine of Y	: 0.000	E-0	Con (4)	: 1.000	E 3
Z-Dir Cosine of Y	: 9.255	E-1	Con (5)	: 1.000	E 3

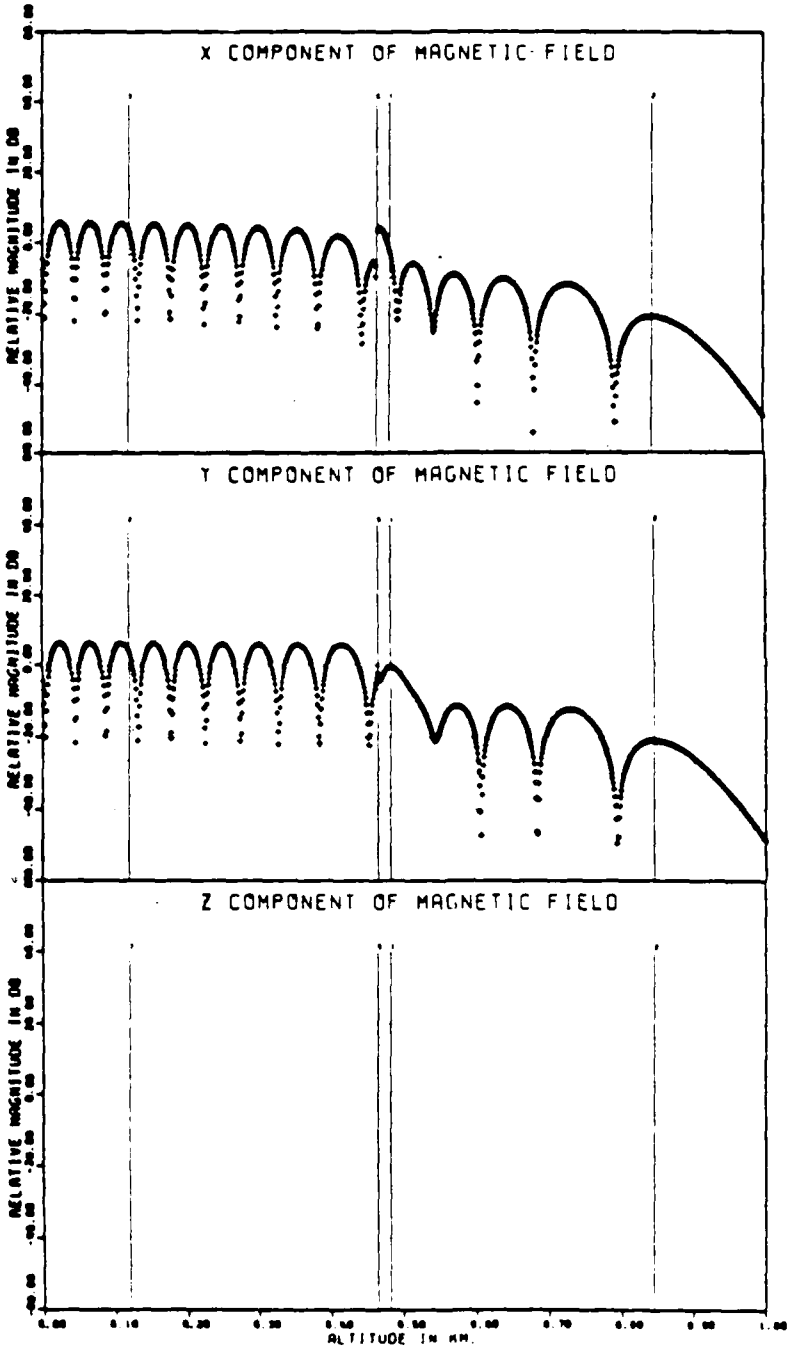

Fig. 4.8 Model 2, x, y, z components of magnetic field for the vertical incidence case

Wave Frequency	: 5.0	E 6	Angle of Incidence	: 1.070	E 1
Magnetic Y Vector	: 3.150	E-1	Con (1)	: 2.700	E 11
Tot. Geomag. Field	: 5.643	E-5	Con (2)	: 1.800	E 11
X-Dir Cosine of Y	:-3.789	E-1	Con (3)	: 1.000	E 3
Y-Dir Cosine of Y	: 0.000	E-0	Con (4)	: 1.000	E 4
Z-Dir Cosine of Y	: 9.255	E-1	Con (5)	: 1.000	E 3

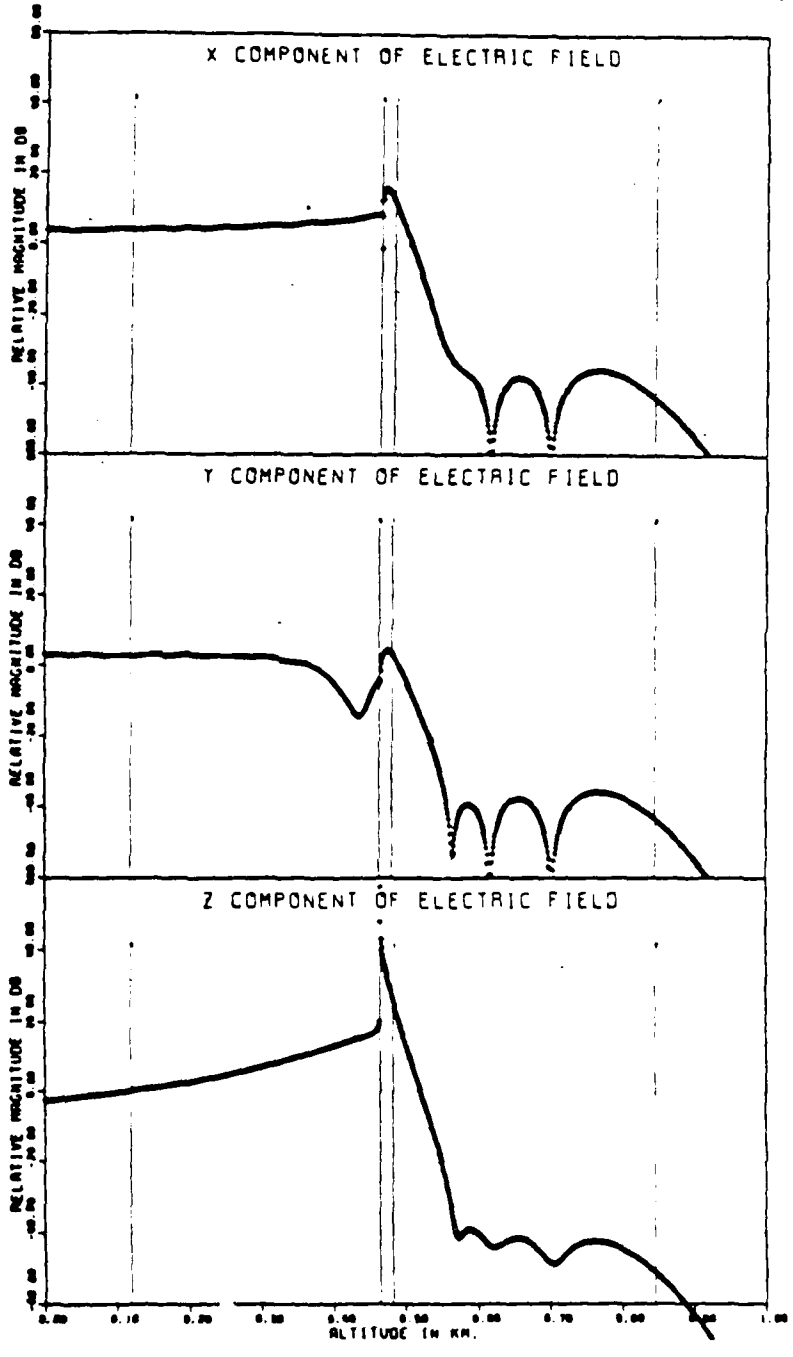

Fig. A.9 Model 2, x, y, z components of electric field for the critical incidence case

Wave Frequency	: 5.0	E 6	Angle of Incidence	: 1.070	E 1
Magnetic Y Vector	: 3.150	E-1	Con (1)	: 2.700	E 11
Tot. Geomag. Field	: 5.643	E-5	Con (2)	: 1.800	E 11
X-Dir Cosine of Y	:-3.789	E-1	Con (3)	: 1.000	E 3
Y-Dir Cosine of Y	: 0.000	E-0	Con (4)	: 1.000	E 4
Z-Dir Cosine of Y	: 9.255	E-1	Con (5)	: 1.000	E 3

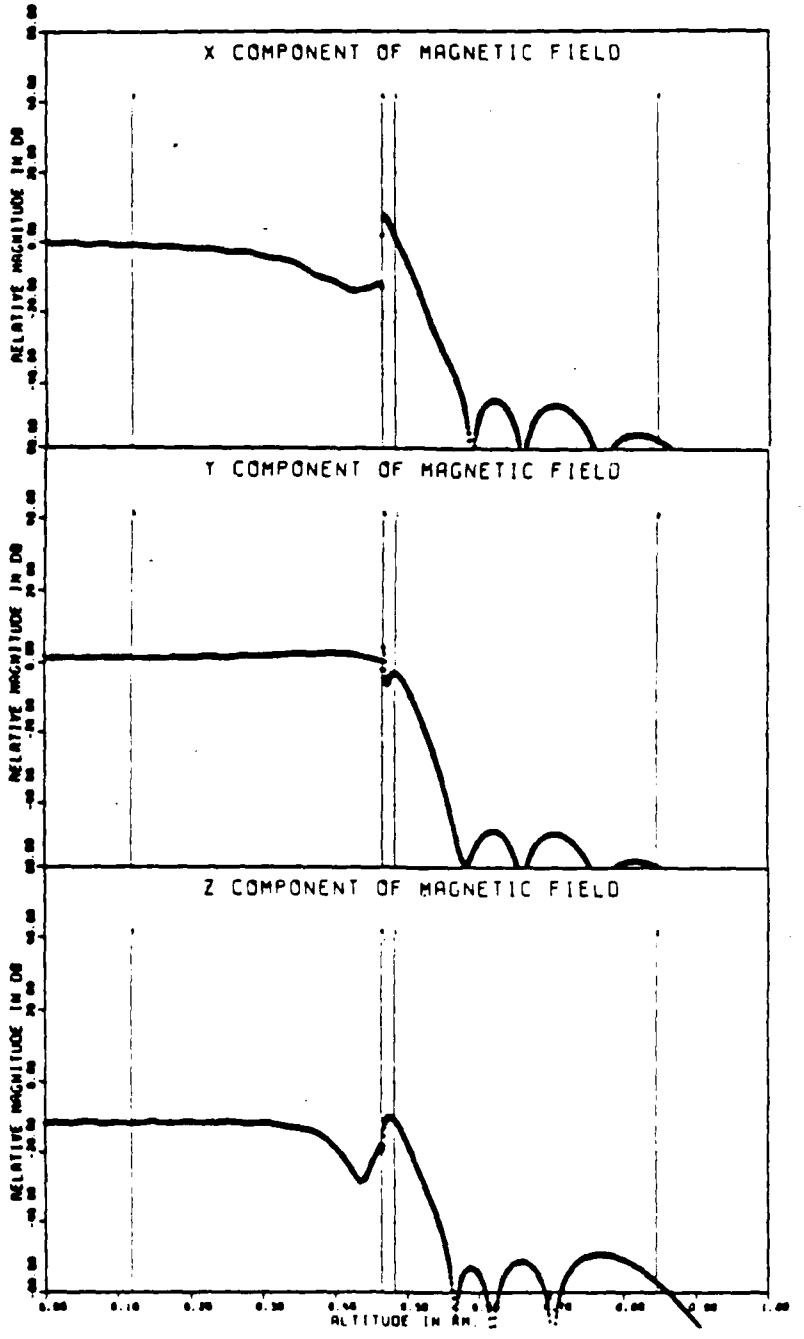

Fig. A.10 Model 3, x, y, z components of magnetic field for the critical incidence case

Wave Frequency	: 3.0	E 6	Angle of Incidence	:-1.070	E 1
Magnetic Y Vector	: 3.150	E-1	Con (1)	: 2.700	E 11
Tot. Geomag. Field	: 5.643	E-5	Con (2)	: 1.800	E 11
X-Dir Cosine of Y	:-3.789	E-1	Con (3)	: 0.000	E 0
Y-Dir Cosine of Y	: 0.000	E-0	Con (4)	: 1.000	E 3
Z-Dir Cosine of Y	: 9.255	E-1	Con (5)	: 1.000	E 3

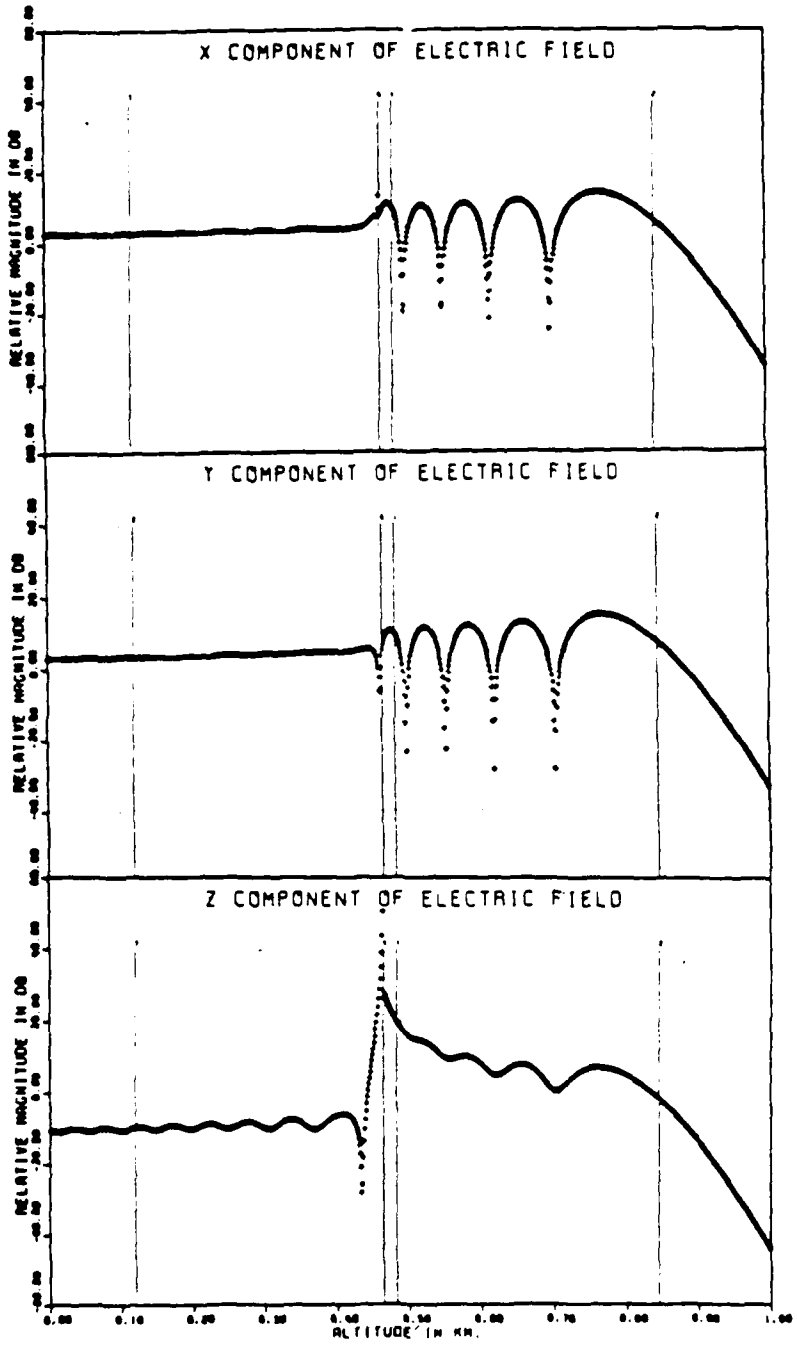

Fig. A.11 Model 2, x, y, z components of electric field for the critical incidence case

Wave Frequency	: 5.0	E 6	Angle of Incidence	:-1.070	E 1
Magnetic Y Vector	: 3.150	E-1	Con (1)	: 2.700	E 11
Tot. Geomag. Field	: 5.643	E-5	Con (2)	: 1.800	E 11
X-Dir Cosine of Y	:-3.789	E-1	Con (3)	: 0.000	E 0
Y-Dir Cosine of Y	: 0.000	E-0	Con (4)	: 1.000	E 3
Z-Dir Cosine of Y	: 9.255	E-1	Con (5)	: 1.000	E 3

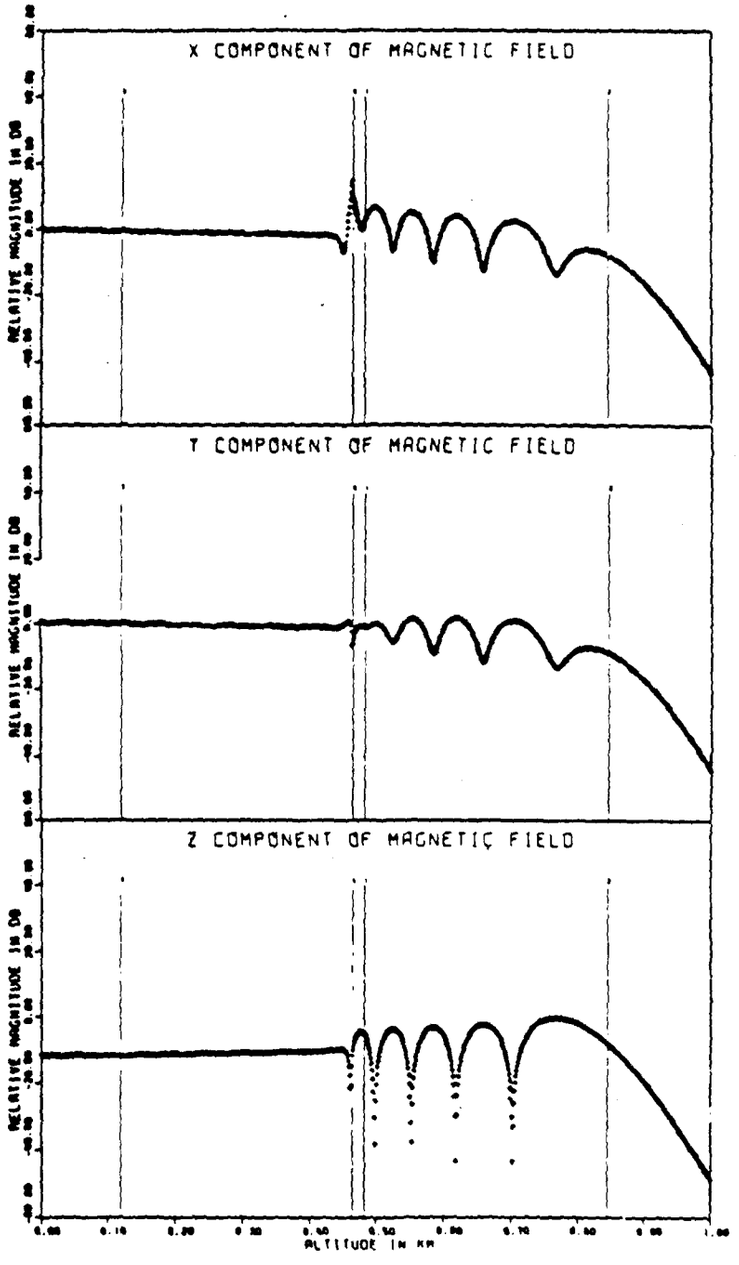

Fig. A.12 Model 2, x, y, z components of magnetic field for the critical incidence case

APPENDIX B

Reflection Coefficients for the Ionospheric Models 1, 2 and 3.

Table B.1 - Reflection Coefficients - Model 1, in the Magnetic Meridian.

WAVE FREQUENCY =	5.0000E+06	CRITICAL INCIDENCE =	1.0696E+01
MAG. Y VECTOR =	3.1590E-01	STARTING HEIGHT =	6.0000E+03
GEOMAG. FIELD =	5.6426E-05	ENDING HEIGHT =	1.0000E+03
X-DIR COS OF Y =	-3.7890E-01	INCREMENT =	-5.0000E-02
Y-DIR COS OF Y =	0.0000E+00	SCALE HEIGHT =	1.0000E+04
Z-DIR COS OF Y =	9.2546E-01	COLLISIONS =	1.0000E+03

REFLECTION COEFFICIENTS

EX	EY	ET	MX	MY	MT	ANGL
8.8877E-01	8.8877E-01	8.8877E-01	8.8877E-01	8.8877E-01	8.8877E-01	0.0000E+00
8.8015E-01	8.9945E-01	8.7709E-01	9.0011E-01	8.7252E-01	8.8561E-01	2.0000E+00
8.7200E-01	9.1101E-01	8.6591E-01	9.2663E-01	8.5765E-01	8.8963E-01	4.0000E+00
8.6381E-01	9.2337E-01	8.5472E-01	9.5117E-01	8.4240E-01	8.9011E-01	6.0000E+00
8.0996E-01	8.8705E-01	7.9853E-01	9.2377E-01	7.8299E-01	8.4295E-01	8.0000E+00
6.5534E-01	7.2697E-01	6.4491E-01	7.4148E-01	6.3067E-01	6.8543E-01	9.0000E+00
5.1032E-01	5.6985E-01	5.0172E-01	5.8871E-01	4.8598E-01	5.3506E-01	9.5000E+00
3.1858E-01	3.5817E-01	3.1293E-01	3.7747E-01	3.0418E-01	3.3466E-01	1.0000E+01
1.3963E-01	1.5785E-01	1.3705E-01	1.6678E-01	1.3356E-01	1.4705E-01	1.0400E+01
4.5700E-03	7.4490E-03	6.4490E-03	7.8964E-03	6.2729E-03	6.9295E-03	1.0700E+01
1.4302E-01	1.6308E-01	1.4022E-01	1.7299E-01	1.3836E-01	1.5107E-01	1.1000E+01
3.6221E-01	4.1605E-01	3.5479E-01	4.4298E-01	3.4451E-01	3.8354E-01	1.1500E+01
7.4284E-01	8.2832E-01	7.3122E-01	8.7107E-01	7.1531E-01	7.7627E-01	1.2000E+01
7.5679E-01	8.8999E-01	7.3922E-01	9.5749E-01	7.1451E-01	8.0730E-01	1.3000E+01
8.2584E-01	1.0270E+00	8.0241E-01	1.1234E+00	7.6761E-01	8.9913E-01	1.4000E+01

WAVE FREQUENCY =	5.0000E+06	CRITICAL INCIDENCE =	-1.0700E+01
MAG. Y VECTOR =	3.1590E-01	STARTING HEIGHT =	9.0000E+03
GEOMAG. FIELD =	5.6426E-05	ENDING HEIGHT =	1.0000E+03
X-DIR COS OF Y =	-3.7890E-01	INCREMENT =	-5.0000E-02
Y-DIR COS OF Y =	0.0000E+00	SCALE HEIGHT =	1.0000E+04
Z-DIR COS OF Y =	9.2546E-01	COLLISIONS =	1.0000E+03

REFLECTION COEFFICIENTS

EX	EY	ET	MX	MY	MT	ANGL
8.8877E-01	8.8877E-01	8.8877E-01	8.8877E-01	8.8877E-01	8.8877E-01	0.0000E+00
8.9799E-01	8.7873E-01	9.0112E-01	8.7035E-01	9.0542E-01	8.8904E-01	-2.0000E+00
9.0792E-01	8.6905E-01	9.1430E-01	8.5239E-01	9.2310E-01	8.8993E-01	-4.0000E+00
9.1831E-01	8.5908E-01	9.2906E-01	8.3403E-01	9.4167E-01	8.9118E-01	-6.0000E+00
8.7986E-01	8.0341E-01	8.9244E-01	7.7150E-01	9.1016E-01	8.4543E-01	-8.0000E+00
7.1994E-01	6.4902E-01	7.3159E-01	6.1963E-01	7.4281CE-01	6.8835E-01	-9.0000E+00
4.6366E-01	5.0480E-01	4.7331E-01	4.8048E-01	5.8706E-01	5.3761E-01	-9.5000E+00
3.5569E-01	3.1635E-01	3.6206E-01	3.0018E-01	3.7126E-01	3.3836E-01	-1.0000E+01
1.4876E-01	1.3159E-01	1.5156E-01	1.2455E-01	1.5559E-01	1.4126E-01	-1.0400E+01
8.2386E-03	7.2569E-03	8.3981E-03	6.8551E-03	8.6288E-03	7.8112E-03	-1.0700E+01
1.6920E-01	1.4880E-01	1.7259E-01	1.3991E-01	1.7747E-01	1.6019E-01	-1.1000E+01
4.0962E-01	3.5861E-01	4.1818E-01	3.3508E-01	4.3088E-01	3.8684E-01	-1.1500E+01
8.3859E-01	7.1309E-01	8.5847E-01	6.6277E-01	8.8814E-01	7.8609E-01	-1.2000E+01
9.6301E-01	8.0505E-01	9.8771E-01	7.4239E-01	1.0252E+00	8.9834E-01	-1.3000E+01
1.0094E+00	8.1188E-01	1.0389E+00	7.3556E-01	1.0861E+00	9.3243E-01	-1.4000E+01

Table B.2 - Reflection Coefficients - Model 1, off the Magnetic Meridian.

WAVE FREQUENCY =	5.0000E+06	CRITICAL INCIDENCE =	1.0696E+01
MAG. Y VECTOR =	3.1590E-01	STARTING HEIGHT =	6.0000E+03
GEOMAG. FIELD =	5.6426E-05	ENDING HEIGHT =	1.0000E+03
X-DIR COS OF Y =	-3.7890E-01	INCREMENT =	-5.0000E-02
Y-DIR COS OF Y =	0.0000E+00	SCALE HEIGHT =	1.0000E+04
Z-DIR COS OF Y =	9.2546E-01	COLLISIONS =	1.0000E+03

REFLECTION COEFFICIENTS

EX	EY	EZ	HX	HY	HZ	ANGL
6.5700E-03	7.4590E-03	6.2729E-03	6.4450E-03	7.0964E-03	6.9295E-03	0.0000E+00
2.2008E-01	2.4979E-01	2.1589E-01	2.6442E-01	2.1013E-01	2.3210E-01	5.0000E-01
4.2356E-01	4.8036E-01	4.1548E-01	5.0840E-01	4.0444E-01	4.4657E-01	1.0000E+00
7.0262E-01	7.9567E-01	6.9028E-01	8.4143E-01	6.7219E-01	7.4123E-01	2.0000E+00
8.1886E-01	9.2097E-01	8.0242E-01	9.7277E-01	7.8233E-01	8.6682E-01	3.0000E+00
8.5461E-01	9.4669E-01	8.3762E-01	9.9991E-01	8.1788E-01	8.9347E-01	5.0000E+00
8.6584E-01	9.3011E-01	8.4890E-01	9.6892E-01	8.3290E-01	8.9436E-01	8.0000E+00

WAVE FREQUENCY =	5.0000E+06	CRITICAL INCIDENCE =	-1.0700E+01
MAG. Y VECTOR =	3.1590E-01	STARTING HEIGHT =	9.0000E+03
GEOMAG. FIELD =	5.6426E-05	ENDING HEIGHT =	1.0000E+03
X-DIR COS OF Y =	-3.7890E-01	INCREMENT =	-5.0000E-02
Y-DIR COS OF Y =	0.0000E+00	SCALE HEIGHT =	1.0000E+04
Z-DIR COS OF Y =	9.2546E-01	COLLISIONS =	1.0000E+03

REFLECTION COEFFICIENTS

EX	EY	EZ	HX	HY	HZ	ANGL
8.2386E-03	7.2569E-03	8.6826E-03	8.3981E-03	6.8551E-03	7.8112E-03	0.0000E+00
2.6424E-01	2.3282E-01	2.6936E-01	2.1994E-01	2.7674E-01	2.5056E-01	5.0000E-01
4.8092E-01	4.2407E-01	4.9026E-01	4.0069E-01	5.0366E-01	4.5614E-01	1.0000E+00
7.9140E-01	7.0042E-01	8.0731E-01	6.6231E-01	8.2904E-01	7.5184E-01	2.0000E+00
9.1504E-01	8.1361E-01	9.3317E-01	7.7031E-01	9.5768E-01	8.7044E-01	3.0000E+00
9.3979E-01	8.4846E-01	9.5889E-01	8.0655E-01	9.8207E-01	8.9898E-01	5.0000E+00
9.2851E-01	8.6436E-01	9.4702E-01	8.2976E-01	9.6522E-01	8.9853E-01	8.0000E+00

Table B.3 - Reflection Coefficients - Model 2 - in the Magnetic Meridian.

WAVE FREQUENCY =	5.0000E+06	CRITICAL INCIDENCE =	1.0696E+01
MAG. Y VECTOR =	3.1590E-01	STARTING HEIGHT =	1.0000E+03
GEOMAG. FIELD =	5.6426E-05	ENDING HEIGHT =	0.0000E+00
X-DIR COS OF Y =	-3.7890E-01	INCREMENT =	-1.0000E-01
Y-DIR COS OF Y =	0.0000E+00	SCALE HEIGHT =	1.0000E+03
Z-DIR COS OF Y =	9.2546E-01	COLLISIONS =	1.0000E+03

REFLECTION COEFFICIENTS

EX	EY	EZ	HX	HY	HZ	ANGL
9.2259E-01	9.2259E-01	9.2259E-01	9.2259E-01	9.2259E-01	9.2259E-01	0.0000E+00
8.9498E-01	9.1092E-01	8.9530E-01	9.1653E-01	8.9011E-01	9.0243E-01	2.0000E+00
8.1643E-01	8.4595E-01	8.1699E-01	8.5651E-01	8.0752E-01	8.3009E-01	4.0000E+00
6.8333E-01	7.0005E-01	6.8401E-01	7.1339E-01	6.5242E-01	6.8004E-01	6.0000E+00
4.2422E-01	4.4634E-01	4.2474E-01	4.6822E-01	4.1484E-01	4.3854E-01	8.0000E+00
3.5236E-01	3.8092E-01	3.5287E-01	3.9153E-01	3.4467E-01	3.6502E-01	8.5000E+00
2.7654E-01	3.0045E-01	2.7696E-01	3.0938E-01	2.6936E-01	2.8707E-01	9.0000E+00
1.9741E-01	2.1557E-01	1.9772E-01	2.2239E-01	1.9219E-01	2.0536E-01	9.5000E+00
1.1611E-01	1.2745E-01	1.1630E-01	1.3173E-01	1.1287E-01	1.2103E-01	1.0000E+01
8.3564E-02	9.1917E-02	8.3706E-02	9.5077E-02	8.1181E-02	8.7181E-02	1.0200E+01
5.1987E-02	5.7305E-02	5.2077E-02	5.9321E-02	5.0474E-02	5.4263E-02	1.0400E+01
2.6146E-02	2.8875E-02	2.6186E-02	2.9914E-02	2.5363E-02	2.7317E-02	1.0600E+01
2.2491E-02	2.5426E-02	2.3014E-02	2.6342E-02	2.2303E-02	2.4039E-02	1.0700E+01
3.0741E-02	3.4030E-02	3.0746E-02	3.5282E-02	2.9866E-02	3.2142E-02	1.0800E+01
4.9018E-02	6.5479E-02	5.9129E-02	6.7937E-02	5.7139E-02	6.1779E-02	1.1000E+01
1.3937E-01	1.5987E-01	1.4000E-01	1.6206E-01	1.3520E-01	1.4668E-01	1.1500E+01
2.2000E-01	2.4678E-01	2.2044E-01	2.5112E-01	2.1259E-01	2.3126E-01	1.2000E+01
3.7003E-01	4.1991E-01	3.7083E-01	4.3939E-01	3.5631E-01	3.9061E-01	1.3000E+01
6.1771E-01	7.1831E-01	6.1892E-01	7.5871E-01	5.9049E-01	6.5723E-01	1.5000E+01
7.7863E-01	9.3127E-01	7.8046E-01	9.9424E-01	7.3998E-01	8.3540E-01	1.7000E+01

WAVE FREQUENCY =	5.0000E+06	CRITICAL INCIDENCE =	-1.0700E+01
MAG. Y VECTOR =	3.1590E-01	STARTING HEIGHT =	1.0000E+03
GEOMAG. FIELD =	5.6426E-05	ENDING HEIGHT =	0.0000E+00
X-DIR COS OF Y =	-3.7890E-01	INCREMENT =	-1.0000E-01
Y-DIR COS OF Y =	0.0000E+00	SCALE HEIGHT =	1.0000E+03
Z-DIR COS OF Y =	9.2546E-01	COLLISIONS =	1.0000E+03

REFLECTION COEFFICIENTS

EX	EY	EZ	HX	HY	HZ	ANGL
9.2259E-01	9.2259E-01	9.2259E-01	9.2259E-01	9.2259E-01	9.2259E-01	0.0000E+00
9.1000E-01	8.9404E-01	9.0968E-01	8.8860E-01	9.1499E-01	9.0249E-01	-2.0000E+00
8.4413E-01	8.1466E-01	8.4354E-01	8.0662E-01	8.5344E-01	8.3029E-01	-4.0000E+00
6.9755E-01	6.6096E-01	6.9683E-01	6.4864E-01	7.0822E-01	6.8040E-01	-6.0000E+00
4.5477E-01	4.2276E-01	4.5416E-01	4.1203E-01	4.6405E-01	4.3542E-01	-8.0000E+00
3.8004E-01	3.5155E-01	3.7949E-01	3.4202E-01	3.8920E-01	3.6686E-01	-8.5000E+00
3.0042E-01	2.7652E-01	2.9997E-01	2.6893E-01	3.0812E-01	2.8540E-01	-9.0000E+00
2.1651E-01	1.9827E-01	2.1617E-01	1.9219E-01	2.2239E-01	2.0614E-01	-9.5000E+00
1.2934E-01	1.1783E-01	1.2912E-01	1.1400E-01	1.3305E-01	1.2407E-01	-1.0000E+01
4.4119E-02	3.5562E-02	4.3956E-02	3.2718E-02	4.6873E-02	4.0210E-02	-1.0200E+01
7.9620E-02	5.4088E-02	5.9518E-02	5.2250E-02	6.1402E-02	5.7559E-02	-1.0400E+01
3.0117E-02	2.7264E-02	3.0064E-02	2.6317E-02	3.1040E-02	2.8819E-02	-1.0600E+01
2.4499E-02	2.2155E-02	2.4455E-02	2.1377E-02	2.5257E-02	2.3433E-02	-1.0700E+01
3.1292E-02	2.8267E-02	3.1236E-02	2.7264E-02	3.2270E-02	2.9918E-02	-1.0800E+01
6.1705E-02	5.5620E-02	6.1593E-02	5.3604E-02	6.3674E-02	5.8947E-02	-1.1000E+01
1.5134E-01	1.3567E-01	1.5106E-01	1.3044E-01	1.5642E-01	1.4479E-01	-1.1500E+01
2.4182E-01	2.1556E-01	2.4132E-01	2.0699E-01	2.5030E-01	2.3003E-01	-1.2000E+01
4.1433E-01	3.6512E-01	4.1344E-01	3.4893E-01	4.3029E-01	3.9250E-01	-1.3000E+01
7.0964E-01	6.0988E-01	7.0792E-01	5.7740E-01	7.4155E-01	6.6496E-01	-1.5000E+01
9.1354E-01	7.8322E-01	9.1069E-01	7.1488E-01	9.6156E-01	8.5070E-01	-1.7000E+01

Table B.4 - Reflection Coefficients - Model 2, off the Magnetic Meridian.

MAG. Y VECTOR	= 3.1590E-01	STARTING HEIGHT	= 1.0000E+03
GEOMAG. FIELD	= 5.6426E-05	ENDING HEIGHT	= 0.0000E+00
X-DIR COS OF Y	= -3.7890E-01	INCREMENT	= -1.0000E-01
Y-DIR COS OF Y	= 0.0000E+00	SCALE HEIGHT	= 1.0000E+03
Z-DIR COS OF Y	= 9.2546E-01	COLLISIONS	= 1.0000E+03

REFLECTION COEFFICIENTS

EX	EY	ET	MX	MY	MT	ANGL
2.4506E-02	2.2162E-02	2.4463E-02	2.1384E-02	2.5264E-02	2.3440E-02	0.0000E+00
4.2292E-02	3.8246E-02	4.2217E-02	3.6904E-02	4.3600E-02	4.0443E-02	1.0000E-01
6.0066E-02	5.4317E-02	5.9955E-02	5.2410E-02	6.1919E-02	5.7450E-02	2.0000E-01
1.1311E-01	1.0236E-01	1.1257E-01	9.8770E-02	1.1666E-01	1.0825E-01	5.0000E-01
1.4812E-01	1.3418E-01	1.4806E-01	1.2948E-01	1.5290E-01	1.4179E-01	7.0000E-01
2.0055E-01	1.8146E-01	2.0017E-01	1.7512E-01	2.0669E-01	1.9184E-01	1.0000E+00
3.6739E-01	3.3322E-01	3.6684E-01	3.2127E-01	3.7841E-01	3.5178E-01	2.0000E+00
5.1821E-01	4.7183E-01	5.1775E-01	4.5591E-01	5.3391E-01	4.9696E-01	3.0000E+00
6.4822E-01	5.9317E-01	6.4456E-01	5.7375E-01	6.6756E-01	6.2278E-01	4.0000E+00
8.3761E-01	7.7671E-01	8.3873E-01	7.5371E-01	8.6109E-01	8.0913E-01	6.0000E+00

WAVE FREQUENCY	= 5.0000E+06	CRITICAL INCICENCE	= 1.0696E+01
MAG. Y VECTOR	= 3.1590E-01	STARTING HEIGHT	= 1.0000E+03
GEOMAG. FIELD	= 5.6426E-05	ENDING HEIGHT	= 0.0000E+00
X-DIR COS OF Y	= -3.7890E-01	INCREMENT	= -1.0000E-01
Y-DIR COS OF Y	= 0.0000E+00	SCALE HEIGHT	= 1.0000E+03
Z-DIR COS OF Y	= 9.2546E-01	COLLISIONS	= 1.0000E+03

REFLECTION COEFFICIENTS

EX	EY	ET	MX	MY	MT	ANGL
2.2931E-02	2.5363E-02	2.2979E-02	2.6285E-02	2.2249E-02	2.3980E-02	0.0000E+00
7.1666E-03	7.9243E-03	7.1793E-03	8.2125E-03	6.9516E-03	7.4923E-03	1.0000E-01
1.0169E-02	1.1239E-02	1.0187E-02	1.1648E-02	9.8599E-03	1.0627E-02	2.0000E-01
5.8943E-02	6.4609E-02	5.8544E-02	6.6956E-02	5.6650E-02	6.1053E-02	5.0000E-01
9.0746E-02	1.0030E-01	9.0902E-02	1.0394E-01	8.8026E-02	9.4856E-02	7.0000E-01
1.3893E-01	1.5350E-01	1.3916E-01	1.5906E-01	1.3477E-01	1.4520E-01	1.0000E+00
2.9489E-01	3.2507E-01	2.9529E-01	3.3668E-01	2.8612E-01	3.0793E-01	2.0000E+00
4.3901E-01	4.8215E-01	4.3940E-01	4.9898E-01	4.2611E-01	4.5773E-01	3.0000E+00
5.6651E-01	6.1907E-01	5.6665E-01	6.3996E-01	5.5016E-01	5.8958E-01	4.0000E+00
7.6178E-01	8.2155E-01	7.6083E-01	8.4660E-01	7.4107E-01	7.8865E-01	6.0000E+00

Table B.5 - Reflection Coefficients - Model 3, in the Magnetic Meridian.

WAVE FREQUENCY =	5.0000E+06	CRITICAL INCIDENCE =	1.0696E+01
MAG. Y VECTOR =	3.1590E-01	STARTING HEIGHT =	1.0000E+03
GEOMAG. FIELD =	5.6426E-05	ENDING HEIGHT =	0.0000E+00
X-DIR COS OF Y =	-3.7890E-01	INCREMENT =	-2.0000E-02
Y-DIR COS OF Y =	0.0000E+00	SCALE HEIGHT =	1.0000E+03
Z-DIR COS OF Y =	9.2546E-01	COLLISIONS =	2.0000E+02

REFLECTION COEFFICIENTS

EX	EY	EZ	HX	HY	HZ	ANGL
9.3169E-01	9.3169E-01	9.3169E-01	9.3169E-01	9.3169E-01	9.3169E-01	0.0000E+00
9.0379E-01	9.1498E-01	9.0410E-01	9.2554E-01	8.9886E-01	9.1131E-01	2.0000E+00
8.2440E-01	8.5471E-01	8.2497E-01	8.6487E-01	8.1540E-01	8.3819E-01	4.0000E+00
6.7000E-01	7.0709E-01	6.7069E-01	7.2057E-01	6.5859E-01	6.8669E-01	6.0000E+00
4.2958E-01	4.8210E-01	4.3016E-01	4.7413E-01	4.2CCBE-01	4.4408E-01	8.0000E+00
3.5730E-01	3.8626E-01	3.5782E-01	3.9702E-01	3.4P89E-01	3.7C14E-01	9.5000E+00
2.8094E-01	3.0522E-01	2.8136E-01	3.1430E-01	2.7392E-01	2.9163E-01	9.0000E+00
2.0106E-01	2.1956E-01	2.0139E-01	2.2650E-01	1.9574E-01	2.0915E-01	9.5000E+00
1.1967E-01	1.3026E-01	1.1987E-01	1.3464E-01	1.1536E-01	1.2371E-01	1.0000E+01
8.5515E-02	9.40A2E-02	8.5660E-02	9.7294E-02	8.3076E-02	8.9216E-02	1.0200E+01
5.3023E-02	5.8444E-02	5.3114E-02	6.0501E-02	5.1479E-02	5.5364E-02	1.0400E+01
2.5122E-02	2.7749E-02	2.5164E-02	2.8746E-02	2.4374E-02	2.6251E-02	1.0600E+01
2.0516E-02	2.26A7E-02	2.0553E-02	2.3512E-02	1.99CCE-02	2.1449E-02	1.0700E+01
2.8276E-02	3.1301E-02	2.8327E-02	3.2453E-02	2.7415E-02	2.9574E-02	1.0800E+01
5.7611E-02	6.3912E-02	5.7716E-02	6.6317E-02	5.583CE-02	6.03C6E-02	1.1000E+01
1.4029E-01	1.5644E-01	1.4052E-01	1.6266E-01	1.357CE-01	1.4712E-01	1.1500E+01
2.2219E-01	2.4934E-01	2.2263E-01	2.5867E-01	2.1464E-01	2.3356E-01	1.2000E+01
3.7523E-01	4.2580E-01	3.7604E-01	4.4554E-01	3.6131E-01	3.9469E-01	1.3000E+01
6.2511E-01	7.2811E-01	6.2714E-01	7.6900AE-01	5.9852E-01	6.6621E-01	1.5000E+01
7.8501E-01	9.1961E-01	7.8747E-01	1.0031E+00	7.4950E-01	8.4306E-01	1.7000E+01

WAVE FREQUENCY =	5.0000E+06	CRITICAL INCIDENCE =	-1.0700E+01
MAG. Y VECTOR =	3.1590E-01	STARTING HEIGHT =	1.0000E+03
GEOMAG. FIELD =	5.6426E-05	ENDING HEIGHT =	0.0000E+00
X-DIR COS OF Y =	-3.7890E-01	INCREMENT =	-2.0000E-02
Y-DIR COS OF Y =	0.0000E+00	SCALE HEIGHT =	1.0000E+03
Z-DIR COS OF Y =	9.2546E-01	COLLISIONS =	2.0000E+02

REFLECTION COEFFICIENTS

EX	EY	EZ	HX	HY	HZ	ANGL
9.0633E-01	9.0630E-01	9.0630E-01	9.0630E-01	9.0630E-01	9.0630E-01	0.0000E+00
9.0100E-01	8.8529E-01	9.0069E-01	8.7982E-01	9.0094E-01	8.9356E-01	-2.0000E+00
8.4174E-01	8.1236E-01	8.4115E-01	8.0234E-01	8.5103E-01	8.2788E-01	-4.0000E+00
7.0118E-01	6.6502E-01	7.0112E-01	6.5258E-01	7.1358E-01	6.8449E-01	-6.0000E+00
4.6134E-01	4.2866E-01	4.6071E-01	4.1794E-01	4.7176E-01	4.4627E-01	-8.0000E+00
3.8606E-01	3.5712E-01	3.8551E-01	3.4744E-01	3.9537E-01	3.7268E-01	-8.5000E+00
3.0595E-01	2.8124E-01	3.0510E-01	2.7312E-01	3.1339E-01	2.9035E-01	-9.0000E+00
2.2049E-01	2.0192E-01	2.2014E-01	1.9577E-01	2.2648E-01	2.1196E-01	-9.5000E+00
1.3203E-01	1.202AE-01	1.3181E-01	1.1643E-01	1.3583E-01	1.2666E-01	-1.0000E+01
8.6285E-02	8.7535E-02	9.4122E-02	8.4626E-02	9.9112E-02	5.2250E-02	-1.0200E+01
4.1257E-02	5.5573E-02	6.1151E-02	5.3084E-02	6.3C94E-02	4.8666E-02	-1.0400E+01
3.1089E-02	2.8144E-02	3.1035E-02	2.7167E-02	3.2041E-02	2.9749E-02	-1.0600E+01
2.4883E-02	2.2502E-02	2.4839E-02	2.1712E-02	2.5653E-02	2.3FC0E-02	-1.0700E+01
3.1246E-02	2.8276E-02	3.1190E-02	2.7224E-02	3.2223E-02	2.9875E-02	-1.0800E+01
6.1770E-02	5.5679E-02	6.1658E-02	5.3660E-02	6.3740E-02	5.9009E-02	-1.1000E+01
1.5241E-01	1.3663E-01	1.5212E-01	1.3142E-01	1.5752E-01	1.4530E-01	-1.1500E+01
2.4383E-01	2.1737E-01	2.4335E-01	2.0863E-01	2.5241E-01	2.3196E-01	-1.2000E+01
4.1791E-01	3.6832E-01	4.1707E-01	3.5199E-01	4.3407E-01	3.9594E-01	-1.3000E+01
7.1571E-01	6.1510E-01	7.1388E-01	5.8234E-01	7.4830E-01	6.7226E-01	-1.5000E+01
9.2107E-01	7.6951E-01	9.1820E-01	7.2077E-01	9.6989E-01	8.5771E-01	-1.7000E+01

Table B.6 - Reflection Coefficients - Model 3, off the Magnetic Meridian.

WAVE FREQUENCY =	5.0000E+06	CRITICAL INCIDENCE =	1.0696E+01
MAG. Y VECTOR =	3.1590E-01	STARTING HEIGHT =	1.0000E+03
GEOMAG. FIELD =	5.6426E-05	ENDING HEIGHT =	0.0000E+00
X-DIR COS OF Y =	-3.7890E-01	INCREMENT =	-2.0000E-02
Y-DIR COS OF Y =	0.0000E+00	SCALE HEIGHT =	1.0000E+03
Z-DIR COS OF Y =	9.2546E-01	COLLISIONS =	2.0000E+02

REFLECTION COEFFICIENTS

EX	EY	ET	MX	MY	MT	ANGL
2.0479E-02	2.2640E-02	2.0511E-02	2.3663E-02	1.9861E-02	2.1406E-02	0.0000E+00
4.3837E-03	4.8471E-03	4.3914E-03	5.0234E-03	4.2522E-03	4.5828E-03	1.0000E-01
1.2480E-02	1.3798E-02	1.2502E-02	1.4300E-02	1.2105E-02	1.3046E-02	2.0000E-01
6.1468E-02	6.7954E-02	6.1576E-02	7.0422E-02	5.9626E-02	6.4257E-02	5.0000E-01
9.4071E-02	1.0398E-01	9.4233E-02	1.0775E-01	9.1252E-02	9.8331E-02	7.0000E-01
1.4263E-01	1.5763E-01	1.4291E-01	1.6334E-01	1.3840E-01	1.4911E-01	1.0000E+00
2.9982E-01	3.3051E-01	3.0023E-01	3.4231E-01	2.9091E-01	3.1309E-01	2.0000E+00
4.4491E-01	4.8862E-01	4.4530E-01	5.0567E-01	4.3182E-01	4.6392E-01	3.0000E+00
6.8162E-01	7.4039E-01	6.8130E-01	7.6619E-01	6.6244E-01	7.0767E-01	5.0000E+00
8.8791E-01	9.4244E-01	8.8959E-01	9.6690E-01	8.6634E-01	9.1314E-01	8.0000E+00

WAVE FREQUENCY =	5.0000E+06	CRITICAL INCIDENCE =	-1.0700E+01
MAG. Y VECTOR =	3.1590E-01	STARTING HEIGHT =	1.0000E+03
GEOMAG. FIELD =	5.6426E-05	ENDING HEIGHT =	0.0000E+00
X-DIR COS OF Y =	-3.7890E-01	INCREMENT =	-1.0000E-01
Y-DIR COS OF Y =	0.0000E+00	SCALE HEIGHT =	1.0000E+03
Z-DIR COS OF Y =	9.2546E-01	COLLISIONS =	2.0000E+02

REFLECTION COEFFICIENTS

EX	EY	ET	MX	MY	MT	ANGL
2.4879E-02	2.2495E-02	2.4831E-02	2.1706E-02	2.5644E-02	2.3793E-02	0.0000E+00
4.2831E-02	3.8734E-02	4.2756E-02	3.7374E-02	4.4157E-02	4.0969E-02	1.0000E-01
6.0761E-02	5.4955E-02	6.0686E-02	5.3026E-02	6.2646E-02	5.8125E-02	2.0000E-01
1.1436E-01	1.0344E-01	1.1417E-01	9.9836E-02	1.1790E-01	1.0940E-01	5.0000E-01
1.4984E-01	1.3556E-01	1.4958E-01	1.3081E-01	1.5447E-01	1.4335E-01	7.0000E-01
2.0251E-01	1.8328E-01	2.0211E-01	1.7687E-01	2.0876E-01	1.9376E-01	1.0000E+00
3.7089E-01	3.3644E-01	3.7038E-01	3.2983E-01	3.8226E-01	3.5517E-01	2.0000E+00
5.2315E-01	4.7632E-01	5.2269E-01	4.6025E-01	5.3899E-01	5.0169E-01	3.0000E+00
7.6194E-01	7.0152E-01	7.6236E-01	6.7957E-01	7.8401E-01	7.3398E-01	5.0000E+00
9.4970E-01	8.9479E-01	9.5227E-01	8.7214E-01	9.7343E-01	9.2351E-01	8.0000E+00

END

DATE

FILMED

8-88

DTIC